Department of Civil Engineering DTU

Jesper L. Asferg

Modeling of Concrete Fracture Applying the eXtended Finite Element Method

PHD THESIS

BYG • DTU

Modeling of Concrete Fracture Applying the eXtended Finite Element Method

Jesper L. Asferg

Ph.D. Thesis

Department of Civil Engineering
Technical University of Denmark

2006

Modeling of Concrete Fracture Applying the eXtended Finite Element Method

Printed by DTU Tryk
Department of Civil Engineering
Technical University of Denmark
87 7877 214 1
1601-2917

Preface

This thesis is submitted as a partial fulfilment of the requirements for the Danish Ph.d. degree. The thesis is divided into two parts. The first part concerns the background of the research, motivates the work carried out and highlights the major findings and conclusions. The second part is a collection of three papers, presenting the research in greater details.

Lyngby the 15$^{\text{th}}$ of September 2006

Jesper L. Asferg

Preface to published version of thesis

The thesis was defended at a public defence on Friday the 2$^{\text{nd}}$ of February 2007. Official opponents were Professor Bhushan L. Karihaloo, Cardiff University, Professor Dr. Ir. L. J. Sluys, Delft University of Technology, and Professor Jeppe Jönsson, The Technical University of Denmark. Subsequently the Ph.D. degree was awarded from The Technical University of Denmark.

Compared to the original submitted version of the thesis a number of minor editorial corrections have been implemented and the status of two of the papers on which the thesis is based has changed from submitted to published.

Acknowledgements

I gratefully acknowledge the support and fruitful discussion with my supervising team - Professor Henrik Stang, Associate Professor Peter Noe Poulsen and Associate Professor John Forbes Olesen all from the Department of Civil Engineering, Section for Structural Engineering at the Technical University of Denmark.

I am most grateful for the support and fine cooperation with Associate Professor Leif Otto Nielsen also from the Department of Civil Engineering, Section for Structural Engineering at the Technical University of Denmark with whom I have had an excellent cooperation regarding the coding of the extended finite element scheme.

Furthermore, I would like to thank Professor Ted Belytschko, Northwestern University, Evanston, IL, USA for a very fruitful stay with his research group. I would also like to thank Ph.D. student Robert Gracie, Post doc. Pedro M. A. Areias, Ph.D. student Jeong-Hoon Song and Ph.D. student Hongwu Wang for many fruitful discussions during my stay at Northwestern.

A sincere thanks to Associate Professor Lennart Østergaard, Ph.D. Rasmus Walter and Ph.D. student Lars Dick-Nielsen for many interesting discussions related to fracture mechanics and FE modeling during the three years at DTU. Finally, a great thanks to my fellow Ph.D. students at the "Ph.D-office" who all contributed to three excellent years at the Department of Civil Engineering.

Without external funding the stay at Northwestern University, my participation in international advanced courses and international conferences could not have been realized. I therefore wish to thank the following foundations for their economical support: The Otto Mønsted Foundation, The Knud Højgaard Foundation, The Reinholdt W. Jorck Foundation, The Alexandre and Nina Haynman Foundation, The Berg Nielsen Scholarship, The Christiani and Nielsen Foundation, The Poul V. Andresens Foundation, The Idella Foundation and the BYG-DTU travel foundation for PhD-students.

Abstract

At present no consistent methods are available for a complete structural analysis of concrete structures. There are no methods which are capable of predicting crack pattern, crack widths and development in structural stiffness in the serviceability state while at the same time being able to model the response of the structure all the way to failure. With respects to models dealing with durability and life time predictions of RC structures there is a lack of methods capable of supplying information about cracking to the durability estimates. Thus models capable of predicting crack growth, crack patterns and crack widths in RC structures are required.

Analysis of structures with complex geometry will often require the use of numerical tools such as the finite element method. Therefore it is seen as essential that a model for cracking of RC structures fits within the framework of this method.

This thesis is concerned with the modeling of cohesive crack growth in concrete within the framework of the eXtended Finite Element Method (XFEM). The major part of the work is concerned with the modeling of crack growth in the bulk concrete from a computational point of view.

The cornerstone in the XFEM is the enrichment of the displacement field in elements cut by the discontinuity. The development of proper enrichment schemes for elements for cohesive crack growth has been a focus area in the research presented in this thesis. The proposed enrichments are based on local partitions of unity and the enrichments only influence elements cut by the discontinuity. A direct enrichment scheme for fully cracked elements is proposed. The enrichment scheme is able to model the same variations in the displacement field as other XFEM elements found in the literature. The proposed enrichment scheme is, however, more straight forward and is easily implemented. The enrichment is implemented for the constant strain triangle (CST) and the linear strain triangle (LST). The performance of the elements is illustrated by modeling of fracture in two benchmark fracture tests for concrete - the notched three point bending test (TPBT) and the notched four point shear beam (FPSB). Good results are obtained with respect to predicting crack paths and determining the full load-deformation responses applying the fully cracked elements.

Applying the enrichment scheme proposed for fully cracked elements or the schemes found in the literature, the crack-tip element is not capable of modeling equal stresses at each side of the crack. Furthermore elements that are not capable of holding the crack tip within

the interior of the element do not allow computation of all possible load-displacement states as it is normally required in a general non-linear procedure. Therefore, a consistent XFEM element, capable of modeling equal stresses at each side of the crack in the tip-element, and capable of holding the crack tip at any point within the element, is proposed. The capability to model equal stresses at each side of the crack in the crack-tip element is achieved by addition of extra enrichments to elements cut by the discontinuity. The extra enrichments are, like the enrichment applied for the fully cracked elements, element local and influence only elements cut by the crack. This enrichment scheme is developed for the CST element and the performance of the partly cracked element is illustrated by modeling of fracture in the TPBT specimen and in the FPSB. Applying the partly cracked CST element the prediction of the crack paths are improved and more smooth crack paths are achieved. Also more smooth load-deformation responses are obtained.

The interaction between the bulk concrete and the reinforcement is the governing factor for the load carrying capacity of RC structures. Regarding the capability of the model to include reinforcement the long time goal may be the formulation of a "super" element capable of modeling the overall physical behavior of reinforcement embedded in concrete. As a step towards a super element a cohesive XFEM interface element for modeling of the bond zone between reinforcement and concrete is developed. The interface element is developed in a plane 2D version capable of being partly cracked. The performance of the interface element is tested by modeling of fracture in the previous considered TPBT specimen. A nice smooth crack profile is obtained applying the interface element and good results are obtained with regard to the load-deformation response when the crack is propagated element by element. When the crack-tip is located inside an element the load-deformation response becomes somewhat tortious.

Resumé

På nuværende tidspunkt er der ingen tilgængelige konsistente metoder for en fuldstændig analyse af betonkonstruktioner. Der er ingen metoder, der er i stand til at forudsige revnemønstre, revnevidder samt udvikling i stivheden for konstruktioner i anvendelsesgrænsetilstanden samtidig med, at de er i stand til at modellere det strukturelle respons hele vejen frem til brud. I relation til levetidsmodeller for betonkonstruktioner er der mangel på metoder, der er i stand til at tilføre levetidsmodellerne information om revnedannelse. Modeller, der kan forudsige revnevækst, revnemønstre og revnevidder i armerede betonkonstruktioner, er påkrævede.

Analyse af konstruktioner med komplekse geometrier vil ofte kræve anvendelse af numeriske værktøjer som fx. den finitte element metode. Derfor vil det være fordelagtigt såfremt metoder til modellering af revnevækst er kompatible med den finitte element metode.

Denne ph.d.-afhandling omhandler kohæsiv revnevækst i beton inden for rammerne af "the eXtended Finite Element Method", XFEM. Hovedparten af forskningsarbejdet er relateret til modellering af revnevækst i uarmeret beton ud fra et modelleringsteknisk perspektiv.

XFEM er baseret på berigelse af flytningsfeltet i elementer, der er gennemskåret af en diskontinuitet. Udviklingen af fornuftige koncepter til berigelse af flytningsfeltet - i elementer til kohæsiv revnevækst - har været i fokus i den udførte forskning. De præsenterede koncepter for berigelsen er baseret på lokale enhedsflytningsfelter (partition of unity). De foreslåede berigelser er elementlokale, og kun elementer der er gennemskåret af diskontinuiteten berøres af berigelsen. Et direkte og enkelt koncept for berigelsen af elementer, der er gennemskåret af en diskontinuitet i elementets fulde længe, er præsenteret. De foreslåede elementer er i stand til at modellere samme variation i flytningsfeltet som andre XFEM elementer for kohæsiv revnevækst fundet i litteraturen. Den anvendte berigelse af flytningsfelter er imidlertid konceptuelt enklere og lader sig nemt implementere. Den foreslående berigelse er implementeret for CST elementer, der kan reproducere konstante tøjninger, samt for LST elementer, der kan reproducere en lineær tøjningsvariation. Elementernes egenskaber er illustreret ved modellering af revnevækst i traditionelle brudmekaniske tests, som kærvet trepunktsbøjning (TPBT) samt revnevækst i den såkaldte firepunktsforskydningsbjælke (FPSB). Gode resultater er opnået med hensyn til såvel forudsigelse af revnemønster samt bestemmelse af det fulde last-flytningsrespons med anvendelse af de fuldt revnede elementer.

Når berigelseskoncept for de fuldt revnede elementer eller berigelseskoncepter fra litteraturen anvendes, er revnespidselementet ikke i stand til at modellere identiske spændinger på begge sider af revnen. Anvendelsen af elementer, der ikke er i stand til at indeholde revnespidsen i et vilkårligt punkt inden for elementet, muliggør desuden ikke beregning af alle mulige last-flytningstilstande, som det normalt er påkrævet i en generel ikke-lineær beregningsprocedure. Derfor præsenteres også et delvist revnet XFEM revnespidselement, der er i stand til at modellere identiske spændinger på de to sider af revnen. Elementet er i stand til at håndtere en vilkårlig placering af revnespidsen inden for elementet. Muligheden for at modellere identiske spændinger på begge sider af revnen er opnået ved tilføjelse af ekstra berigelser af flytningsfeltet. De ekstra berigelser er som berigelsen af de fuldt revnede elementer baseret på en lokal partion of unity. Det foreslåede berigelseskoncept er implementeret for CST elementet. Elementets egenskaber er illustreret ved modellering af revnevækst i de tidligere anvendte tests, TPBT og FPSB. Ved anvendelsen af det delvist revnede element opnås en bedre bestemmelse af revnemønsteret - det er glattere. Ligeledes fås et glattere last-flytningsrespons.

Sammenvirkningen mellem beton og armering i armerede betonkonstruktioner er den styrende faktor for evnen til at optage last. Vedrørende modellens evne til at inkludere armering er det langsigtede perspektiv formuleringen af et såkaldt superelement, der vil være i stand til at modellere de overordnede fysiske egenskaber af armering indstøbt i beton. Som et skridt frem mod et sådan superelement præsenteres et kohæsivt XFEM interfaceelement til modellering af skillefladen mellem beton og armering. Interfaceelementet er udviklet i en plan udgave og er i stand til at være delvist revnet. Interfaceelementets egenskaber er illustreret ved modellering af revnevækst i TPBT bjælken. Med anvendelsen af interfaceelementet opnås en pæn, glat lukkende revne. Med hensyn til last-flytningsresponset opnås gode resultater, når revnen propageres element for element, mens nogen ujævnhed af responset er konstateret, når revnespidsen er i den indre del af elementet.

Table of Contents

II Appended Papers

Paper I A direct XFEM formulation for cohesive crack growth in concrete,
In: *Computers and Concrete, Vol 4, No.2 (2007), page 83-100*

Paper II A consistent partly cracked XFEM element for cohesive crack growth,
In: *International Journal of Numerical Methods in Engineering*,
Available online/ in press.

Paper III Partly cracked XFEM interface,
In: *Fracture of Nano and Engineering Materials and Structures*,
Proceedings of the 16th European Conference of Fracture, Alexandroupolis, Greece, 2006, E.E. Gdoutos (eds), page 397-398, (Full paper on CD).

Additional work (not included in the thesis)

[1] Asferg J.L., Poulsen P.N., Nielsen L.N.: Modeling of Cohesive Crack Applying the XFEM, In: *5.th International PhD Symposium in Civil Engineering, Delft, The Netherlands, Walraven, Blauwendraad, Scarpas and Snijder (eds) 2004*, page 1261-169.

[2] Asferg J.L., Poulsen P.N., Nielsen L.N.: A simplified XFEM formulation for cohesive crack modeling, in: *Proceedings of the 17th Nordic Seminar on Computational Mechanics, Stockholm, Sweden, 2004, Eriksson, Månsson and Tibert (eds)*, page 35-38.

[3] Asferg J.L., Poulsen P.N., Nielsen L.N.: Cohesive Crack-Tip Element for XFEM, in: *Proceedings of 11th International Conference of Fracture, Turin, Italy, 2005, Carpinteri (eds)*, page 200 (Full paper on CD).

[4] Asferg J.L., Poulsen P.N., Nielsen L.N.: Modeling of crack propagation in concrete applying the XFEM, in: *Computational Modeling of Concrete Structures, Meshke, de Borst, Mang, Bićanić (eds), Taylor Francis Group, London, 2006*, page 33-42.

Part I

Introduction and Summary

Chapter 1

Introduction

Concrete-like materials were used by the Greeks as early as 500-300 BC and it were used for important Roman architectural master pieces such as Colosseum (72-80 AD) and Pantheon (120-125 AD). Portland cement, the basis of modern concrete was, however, not patented until 1824 by Joseph Aspdin. Twenty four years later steel was applied as reinforcement in concrete for the first time when Jean Louise Lambot in 1848 build a boat of concrete with embedded iron bars. In 1868 Joseph Monier patented a system for reinforcing garden tubs and later also concrete beams. Since those early applications of reinforced concrete the technology has developed rapidly and today reinforced concrete is the most widely used construction material in the world. The annual (2005) consumption of concrete has now raised to about 6 billion tons - equivalent to 1 ton per person on the entire planet.

1.1 Analysis of Concrete Structures

Throughout the last century intense research has been carried out regarding methods to determine the ultimate strength of reinforced concrete (RC) structures. Today well-documented methods are available for estimating the ultimate strength of most RC structures. Methods based on the theory of linear elasticity are widely used - e.g. ACI Committee 318 (2002) - but also methods based on the theory of plasticity assuming a rigid-plastic material behavior have proven to be successful and are today highly developed - see e.g. Nielsen (1999). However, most of these methods require the use of empirical factors and do not consider reinforcement arrangement in a fully consistent way. Most of the models are further encumbered with size effects that also need to be handled through empirical factors.

Regarding RC structures in the serviceability limit state the predictive capability of existing methods of analysis is limited. Predictions of the load-deformation-response of RC structures in the serviceability state are often based on empirical rules - see e.g. DS 411 (1999). Attempts have been made to establish more consistent methods to predict the behavior in the serviceability state. Christiansen (2000) and Christiansen and Nielsen (2001) have developed a set of simple models suitable for hand calculation to predict the

structural behavior of reinforced concrete in plane stress. These models are based on the diagonal compression stress field of concrete and have been extended to include a developing crack phase to take into account tension stiffening. The models by Christiansen are semi-analytical and only developed for simple geometries. Analysis of structures with complex geometry will often require the use of the Finite Element Method (FEM) for which the semi analytical approach is not suitable. A complete model for the structural behavior of RC structures in the serviceability limit state must be able to predict the complex cracking which takes place in the concrete during loading. Furthermore, it is preferable if the model fits within the framework of the FEM to allow modeling of structures with complex geometries.

Extended knowledge of the complex mechanical interaction between concrete and reinforcement and the development of methods for modeling of RC structures in the serviceability state will also be of great importance for the development of models capable of describing the response of RC structures subjected to fatigue loading.

In the long term perspective consistent models that are able to predict development of crack patterns and crack widths may also provide information in relation to durability and service life prediction for concrete structures. The connection between the presence of cracks in RC structures and corrosion of reinforcement has been known for a long time. Several design codes specify requirements for allowable crack widths in concrete. On the basis of early studies Beeby (1978) concluded that there is no significant relationship between crack widths and corrosion. However, more recent studies by e.g. Schießl and Raupach (1997) and Mohammed et al. (2001) show that the time to initiation of reinforcement corrosion depends on the crack width. For design purposes the service life of a RC structures is often defined as the time to initiation of reinforcement corrosion. Other studies (Arya and Ofori-Darko, 1996) reveal that the crack spacing is a governing factor in the reduction of the rate of corrosion - i.e. from a corrosion point of view several small cracks are more sever than one large crack. Therefore also the crack pattern plays an important role in relation to durability.

Ongoing efforts in the research community are focused on the scope of developing proper methods for modeling of reinforced concrete structures. A proper method must be capable of predicting crack paths and crack widths in concrete and it must be able to model the complex interaction between reinforcement and concrete.

1.2 A Fracture Mechanics Approach

Any method for structural analysis must be based on an appropriate physical model for the material considered. Several properties of concrete make fracture mechanics relevant when the scope is to model structural concrete. The fact that concrete structures are full of flaws due to pores, air voids and shrinkage cracks, which may initiate further crack growth when the concrete structure is loaded, points toward fracture mechanics. Also the fact that concrete shows tension softening (see e.g. Karihaloo (1995)) due to localized micro cracking motivates the application of fracture mechanics. Furthermore, today the

tensile strength of concrete is neglected in most of the serviceability and the limit state calculations. Ignoring the tensile strength in serviceability calculations maks it difficult to model the presence and effect of cracks. The tensile strength of concrete is often significant compared to the stresses associated with the applied loads in the serviceability state and therefore important to take into account. This may be done applying a fracture mechanics approach.

More than twenty years ago Hawkins (1985) listed twenty-nine provisions in the ACI Code 318 "Building Code Requirements for Reinforced Concrete" that until then did not have a thorough physical explanation but could be explained by the theory of fracture. The twenty-nine provisions were mainly related to issues regarding minimum reinforcement ratios for flexural and shear reinforcement and to ductility requirements. In the beginning of the nineties the work of Hawkins was followed up by ACI Committe 446 (1992) who listed five strong arguments for the application of fracture mechanics to structural concrete:

(i) *Energy requirement for crack growth.*
What is important for cracking in a structure is not how the cracking is initiated but how the cracking will propagate. The growth of any crack requires the consumption of a certain amount of energy. Therefore the crack propagation can only be studied through an energy based propagation criterion. A crack initiation criterion - e.g. a crack strength is not sufficient.

(ii) *Objectivity of load and response calculation*
Early finite element calculations showed dependency on mesh size. The way to obtain reliable results that are independent of element size require the energy dissipated through cracking to be constant. A constant dissipation of energy - the fracture energy - forms the corner stone of fracture mechanics of concrete.

(iii) *Lack of yield plateau*
For materials that exhibit softening the failure process does not result in the formation of plastic hinges at isolated locations, but takes place due to the propagation of a fracture zone throughout the structure.

(iv) *Energy absorbing capability and ductility*
When considering a load displacement diagram for a structure loaded to failure the area under the graph represents the energy consumed during the failure process. For a softening type material the post peak response (the non reversible part) represents the bulk of the absorbed energy and it determines the ductility of the structure. Limit state analysis does not consider tension softening and therefore it can not give an indication of the ductility of the structure.

(v) *Size effect*
Fracture mechanics may opposite to strength criterions predict the effect of the structural size on the failure load and ductility.

Thus fracture mechanics may contribute to physical explanation of phenomena that present codes only take into account using empirical formulas. Phenomena that in many cases will be related to the serviceability state. An introduction to fracture mechanics applicable to concrete will be given in Chapter 2 of this thesis. Cohesive crack models will be identified as very suitable models for modeling of cracks in concrete and the proposed FEM model for modeling of the structural response of concrete structures will be based on fracture mechanics applying a cohesive model.

1.3 Computational Modeling of Reinforced Concrete Structures

Computational modeling of a reinforced concrete beam applying the FEM was carried out almost forty years ago by Ngo and Scordelis (1967). In this seminal work the influence of cracking was investigated assuming a number of different crack patterns. The effects of cracks was modeled by disconnecting nodes located at opposite side of the crack. However the results obtained by Ngo and Scordelis (1967) showed mesh dependency and thus revealed the requirement for energy based crack propagation criterions. Today, FEM computations are often used for analysis of complex concrete structures. However, since the majority of codes of practice are based on the theory of elasticity, e.g. ACI Committee 318 (2002), and since the implementation of models based on linear elasticity is simple, most of the FEM computations for practical purposes are based on the theory of linear elasticity. Commercial FEM codes like DIANA (Diana User Manual, 2003a) have elements that allow the user to embed reinforcement in terms of bars or grids into beam, curved shell or solid elements. The interaction between reinforcement and concrete in such models is assumed to be either full bonding or no bond at all between reinforcement and concrete.

FEM computations based on the theory of plasticity assuming a rigid-plastic material behavior are more difficult but have been carried out in a number of examples. Early examples include Damkilde and Kirk (1981) whereas more recent examples include the work by Damkilde and Krenk (1997) where a system for limit state analysis and material optimization based on the lower-bound theorem is proposed. In this work a number of elements were considered: two- and three dimensional beam elements, truss elements, triangular slab elements and shear and stringer elements for plates with in plane loading. In the work by Poulsen and Damkilde (2000) limit state analysis of RC concrete plates subjected to in-plane forces were considered whereas a lower bound limit analysis of slabs with nonlinear yield criteria was carried out in Krabbenhoft and Damkilde (2002). Despite their advantage in relation to structural optimization the computational methods based on the assumption of a rigid-plastic material behavior are not widely used.

Common for the computational approaches referred to above are that they all focus on the ultimate limit state. They do not predict crack paths and crack widths and are not capable of predicting developments in e.g. stiffness in the serviceability state.

A number of FEM approaches allow modeling of cracks and crack propagation. The models are conceptually different: whereas some require the crack path to be known be-

fore hand others are capable of modeling crack growth independent of the mesh. Some approaches model the cracks in a discrete approach, c.f. Figure 1.1(a), where the crack location and the crack openings are known precisely. Other models smears the crack over an element, c.f. Figure 1.1(b).

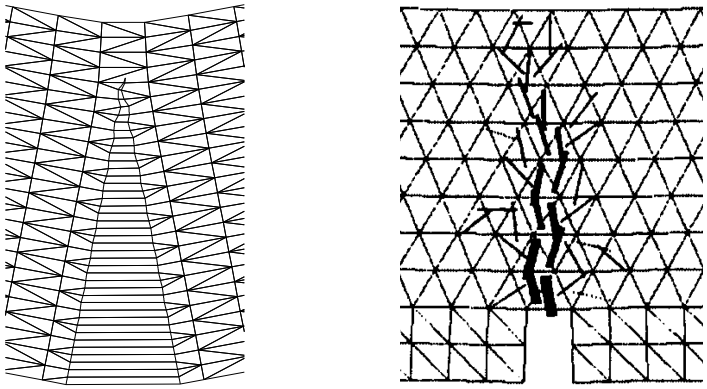

(a) (b)

Figure 1.1 *Different approaches to modeling of crack propagation in three point bending beam: (a) discrete approach applying the XFEM, (b) smeared approach (Jirásek and Zimmermann, 1998a)*

Interface crack models allow inter-elemental crack propagation along predefined paths and model cracks in a discrete approach. Interface models are well suited for modeling of situations where crack paths are known a priori, however, this is rarely the case in real concrete structures. In combination with remeshing techniques interface elements allow modeling of unknown crack paths - see e.g. Yang and Chen (2005). However, remeshing is computationally expensive making this approach less attractive.

Embedded crack models based on the pioneering work of Ortiz et al. (1987) may also model cracks in a discrete approach. In embedded models cracks propagate through an existing mesh independent of element boundaries. However, in embedded crack models the strains on each side of the crack in a cracked element are not fully uncoupled as it is preferred.

Smeared crack models based on the concept of a crack band (Bažant and Oh, 1983) model cracking in a plasticity approach in which the exact location of the crack inside an element is unknown. The interpretation of crack widths is difficult in smeared models and they often show mesh dependency and locking. Models based on damage mechanics (Jirásek, 2004) may also be considered for modeling of fracture in concrete, however, this group of models does not, like the smeared models, model cracks in a discrete approach and hence have some of the drawbacks of the smeared models.

Recent approaches include element free methods (Belytschko et al., 1996) but these models do not fit within the framework of traditional FEM models. Among the most recent

approaches for modeling of crack propagation is also the eXtended Finite Element Method (XFEM) (Belytschko and Black, 1999; Moës et al., 1999). In the XFEM the displacement field is decomposed into a continuous part and a discontinuous part allowing the element to describe a discontinuity discretely within the element. Applying the XFEM, crack growth is independent of the mesh. Furthermore, in the XFEM the uncracked parts on each side of an element are uncoupled and hence XFEM elements have superior kinematic properties compared to embedded crack models.

A more extensive review and discussion of the most relevant computational models for fracture in concrete will be given in Chapter 3. As already indicated XFEM seems to be the best suited method for modeling of crack propagation in concrete. The XFEM fulfills the previous listed requirements in terms of capability to predict crack patterns and crack widths in an efficient and mesh independent way. While most of the models mentioned above have been applied to modeling of crack growth in the bulk concrete it is still an open question how reinforcement may be included in computational models applying fracture mechanics. When modeling the interaction between reinforcement and concrete it is of major importance to include the hoop stress that builds up on the reinforcement. This is known as the confinement pressure - or simply the confinement - and is mainly due to dilation caused by the ribs on the reinforcement. At present there is no standard approach on how to include the effects of confinement. Also regarding the constitutive parameters applicable for the bond zone between reinforcement and concrete more research is still needed.

1.4 Scope of This Study

At present no consistent methods are available for a complete structural analysis of concrete structures. There are no methods which are capable of predicting crack pattern, crack widths and development in structural stiffness in the serviceability state while at the same time being able to model the response of the structure all the way to failure. With respects to models dealing with durability and life time predictions of RC structures there is a lack of methods capable of supplying information about cracking to the durability models. Models capable of predicting crack growth, crack patterns and crack widths in RC structures are required.

This thesis is concerned with the modeling of cohesive crack growth in concrete within the framework of the eXtended Finite Element Method (XFEM). The major part of the work is concerned with the modeling of crack growth in the bulk concrete from a computational point of view. Low order elements in terms of CST and LST elements are considered to allow the modeling of real size civil structures in the long time perspective. Regarding the capability of the model to include reinforcement the long time goal may be the formulation of a "super" element. A super element is an element capable of modeling the overall physical behavior of reinforcement embedded in concrete taking into account effects as confining pressure and combined separation and sliding between reinforcement and concrete. As a step towards such a super element a cohesive XFEM interface element for modeling of the bond zone between reinforcement and concrete is developed.

1.5 Overview of the Thesis

The thesis opens with a short introduction to fracture mechanics and cohesive crack models. Then follows a review of finite element techniques that may be applied for modeling of cohesive crack growth. A general introduction to XFEM will be given before getting into the specific applications of XFEM to cohesive crack propagation .

The original contributions in the work are related to three papers forming the core of the thesis. The scope of each paper will be given in detail in the individual chapters and will not be repeated in great detail here. The two first papers are related to modeling of crack growth in the bulk concrete while the third paper is related to the inclusion of reinforcement in the model.

Paper I, "A direct XFEM formulation for modeling of cohesive crack growth" deals with the development of a direct scheme for cohesive crack growth applying fully cracked XFEM elements. The simplification is related to the so-called enrichment of the displacement field that introduces the discontinuous displacement field in elements cut by a discontinuity. The enrichment scheme is applied to elements that are capable of being either uncracked or fully cracked - i.e. in this work the crack-tip is always located on an element boundary. The developed scheme is implemented for the 3-node constant strain triangle (CST) element and the 6-node linear strain triangle (LST) element. The performance of the scheme is tested by modeling of crack propagation in the notched three point beam bending test (TPBT) and in the notched four point shear beam (FPSB).

Paper II, "A consistent partly cracked XFEM element for cohesive crack growth" introduces a new partly cracked XFEM element for cohesive crack growth. This new element is capable of holding the crack-tip at any point within the element and hence allows the modeling of all possible load-displacement states, as it is normally required in a non-linear analysis. This is not possible when fully cracked elements are applied. From a computational point of view the capability to model all load-displacement states is favorable for the stability of the computations. Furthermore, the proposed crack-tip element allows modeling of equal stresses at each side of the crack in the crack tip element which can not be done applying the previously proposed XFEM elements for cohesive cracking (Wells and Sluys, 2001; Zi and Belytschko, 2003; Mergheim et al., 2005; Asferg et al., 2007b). This improved representation of the stresses in the crack-tip element improves the computation of crack growth direction and the new element yields a more smooth structural response compared to the fully cracked elements. The scheme is implemented for the CST element and by nodal averaging of stresses a stress interpolation is computed for the element allowing solutions where stresses in the crack tip are equal to the tensile material strength. The examples considered for the fully cracked elements are computed applying the partly cracked element and the results are compared.

Paper III, "Partly Cracked XFEM interface element". Whereas the two first papers are

concerned with the modeling of crack propagation in the bulk concrete the third paper is related to the inclusion of reinforcement in the model. The paper is concerned with the finite element aspects of the inclusion of reinforcement and does not concern the constitutive conditions for the bond zone, which in its own possess a large research area. A first step towards a super element modeling the interaction between reinforcement and concrete is a cohesive interface element that is capable of being partly cracked. An XFEM interface element capable of being partly cracked is developed in *paper III* and its performance is illustrated modeling crack growth in the TPBT specimen also considered in *Paper I* and *Paper II*.

In Chapter 7 the findings in the preceding chapters are summarized and final conclusions are drawn. Suggestions for improvements of the proposed XFEM elements are given and areas for further research are pointed out.

Chapter 2

Fracture Mechanics for Concrete

This chapter gives a brief introduction to fracture mechanics applicable to concrete. Although fracture of concrete in most structures must be described by non-linear fracture mechanics the chapter opens by introducing the concepts of linear elastic (LEFM) fracture mechanics, that also forms the basis for the non-linear fracture mechanics. For a more detailed introduction to fracture mechanics reference is made to e.g. Karihaloo (1995) or Shah et al. (1995).

2.1 Linear Elastic Fracture Mechanics

Griffith (1921) was the first to develop an analysis procedure based on energy considerations for the fracture of brittle materials. Griffith explained why the observed tensile strength of brittle materials is significantly lower than the theoretical tensile strength.

Griffith studied the influence of a sharp crack in a sheet of a brittle material loaded by a constant remote stress field. Assuming that the entire fracture process takes place at the crack tip, where the stress field is singular, Griffith found by the principle of superposition, the change in potential energy of the system. From this he formulated the "Griffith" fracture criterion for ideally brittle materials introducing the surface energy density, γ_s, that is the energy required to create a unit traction-free crack surface:

$$\frac{\pi a \sigma_c^2}{E} = 2\gamma_s \tag{2.1}$$

where a is half the initial crack length, E the modulus of elasticity, and σ_c is the maximum applicable remote tensile stress c.f. Figure 2.2. Whereas the quantity $2\gamma_s$ accounts for the energy dissipation in the studies by Griffith later studies revealed that an non-negligible amount of energy is dissipated due to friction when fracture occurs. The material toughness, G_c, includes the surface energy as well as the frictional energy.

Applying the toughness the fracture criterion may also be formulated in terms of a stress criterion for σ_c:

$$\sigma_c = \sqrt{\frac{G_c E}{\pi a}} \tag{2.2}$$

If, for a given load $\sigma < \sigma_c$, the applied elastic energy is lower than the critical energy the crack will not propagate. For loads causing $\sigma > \sigma_c$ the crack will propagate catastrophically since for increasing crack length the critical stress decreases.

Irwin (1957) introduced the stress-intensity factor concept or the so called "Irwin Criterion for fracture of brittle materials". Irwin showed that for the stress variation near a sharp crack tip in a linear elastic material a square-root singularity, $r^{-1/2}$, where r is the distance to the crack tip, for $r << a$, is always found. For the description, of fracture three fundamental modes have been defined for the crack opening. The three modes are depicted in Figure 2.1. Mode I and Mode II are planar modes. Mode I is caused by stresses normal to the crack face while Mode II is due to shear stresses along the crack face. Mode III is an anti-plane mode caused by tearing loading. Like Griffith, Irwin studied the so called Mode I fracture. While the square-root singularity is independent of the crack opening mode, the stress intensity factor depends on the boundary conditions, geometry and loading mode of the system. A stress intensity factor for each mode will be required for the full description of generalized fracture. For Mode I, II and III, respectively, the stress intensity factors are termed K_I, K_{II} and K_{III}.

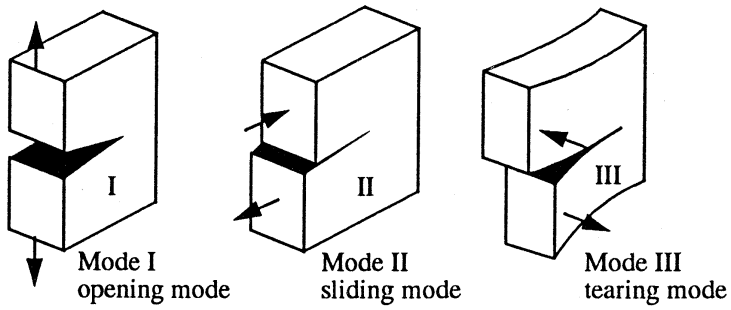

Figure 2.1 *The three opening modes for cracks. Mode I and Mode II are planar modes while Mode III is a anti plane mode of deformation. From (Karihaloo, 1995)*

Applying the stress intensity factor the stress components and the displacement field near the crack tip may be obtained. Introducing a polar coordinate system with origin at the crack tip, c.f. Figure 2.2, the leading terms of the Williams expansion (Williams, 1952), for the stresses and displacements as function of the distance r and the angle θ for Mode I, are:

$$\sigma_{xx} = \frac{K_I}{\sqrt{2\pi r}} \cos\frac{\theta}{2}\left(1 - \sin\frac{\theta}{2}\sin\frac{3\theta}{2}\right)$$

$$\begin{aligned} \sigma_{yy} &= \frac{K_I}{\sqrt{2\pi r}} \cos\frac{\theta}{2}\left(1+\sin\frac{\theta}{2}\sin\frac{3\theta}{2}\right) \\ \sigma_{xy} &= \frac{K_I}{\sqrt{2\pi r}} \cos\frac{\theta}{2}\sin\frac{\theta}{2}\sin\frac{3\theta}{2} \end{aligned} \tag{2.3}$$

$$\begin{aligned} u &= \frac{K_I\,(1+\upsilon)}{E}\sqrt{\frac{2r}{\pi}}\cos\frac{\theta}{2}\left(\frac{\kappa-1}{2}+\sin^2\frac{\theta}{2}\right) \\ v &= \frac{K_I\,(1+\upsilon)}{E}\sqrt{\frac{2r}{\pi}}\sin\frac{\theta}{2}\left(\frac{\kappa-1}{2}+\cos^2\frac{\theta}{2}\right) \end{aligned} \tag{2.4}$$

where u and v are the horizontal and vertical components of the displacement field. The parameter κ is equal to $(3-4\upsilon)$ for plane strain and to $(3-\upsilon)/(1+\upsilon)$ for plane stress.

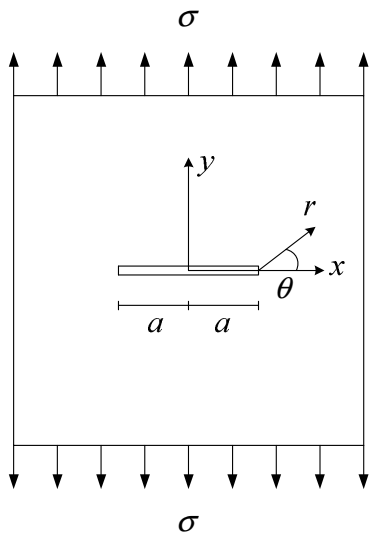

Figure 2.2 *Sharp crack of length 2a in an "infinite" body under Mode I loading.*

The fracture criterion by Irwin (1957) is formulated in terms of the stress intensity factor and introduces a new material parameter, the critical stress intensity factor - for Mode I termed K_{Ic}. In the case where $K_I > K_{Ic}$ uncontrolled crack propagation leading to brittle failure will occur while for $K_I < K_{Ic}$ the crack will not propagate. For the problem studied by Griffith (1921) Irwin's fracture criterion yields:

$$K_{Ic} = \sigma\sqrt{\pi a} \tag{2.5}$$

If Equation 2.2 is substituted into 2.5 the following result is obtained:

$$K_{Ic}^2 = EG_c \tag{2.6}$$

from which it is seen that the global energy balance by Griffith is equivalent to Irwins local stress criteria. Stress intensity factors for a number of problems have been computed and are found in handbooks like Tada et al. (1985).

The Griffith/Irwin theory is based on the assumptions that the stresses and strains at the crack tip tend to infinity and that during the fracture process energy is only dissipated at one point (the crack tip). This contravenes the conditions of the linear elastic theory relating small strains and Hooke's law. Griffith (1921) therefore proposed that the crack faces should be allowed to close smoothly forming a cusp due to large closing forces at the crack tip. However, the first real attempt to include closing forces at the crack tip region within the limits of the elastic theory was made by Barenblatt (1962) (Original paper in Russian in 1959). Barenblatt assumed that smooth closure was achieved due to large stresses with an, in general, unknown distribution acting over a small zone near the crack-tip. The closing forces are also referred to as cohesive forces and the zone along which they are present is refereed to as the cohesive zone, c.f. Figure 2.3, where c indicates the length of the cohesive zone. Even though Barrenblatt's model gives a physical explanation of what is happening in the crack tip, the model essentially corresponds to Griffith's and Irwin's crack models - i.e. Barrenblatt's model reproduces the results of LEFM.

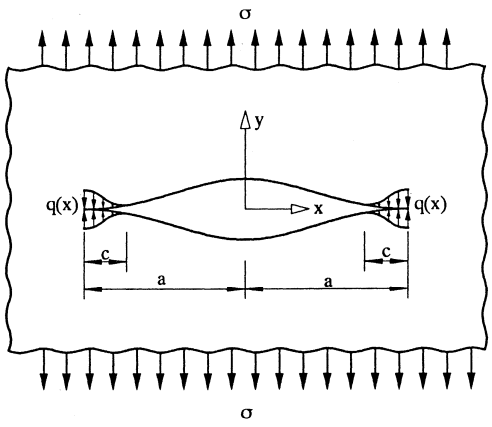

Figure 2.3 *Cohesive crack model due to Barenblatt. The length of the cohesive zone is termed c while $q(x)$ is the distribution of the cohesive stresses. (Karihaloo, 1995)*

Parallel to Barenblatt (1962), Dugdale (1960) proposed a cohesive crack model for a thin elastic-plastic sheet within the concepts of LEFM. In this model the distribution of cohesive stresses is known, and the extend of the cohesive zone is assumed to be within the same order of magnitude as the length of the crack. In Dugdale's model the length

of the cohesive zone is determined by a criterion for smooth crack closure in terms of a criterion for vanishing stress intensity factor at the crack tip. This yields the relation in (2.7) for the length of the cohesive zone, c

$$\frac{c}{a} = 1 - \cos\left(\frac{\pi\sigma}{2\sigma_y}\right) \tag{2.7}$$

The applied stress is termed σ and σ_y is the yield stress of the material. At the crack tip the cohesive stresses are assumed equal to the the yield stress of the thin plate considered. The length of the cohesive zone, c, is normalized by half the initial crack length, cf. Figure 2.3. Also the model of Dugdale essentially reproduces the results of LEFM.

The model of Barrenblatt and Dugdale both assumes smooth closure of the crack and no stress singularity at the crack-tip. In this thesis smooth closing crack models with no stress singularities at the crack-tip will be referred to as cohesive models.

Several attempts to apply LEFM to concrete are found in the literature, for a review see e.g. Karihaloo (1995). In many of those works, experiments revealed that the critical energy release rate or the critical stress intensity factor depends on the specimen size. This contradicts the theory of LEFM in which both measures are postulated to be material parameters. Studies involving measurements of K_{Ic} for mortar and hardened cement paste by e.g. Ohgishi et al. (1986) revealed, that, whereas K_{Ic} was found to be specimen size independent for hardened cement paste, a specimen size dependency was found for mortar. Only if the characteristic structural dimension of a given specimen is much larger than the maximum particle size (45-135 times, c.f. Karihaloo (1995)), the stress intensity factor is found to be independent of the specimen size. Only very few concrete structures have structural dimensions that fulfill this requirement and therefore LEFM is not applicable to most concrete structures. Expressed in other terms, the fracture process zone (FPZ) in concrete is large and therefore LEFM is not applicable to concrete. The length of the FPZ may be estimated applying the relation in Eq. (2.8).

$$l_p \approx \frac{EG_f}{f_t^2} \tag{2.8}$$

Here E is the Young's modulus, G_f the fracture energy and f_t the material tensile strength.

Table 2.1 lists the length of the fracture process zone for various cementitious materials and for glass which was the material Griffith used for his first investigations of fracture mechanics.

Figure 2.4 illustrates the characteristic fracture properties for the three basic types of materials - linear elastic, nonlinear plastic and quasi-brittle. The Griffith (1921) and Irwin (1957) theories are applicable for the brittle fracture in the linear elastic case whereas the cohesive model of Dugdale (1960) may be applied to non-linear plastic fracture when the extended of the non-linear zone is small. Concrete belongs to the group of quasi-brittle materials and in general concrete can not be modeled applying the concepts of linear elastic fracture mechanics.

Table 2.1 *Typical length of fracture process zones for various materials, (Karihaloo, 1995)*

Material	l_p,mm
Glass	10^-6
Cement paste densified by silica fume	1
Hardened cement paste	5-15
Mortar	100-200
High strength concrete (50-100MPa)	150-300
Normal concrete	200-500

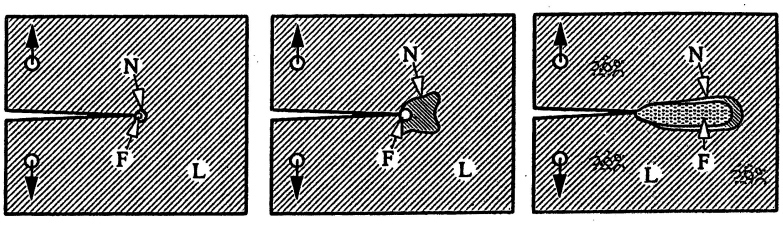

(a) Linear Elastic **(b) Nonlinear plastic** **(c) Nonlinear quasi brittle**

Figure 2.4 *Characteristic features of fracture in (a) a linear elastic material, (b) Nonlinear plastic (ductile metal), (c) a quassi-brittle material. L refers to the linear elastic region, N to the nonlinear region, F to the fracture process zone. (Karihaloo, 1995)*

2.2 Non-linear Fracture Mechanics

According to Table 2.1 the FPZ of cement paste is of the order 1mm while the FPZ of structural concrete is of the order 200-500mm. The aggregates in concrete prevent the brittle failure and a large fracture process zone arises because of progressive softening due to micro cracking and crack bridging. Figure 2.5 shows a typical tensile load-deformation response for concrete and illustrates the tension softening as effect of micro cracking and crack bridging in the FPZ.

2.2.1 The Fictitious Crack Model

One of the most important cohesive crack models is the fictitious crack model (FCM) by Hillerborg et al. (1976). The FCM was the first nonlinear fracture mechanical model for concrete that included the FPZ. Following the concept of the cohesive models of Barenblatt (1962) and Dugdale (1960) a model where closing stresses act near the crack tip and hereby ensure smooth crack closure was proposed. However, Hillerborg et al. (1976) made no assumptions regarding the size of the FPZ and therefore the distribution of the cohesive stresses near the crack tip must be known in the model. In the model the real traction free part of the crack is ending in a fictitious crack, modeling the micro cracked zone ahead of the real traction free crack. The model is known as the fictitious crack model (FCM) and it is illustrated in Figure 2.6. The zone ahead of the fictitious crack tip is assumed to remain elastic.

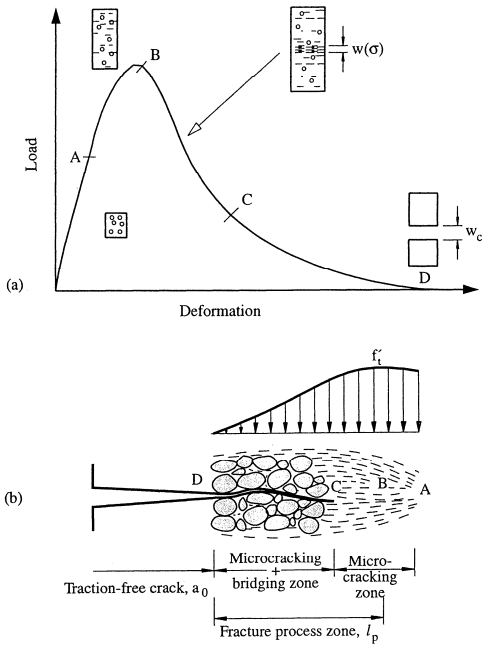

Figure 2.5 *Typical tensile load-deformation response for a concrete specimen (a), and the fracture process zone ahead of the real traction-free crack(b). The fracture process zone extends only over the tension softening region BCD and it can be surrounded by a nonlinear, but not softening region, e.g. the region BA. (Karihaloo, 1995)*

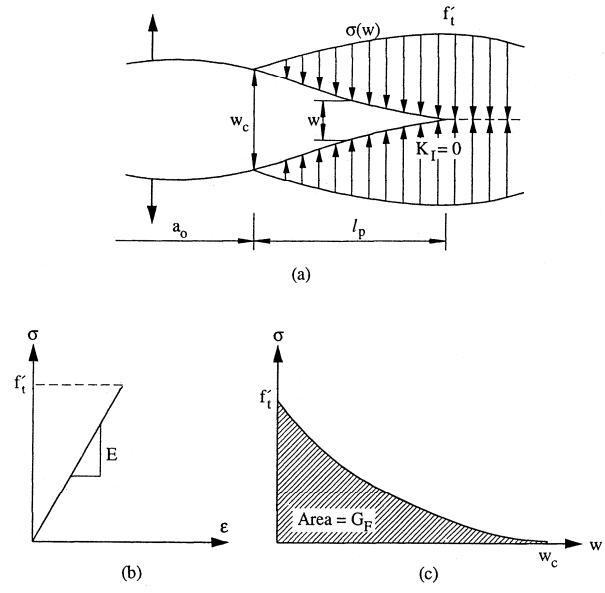

Figure 2.6 *(a) A real traction free crack of length a_0 terminating in a fictitious crack with remaining stress transfer capacity. (b) The material ahead of the fictitious crack is assumed to remain linear elastic. (c) The material within the fracture process zone is softening. (Karihaloo, 1995)*

When the crack propagates, energy is absorbed in the process of overcoming the closing stresses. This amount of energy, the fracture energy, termed G_f, is equal to the area under the tension softening curve, c.f. Figure 2.6.

$$G_f = \int_{f_t}^{0} w(\sigma)d\sigma = \int_{0}^{w_c} \sigma(w)dw \tag{2.9}$$

where f_t is the uniaxial tensile strength of the material (In Figure 2.6 termed $f_t^{'}$), $w(\sigma)$ is the stress-displacement relation $\sigma(w)$ in the softening zone and w_c is the critical crack tip opening at which the crack becomes stress-free.

In the FCM the process of fracture is described through the stress-displacement relationship (also known as the softening curve) $\sigma(w)$ for the softening zone. G_f is equal to the area under the softening curve.

Finally, it shall be emphasized that the fictitious crack model assumes the fracture process zone to be of negligible thickness and hence models the cracks discretely.

2.2.2 The Crack Band Model

Another nonlinear approach for modeling of fracture in concrete is the crack band model (CBM) proposed by Bažant and Cedolin (1979a,b, 1983) and further developed by Bažant and Oh (1983). It is based on the hypothesis "that fracture in a heterogenous material can be modeled as a band of parallel, densely distributed micro-cracks with a blunt front". The application of the CBM to concrete is justified by the crack morphology in concrete with aggregates of various sizes; a crack will not follow a straight line but be tortuous as illustrated in Figure 2.7.

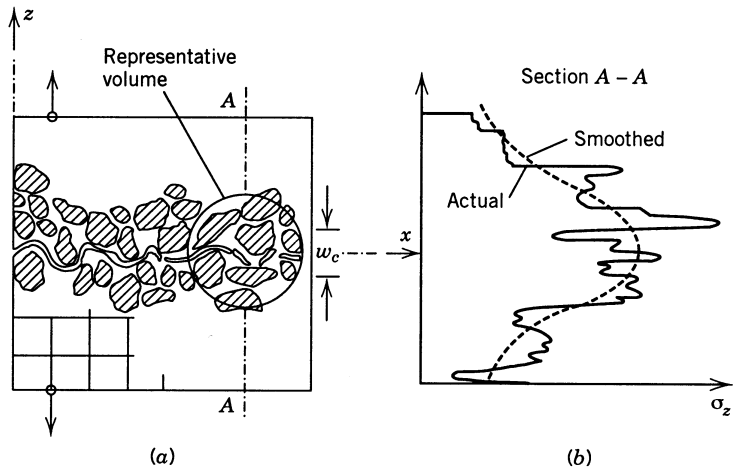

Figure 2.7 *(a) Actual crack morphology, (b) actual stresses and their smoothing for a cross section in the tension softening zone. (Bažant and Oh, 1983)*

In the CBM the fracture process zone is modeled as a band of parallel and uniformly distributed micro-cracks over a given crack band width h_c and the deformation due to cracking is interpreted as an inelastic strain. Stable crack propagation is modeled by progressive micro-cracking within the crack band and the crack propagation is described by a the stress strain relationship c.f. Figure 2.8(b)

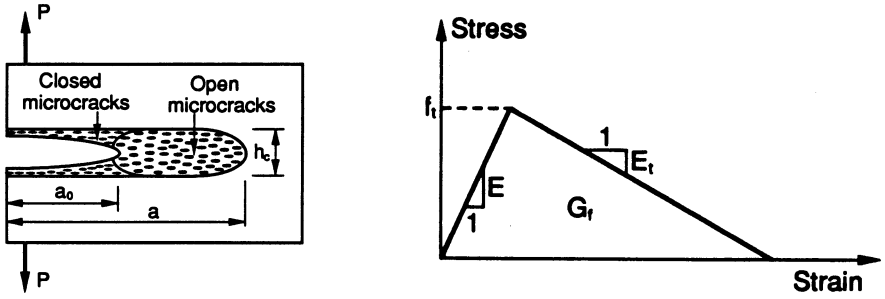

(a) Crack band (b) Stress strain curve

Figure 2.8 *Crack band model for fracture of concrete: (a) microcrack band fracture, (b) stress-strain curve for the microcrack band. (Shah et al., 1995)*

In the CBM the crack opening displacement is equal to the product of the crack band width and the fracture strain. The fracture energy - the energy consumed due to the crack advance per unit area of the crack band - is the product of the area under the stress-strain curve in Figure 2.8(b) and the band width:

$$G_f = h_c \left(1 + \frac{E}{E_t}\right) \frac{f_t'^2}{2E} \tag{2.10}$$

E being the modulus of elasticity, E_t the strain-softening modulus, $f_t^{'}$ the tensile strength of the material and h_c the crack band width.

The ultimate strain at rupture is therefore related to the width of the crack band

$$\varepsilon_u = \frac{2G_f}{f_t' h_c} \tag{2.11}$$

The CBM was proposed with reference to finite element modeling and due to the expression of the displacement jump in terms of inelastic strains it is easily implemented in FE codes. In FE analysis the crack band is related to the element size and Bažant and Oh (1983) recommends h_c to be taken as three times the maximum aggregate size.

2.3 Bridged Crack Models

In a material like concrete the process of fracture may be observed on different scales spanning from the fracture of atomic bonds on the smallest scale to phenomena as aggregate and fiber bridging on the largest scale. Crack propagation in concrete may thus

be seen as a multi-scale problem that requires cohesive laws to be introduced at different length scales. The multi-scale concept of cracking has been discussed by a number of authors - see e.g. Bao and Suo (1992) or Li and Maalej (1996). The concept of a multi-scale cohesive law is illustrated in Figure 2.9 (Stang et al., 2006b). On each scale the cohesive law represents a characteristic mechanism reflecting the average nature of the bond including the presence of defects: atomic bond seperation on the smallest scale, separation of grain interfaces, micro-crack ligament stress-transfer, and aggregate or fibre bridging at the largest scale. The concept that a cohesive law introduces a length scale through a characteristic crack opening w_c was proposed by Needlemann (1990).

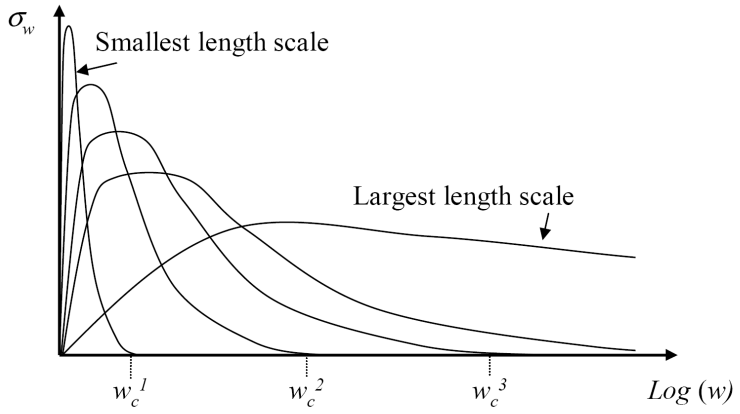

Figure 2.9 *Schematic illustration of a multi-scale cohesive law. Note that the x-axis is logarithmic. (Stang et al., 2006b)*

I principle all the cohesive laws would have to be considered in an analysis, however, such a level of detailing in e.g. a finite element analysis would require unreasonable fine meshes. In bridged crack models the energy corresponding to length scales smaller than a certain scale w_c^i is lumped into a single point corresponding to applying LEFM to scales smaller than w_c^i and only applying the cohesive law to the larger length scales. The concept of a bridge crack is depicted in Figure 2.10

The criterion for crack propagation for bridged crack models is expressed in terms of a stress intensity factor criterion: a crack propagates in Mode I when $K_I = K_{Ic}$ where

$$K_{Ic} = \sqrt{E' G_F^i} \tag{2.12}$$

and

$$G_F^i = \int_0^{w_c^i} \sigma_w(w)\, dw \tag{2.13}$$

Bridged crack models have been applied to modeling of crack propagation in various reinforced materials and was recently also applied for modeling of crack propagation in cementitious composites by Ferro (2002).

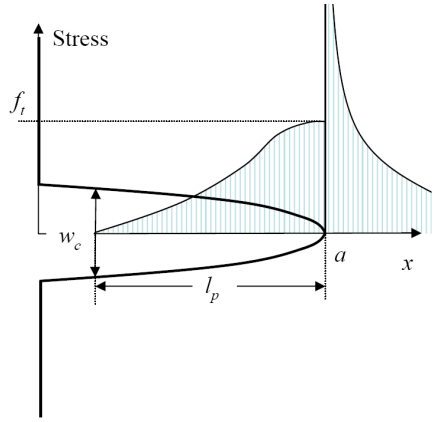

Figure 2.10 *Bridged crack model. (Stang et al., 2006b)*

According to Cox and Marshall (1991) cohesive crack models with smooth crack closure, i.e. vanishing stress intensity factor at the crack-tip, may be considered as a special case of the general bridged crack model. Whether a bridged crack model may be approximated with a cohesive crack model depends on the ratio between the fracture energy associated with the crack tip and the fracture energy associated with the cohesive law. In Stang et al. (2006b) the applicability of bridged crack models versus the FCM for modeling of concrete fracture was investigated. Based on a semi-analytic model it was found that the FCM gives a good description of fracture in concrete.

2.4 Determination of Fracture Mechanical Parameters

From the above discussion of models for crack propagation it appears that the FCM proposed by Hillerborg et al. (1976) possess the required properties for modeling of discrete crack growth in concrete. In the models developed later in this thesis the FCM will be applied, however, before applying the FCM, it is relevant to shortly discuss how the required fracture mechanical parameters are obtained from experiments.

The FCM requires the stress-displacement relation $\sigma(w)$ in the softening zone to be known. In the work by Østergaard (2003) fracture mechanical test methods for the determination of fracture mechanical parameters were investigated in details. This study illustrates that an uniaxial tension test applying non-rotating boundary plates is the direct method to obtain the softening curve. As alternative to the uniaxial tension test the fracture mechanical parameters may be be determined either by the notched three point bending test (see e.g. RILEM (1985)) or by the wedge splitting test, originally proposed by Linsbauer and Tschegg (1986) and further developed by Brühwiler and Wittmann (1990).

Whereas the uniaxial tension test is the direct way to the fracture mechanical parame-

ters, the three point bending test and the wedge splitting test requires inverse analysis to determine the fracture mechanical properties. An effective procedure for inverse analysis was proposed by Østergaard (2003). In this case the inverse analysis is based on the hinge model proposed by Olesen (2001). For a more general review of methods for inverse analysis reference is made to Østergaard (2003).

Focus in this thesis is on the modeling of Mode I fracture and hence this introduction to fracture mechanics has been focused on Mode I. However, the model that is proposed for modeling of fracture in concrete is general with respect to handling of different modes of fracture including mixed mode fracture. Determination of mixed mode constitutive parameters is, however, not a trivial task and considerable efforts are focused on this task in the concrete research community. Published works regarding mixed mode parameters for concrete includes the works by Hassanzadeh (1991) and Nooru-Mohamed (1992). Mixed-mode constitutive models were also considered by Carol et al. (1997, 2001), who proposed the concept of a shrinking crack surface. This mixed-mode model was applied by Gálvez et al. (2002) in their study of mixed-mode modeling of fracture in concrete. Walter and Olesen (2006) proposed a mixed-mode model for modeling of the interface between concrete and steel.

Chapter 3

FE Modeling of Crack Growth in Concrete

In general the basic objective of a computational analysis of a reinforced concrete structure is to predict not only the load deformation response at any load level up to failure of the structure but also the formation of cracks. To handle the process of cracking the method applied must be able to:

- ◇ Identify locations where cracks will initiate.
- ◇ Model crack propagation.
- ◇ Model development in crack widths.
- ◇ Model crack coalescence and hereby localization phenomena.
- ◇ Model the process all the way to rupture.

As indicated in the previous sections the application of non-linear fracture mechanics may contribute to the fulfillment of this goal.

In this chapter a brief review will be given of the most popular techniques available for computational modeling of localized crack propagation in concrete within the framework of finite element modeling. Methods like the element free Galerkin method (Belytschko et al., 1996), which is capable of modeling fracture but does not fit within the framework of standard FE codes, will not be treated. For a more thorough review also including a thorough introduction to damage mechanics, which is outside the scoop of the present thesis, reference is made to e.g. Jirásek (2004).

3.1 Interface Elements

When Hillerborg et al. (1976) proposed the concept of the fictitious crack model, they also illustrated its applicability to finite elements by modeling of crack propagation in a concrete beam subjected to pure bending. The symmetry of the problem was utilized and

only half the beam was considered. The crack was propagated node by node along the symmetry line. Corresponding values of crack depth and the moment yielding stresses equal to the tensile stresses in the node at the crack tip was computed. This modeling strategy may be seen as an early application of the, today well known, interface technique that has been adopted in several of the commercial FE programmes. Among others ABAQUS (2004b) and DIANA (Diana User Manual, 2003a) have a number of cohesive interface elements based on traction-separation descriptions for modeling of cohesive crack growth. Figure 3.1 depicts the configuration of a standard 3-node two dimensional interface element where σ and τ are the normal, respectively, the shear stresses acting across the interface. δ_n and δ_t are the corresponding crack openings. As indicated in the figure the thickness of the interface element is often set to zero and a large dummy stiffness is applied for the interface until the crack opens.

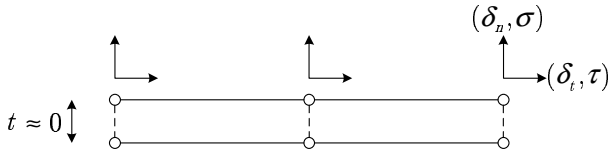

Figure 3.1 *Configuration of standard 2D interface element*

The relationship between the gradients of stress and crack opening in the normal and tangential direction is given by:

$$\begin{bmatrix} \dot{\sigma} \\ \dot{\tau} \end{bmatrix} = \begin{bmatrix} D_{11} & D_{12} \\ D_{21} & D_{22} \end{bmatrix} \begin{bmatrix} \dot{\delta}_n \\ \dot{\delta}_t \end{bmatrix} \tag{3.1}$$

Regarding modeling of crack growth in concrete, interface elements have been used in a number of applications, e.g. Rots (1988) and Stankowski et al. (1993). More recent examples include 3D modeling of bond between reinforcement and concrete in frame corners (Lundgren, 1999) and axisymmetric modeling of pull out of reinforcement in early age concrete (Østergaard, 2003). An other example is given in Walter (2005) where the bond between steel and cement based overlays for strengthening of orthotropic steel bridge decks was modeled applying interface elements capable of handling mixed mode cohesive cracking. Interface elements were also applied for fiber pull out of fibers in "Engineered Cementitious Composites" by Dick-Nielsen et al. (2006). Also when notched specimens subjected to symmetric loading are considered, e.g. in conjunction with fracture mechanical experiments, interface elements may be applied - examples of this will be given later in this thesis.

If the crack path is not known beforehand interface elements have been placed along all element boundaries in a given mesh to allow propagation of cracks along different paths. This technique poses improved capabilities for modeling of unknown crack path but unless very fine FE meshes are considered the results of the analysis will be locked to the chosen

mesh in the sense that only predefined crack paths may be modeled. Examples of this technique includes a micro-mechanical analysis of concrete performed by Carol et al. (2001). An alternative approach to the modeling of an a-priori unknown crack path is the coupling of interface elements with methods for remeshing where the mesh is updated to conform with the propagating crack. Recent examples of combined use of interface elements and remeshing for modeling of crack propagation in concrete includes the works of Prasad and Krishnamoorthy (2002) and Yang and Chen (2004, 2005). Remeshing is, however, computationally costly and hence interface elements are not preferable for modeling of fracture in real RC structures.

3.2 Smeared Crack Models

Another fairly widespread group of models in commercial finite element programs is the group of smeared models - see e.g. ABAQUS (2004a) or (Diana User Manual, 2003b). In the smeared approach the displacement jump across a crack is not modeled explicitly in terms of a discontinuity in the displacement field for the cracked element. One "model" crack in the smeared approach does not necessarily model one single physical crack but may model the average effect of micro-cracks in a given volume surrounding a given material point. This property makes it difficult to interpret the outcome of a smeared analysis with respect to estimating e.g. crack widths. The smeared approach follows the concept applied in modeling of plasticity and the total strain is, c.f. Eq. (3.2), decomposed into an elastic part, ε_e, modeling the deformation of the uncracked material and an inelastic part, ε_{cr}, modeling the contribution due to cracking. The inelastic part is also refereed to as "the cracking strain"

$$\varepsilon = \varepsilon_e + \varepsilon_{cr} \tag{3.2}$$

In the discrete approach, applied for e.g. interface elements, the traction-separation relation in terms of the softening curve (see e.g. Figure 2.6(c)) is applied directly. In the smeared approach the traction-separation relation has to be transformed into a stress-strain relation. The cracking strain, ε_{cr}, is set equal to the crack opening, w, divided by the width of the localization band, h. In a simple model h may be set equal to the width of the finite elements in which cracking localizes:

$$\varepsilon_{cr} = \frac{w}{h} \tag{3.3}$$

Assuming a local coordinate system, (m, n), aligned with the crack, n being normal to the crack, stresses and strains are related through a function f. Considering pure Mode I the relation for the normal traction, σ^n, and the normal strain,ε^n, across the element is:

$$\sigma^n = f\left(\varepsilon_{cr}^n\right) \tag{3.4}$$

Utilizing the relation between crack opening and band width, the stresses may be expressed in terms of the crack opening, w:

$$f\left(\varepsilon_{cr}^n\right) \quad = \quad f_w\left(h\varepsilon_{cr}^n\right)$$

$$\sigma^n = f_w(w) \tag{3.5}$$

Where f_w is the softening law, previously termed $\sigma(w)$, that may be obtained by fitting of experiments. A number of sophisticated models have been proposed for fitting of the softening curve for concrete - se e.g. Hordijk (1991) or Østergaard (2003). However, often an exponential, bilinear or linear softening law is applied in computations.

The first examples of modeling of cracking in concrete applying the smeared approach dates back to the sixties (Rashid, 1968) - i.e. before Hillerborg et al. (1976) proposed the fictitious crack model and Bažant and Oh (1983) proposed the concept of a crack band. In this early application of the smeared approach the stiffness orthogonal to the crack was set to zero when cracking occurred - i.e. the effect of softening was not modeled and no post-peak response was obtained in the numerical computations. However, the crack band model by Bažant and Oh (1983) introduced in Chapter 2 is capable of modeling various softening laws and hence may model the post peak response too.

In Bažant and Oh (1983) the crack direction is assumed to remain fixed i.e. it is assumed that all micro cracks referring to a given material point have almost the same orientation. In general the crack in a fixed model transfers shear tractions that produce relative sliding of the crack faces and in simple models the shear traction is taken as proportional to the shear crack strain. Introducing the so-called shear retention factor, β, the proportionality factor is βG, where G is the shear modulus of elasticity and $\beta < 1$. In the later approach by de Borst and Nauta (1985) the fixed crack formulation was generalized to a multiple crack model, allowing several model cracks with different orientations, to be introduced at the same material point. Another way of taking into account changes in the crack pattern due to changing stresses is the rotating crack concept (Gupta and Akbar, 1984). In this model the possible existence of cracks with various orientations is taken into account by continuously adjusting the orientation of a single crack.

Rots (1988) performed a thorough analysis of smeared models for crack growth in concrete and observed that the models suffer from stress locking in terms of spurious stress transfer across widely open cracks. For fixed crack models applying a nonzero shear retention factor, locking is primarily due to shear stresses generated by rotation of the principal stress direction after crack initiation. For the rotating crack models the spurious stress transfer is due to a poor kinematic representation of the discontinuous displacement field around the macroscopic crack, c.f. Jirásek and Zimmermann (1998b). Figure 3.2 depicts an example of stress locking in a notched three point beam bending specimen modeled applying CST elements and a rotating smeared crack model (from Jirásek (2004)). Whereas good results are obtained for the pre-peak response the post-peak response is incorrect. When the crack has propagated all the way to the top of the beam the model predicts a significant non-negligible load carrying capacity.

To avoid the locking problems Jirásek and Zimmermann (1998b) proposed that the rotating crack model was combined with a damage mechanics model through a transition

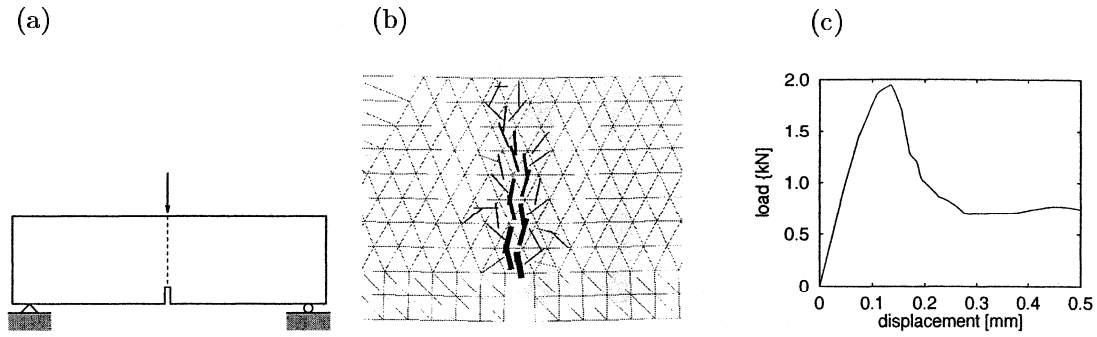

Figure 3.2 *Locking in modeling of fracture in three point bending applying smeared rotating crack model. (a) Geometry and loading, (b) fracture pattern, (c) load-displacement diagram. From (Jirásek, 2004)*

to scalar damage, whereby the model becomes capable of modeling the entire load deformation response in a correct way. However, locking is not the only problem related to the smeared models. Due to the relation between element size and crack bandwidth the method may show mesh dependency. Instability due to the appearance of spurious kinematic modes was also observed by Rots (1988). Furthermore the non-continuous modeling of the crack path as depicted in Figure 3.2 (b) is also counting against the application of smeared models when the aim is to model localized crack growth.

3.3 Embedded Crack Models

A more recent approach to handle discontinuities within the framework of finite elements is the concept of strain or displacement discontinuities embedded into standard finite elements. By embedding the discontinuity the kinematic representation of highly localized strains is improved and stress locking, as observed in smeared models, may be avoided. Embedded crack models may be seen as a method that combines the strongholds of the traditional discrete models and the smeared concept. This section focuses on the concepts of the embedded models more than the mathematical formulations behind them. For a more extensive review of embedded crack models reference is made to e.g. Jirásek (2000) or Jirásek (2004).

In most of the embedded crack models the parameters representing the discontinuity are eliminated by condensation at the element level. Therefore, the enhancements of the strain or displacement fields in embedded models are element local and do not have to be treated as global unknowns like other degrees of freedom e.g. the nodal displacements.

Embedded crack models which describe a jump in the strain field, while the displacement field remains continuous are referred to as weak discontinuity models whereas models capable of modeling a jump in the displacement field are referred to as strong discontinuity models. Figure 3.3 depicts two types of weak discontinuities and one example of a strong discontinuity.

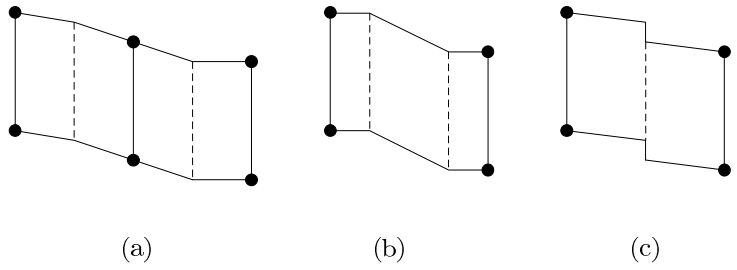

Figure 3.3 *Elements with embedded discontinuities: (a) Elements with one weak discontinuity (b) Element with two weak discontinuities (c) Element with one strong discontinuity. After Jirásek (2000)*

In the pioneering work of Ortiz et al. (1987) the resolution of shear bands was improved by enhancing the strain field in quadrilateral elements such that a discontinuity in the strain field could be captured - i.e. the discontinuity was modeled in a weak sense. Each element was capable of holding one weak discontinuity line and hence two elements were required to model the shear band - c.f. Figure 3.3 (a). The applied enhancement was based on the individual approximation of stress and strains following the Hellinger-Reissner principle (see e.g. Zienkiewicz and Taylor (2000)). The requirement for two elements to model the entire localization band, however, makes the width of the band element size dependent.

The weak discontinuity approach was improved by Belytschko et al. (1988) who proposed two weak discontinuities to be included in one element whereby one element became capable of modeling the full width of the localization band, c.f. Figure 3.3(b). By doing so the element size dependency of the model by Ortiz et al. (1987) was further reduced. In the proposed model the width of the localization band is not determined by the computations but is assumed a material parameter that has to be specified. The enhancement in Belytschko et al. (1988) is based on the three field Hu-Washizu variational principle (see e.g. Zienkiewicz and Taylor (2000)) in which the displacement field, the strain field and the stress field all are assumed independent. A number of improvements and extensions of the applicability for the element holding two weak discontinuity lines were proposed by the group of Belytschko, however, for further details and reference regarding those improvements reference is made to Jirásek (2000). In the context of modeling of fracture in concrete Sluys and Berends (1998) applied elements with a band of localized strains similar to the concept suggested by Belytschko et al. (1988).

Among the first to consider a strong discontinuity to be embedded in an element was Dvorkin et al. (1990) who considered cohesive cracking in concrete. However, the first fully consistent variational derivation of an element with a strong discontinuity was carried out by Lotfi and Shing (1995) who also considered the cracking of concrete. They applied the Hu-Washizu principle and added a term representing the work of the cohesive tractions and presented their model in the assumed strain concept (see e.g. Zienkiewicz and Taylor (2000)).

In the above short review, the different approaches have been categorized due to how the discontinuity is modeled in terms of one or two weak discontinuity lines or one strong discontinuity line within an element. Jirásek (2000) categorizes the elements due to how the statics and the kinematics are modeled. Elements which satisfy the traction continuity condition but do not model the kinematics of a strain or displacement discontinuity properly are said to be formulated in a *statically optimal symmetric* (SOS) formulation. The major drawback of the SOS models is that in the general case the SOS formulation cannot reproduce the full stress relaxation around a widely open crack. SOS models therefore leads to spurious stress transfer. The elements suggested by Belytschko et al. (1988) and Sluys and Berends (1998), both being based on weak discontinuities belong to the group of SOS elements. However, also a number of elements with strong discontinuities, belong to the group of SOS elements - se e.g. Jirásek (2000). Elements that are able to reproduce the kinematics of the discontinuity but lead to an awkward approximation of the traction continuity condition - i.e. the relationship between stresses in the bulk of the element and the tractions across the discontinuity line - are referred to as belonging to the *kinematically optimal symmetric* (KOS) formulation. In this formulation spurious stress transfer is eliminated. The element of Lotfi and Shing (1995) belongs to the KOS formulation. The third and last group of elements is the one that includes elements that are capable of representing both the kinematic and the static aspect properly and those elements are formulated within the *statically and kinematically optimal nonsymmetric* (SKON) formulation. The formulation is refereed to as being nonsymmetric due to a nonsymmetric tangential stiffness matrix. The SKON approach is capable of properly representing complete separation at late stages of fracture without spurious stress transfer. Elements belonging to the SKON formulation are based on the strong discontinuity approach and examples of SKON elements are the ones by Dvorkin et al. (1990) and Oliver (1996). In the SKON formulation there is no requirement for specifying the length of the localization band. This is favorable because in general, it is not an objective quantity but depends of the positioning of the discontinuity in the element.

A more recent application of embedded crack models for modeling of fracture in concrete is by Jirásek and Zimmermann (2001). In this work an embedded crack model in the SKON formulation is combined with smeared cracking. Transition from a smeared crack to an embedded crack is implemented to stabilize the crack pattern and good results are obtained for a number of benchmark tests such as the notched three point bending beam, the notched four point shear beam and crack propagation in a concrete gravity dam.

From the review above it is evident that embedded crack models exhibit better performance than the previous discussed approaches for modeling of fracture - interface elements and the smeared approach. However, the drawbacks for the embedded models are that the displacement approximation is nonconforming, strains in the separated parts of an element remain partially coupled and in the case of the favorable SKON formulations the stiffness matrix is nonsymmetric. Further comments will be given regarding the two first drawbacks when comparing the embedded concept to the XFEM in the following section.

3.4 The eXtended Finite Element Method

In this section a short introduction will be given to the eXtended Finite Element Method, XFEM, focusing on the concepts for the method and the historical development. XFEM is today probably the most widely used expression for this group of models, however, in the literature similar models may also be found under expressions like Generalized Finite Element (GFEM) or Partition of Unity Methods (PUM).

XFEM and embedded crack models (ECM) may at first be seen as fairly similar, they are, however, conceptually quite different and the differences between the two models will be pointed out through some illustrative conceptual examples.

In the XFEM proposed by Belytschko and Black (1999) and Moës et al. (1999) discontinuities may propagate independently of the mesh. Like in the ECM models, XFEM elements crossed by a discontinuity are enriched whereby the elements become capable of describing the discontinuity. In the XFEM the displacement field consists of two parts, a continuous and a discontinuous part. The continuous part is the standard displacement field corresponding to the situation without any cracks. The discontinuous displacement field is based on local partitions of unity (Mellenk and Babuška, 1996) and enables the element to include a discontinuity, in the present case a cohesive crack. In general the enriched displacement approximation takes the form:

$$u(x) = \sum_{i \in I} N_i(x) u_i + \sum_{j \in E} N_j(x) \psi(x) e_j \tag{3.6}$$

where I is the set of nodes in the system, $N_i(x)$ is the shape function at node i and u_i are the nodal displacements. E is the set of enriched nodes, $N_j(x)$ is the nodal shape functions for the enriched nodes, e_j are additional degrees of freedom and $\psi(x)$ is the enrichment function.

The following one dimensional example from Jirásek and Belytschko (2002) illustrates the difference between the discontinuous approximation applied in the ECM and in the XFEM. A one dimensional body is separated into the two domains Ω_- and Ω_+ by the discontinuity point Γ_d, c.f. Figure 3.4. Considering an element with an embedded discontinuity based on the enhanced assumed strain method (EED-EAS) the enhancement function $G(x)$ is given in terms of the Heaviside step function $H(x)$ and the standard nodal shape functions N_i associated with node I:

$$G(x) = H(x) - \sum_{x_i \in \Omega_+} N_i(x) \tag{3.7}$$

where the Heaviside step function is equal to 1 in Ω_+ and 0 in Ω_-. The coordinate of node I is termed x_i.

The enrichment in Eq. (3.7) is illustrated in Figure 3.4(a). From the Figure it may be noticed that one additional degree of freedom e is added. e is the displacement jump while the other degrees of freedom are the usual nodal displacements.

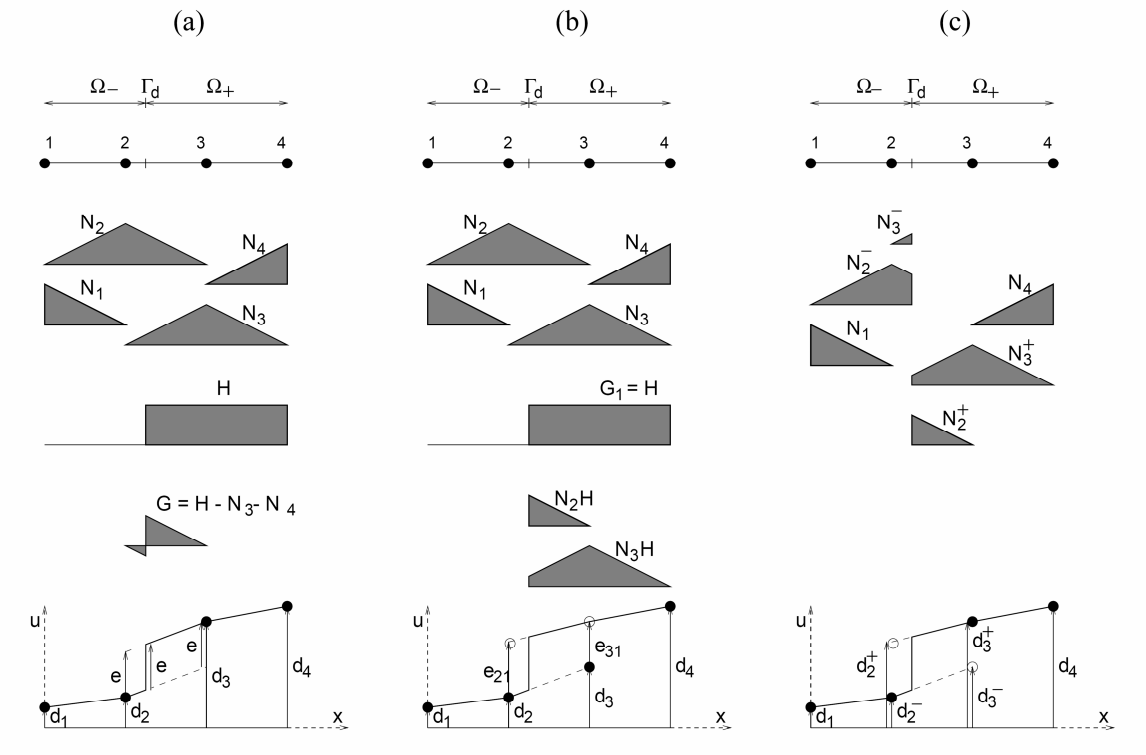

Figure 3.4 *Discontinuous approximation in one dimension: (a)Elements with embedded discontinuity, (b) Extended finite elements, (c) Extended finite elements with transformed basis. (Jirásek and Belytschko, 2002).*

Applying the same Heaviside step function for the enrichment in the XFEM formulation the enriched displacement approximation in Eq. (3.6) takes the form:

$$u(x) = \sum_{i \in I} N_i(x) u_i + \sum_{x_i \in \Omega_+} H N_i(x) e_j \tag{3.8}$$

The XFEM enrichment is depicted in Figure 3.4 (b). Whereas there was only one additional degree of freedom in the EED-EAS enrichment two additional degrees of freedom, e_{21} and e_{31}, appears in the XFEM enrichment. The physical meaning of e_{21} and e_{31} is depicted in the bottom part of the figure. Figure 3.4(c) illustrates how a set of shape functions can be constructed by linear transformation of the basis for which the corresponding degrees of freedom d_1, d_2^-, d_3^-, d_2^+, d_3^+ and d_4 directly have the meaning of nodal displacements on the right respectively the left side of the discontinuity.

In the one dimensional case discussed above and depicted in Figure 3.4 the EED-EAS enrichment in Eq. (3.7) is continuous and vanishing outside the element crossed by the discontinuity. However, in the general case the EED-EAS enrichment is discontinuous not only at Γ_d but also at the element boundaries. Therefore the EED-EAS enrichment is nonconforming and compatibility of the strain field is only enforced in a week sense. The XFEM enrichment in Eq. (3.8) is only discontinuous at Γ_d and continuous everywhere else, also in the multi-dimensional case ensuring conformity and compatibility.

The physical interpretation of the additional degree of freedom, e, in the EED-EAS formulation is that the EED-EAS formulation can reproduce an arbitrary displacement jump at a given discontinuity point but that the strains on each side of the discontinuity must remain the same in the element split by the discontinuity. The presence of two additional degrees of freedom, e_{21} and e_{31}, in the XFEM formulation on the other hand can be interpreted as an approximation of two completely independent meshes with no kinematic constraints - the only interaction takes places through the applied traction-separation law.

Jirásek and Belytschko (2002) illustrated the difference between the kinematic capabilities of the EED-EAS and the XFEM by considering the splitting of a rectangular piece of material into two parts by a vertical stress-free crack as illustrated in the top row of Figure 3.5. First the separated parts are subjected to a relative motion of the two parts parallel to the crack, c.f. the middle row, and then the right part is compressed in the direction, parallel to the crack, c.f. the lower row. Figure 3.5 (a) depicts the actual physical process while Figure 3.5(b) shows the approximation obtained with a standard finite element with a bilinear interpolation for the displacement field and a smeared representation of fracture. The outcome of the relative motion is normal and shear strains, and the force imposed on the right part influences the entire element. Figure 3.5(c) depicts the approximation achieved applying an element with an embedded discontinuity. The element reproduces the rigid body separation nicely but forces are transmitted from the right to the left part when compressing the right part. This is due to the strain in the bulk material being interpolated in a continuous way. The XFEM approximation is illustrated in 3.5(d) by interpretation of the method in terms of two independent overlayed elements. The two independent elements are plotted by dotted and dashed lines respectively. Solid circles mark physical nodes while empty circles mark virtual nodes corresponding to a continuous extension of the displacement field beyond the discontinuity line. The "dotted" element represents the displacement interpolation to the left of the crack while the "dashed" element is valid to the right of the crack. In 3.5(e) the fully drawn lines illustrate the "final" XFEM approximation. As seen from Figure 3.5(e) the XFEM approximation reproduces both the separation and the independent deformation of one part exactly. From the example above the superior kinematic properties of the XFEM element is evident.

The introduction of extra global degrees of freedom at system level in the XFEM makes the implementation efforts of XFEM greater than the effort required to implement the EED-EAS element holding only additional degrees of freedom, that may be eliminated on the element level. The numerical robustness is, however, better for the XFEM element than for the EED-EAS element for which very strict requirements for the shape of the

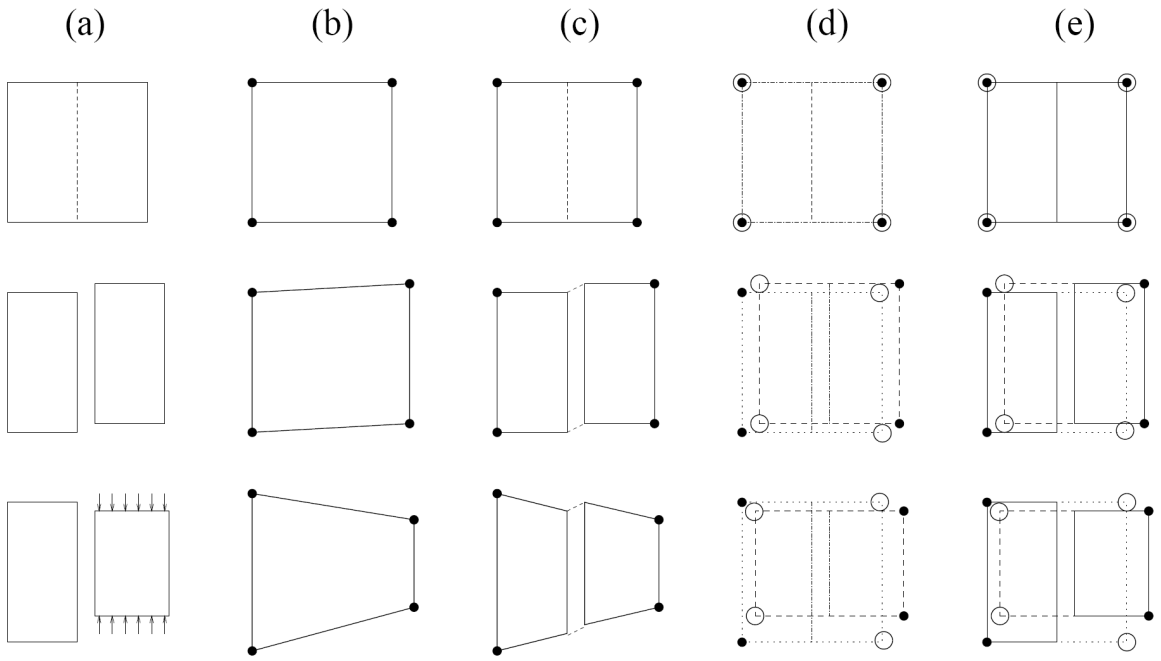

Figure 3.5 *Separation test: (a)Real body split into two independent parts (b) standard finite element with smeared representation of fracture (c) element with embedded discontinuity, (d-e) Extended finite element. The XFEM can be interpreted in terms of two independent overlayed elements. The two independent elements are plotted by dotted and dashed lines respectively. Solid circles mark physical nodes while empty circles mark virtual nodes corresponding to a continuous extension of the displacement field beyond the discontinuity line. The "dotted" element represents the displacement interpolation to the left of the crack while the "dashed" element is valid to the right of the crack. The fully drawn lines in (e) illustrate the "final" XFEM approximation (Jirásek and Belytschko, 2002).*

elements have to be fulfilled to avoid numerical problems. The numerical problems for the EED-EAS elements are related to the requirements for uniqueness of the rate problem and are explained in more details in (Jirásek and Belytschko, 2002).

From the discussion above some of the important differences between embedded crack models and the eXtended Finite Element Method have been highlighted. Table 3.1 summarizes the comparison of the EED-EAS element and the XFEM element.

Table 3.1 *Comparison of properties for embedded crack model and XFEM model. After Jirásek and Belytschko (2002)*

	EED-EAS	XFEM
Added degrees of freedom	internal	global
associated with	elements	nodes
Displacement approximation	nonconforming	conforming
Stiffness matrix	always nonsymmetric	can be symmetric
Strains in separated parts	partially coupled	independent
Implementation effort	smaller	greater
Numerical robustness	limited	good

From the review of computational techniques the XFEM appears to be a preferable choice for modeling of fracture in concrete. XFEM has already been applied to different problems within the area of fracture mechanics. While it was first developed for linear elastic fracture mechanics se e.g. Belytschko and Black (1999); Moës et al. (1999); Stolarska et al. (2001) it has now been applied to different problems. Cohesive cracking has been considered by a number of authors, e.g. Wells and Sluys (2001); Moës and Belytschko (2002); Zi and Belytschko (2003); Asferg et al. (2007b,a). Arbitrary branched and intersecting cracks were considered by Daux et al. (2000), while three dimensional crack propagation was treated by Sukumar et al. (2000) and Areias and Belytschko (2005a). The applicability of the XFEM for cracks in shells was illustrated by Areias and Belytschko (2005b). For an overview of the earlier works regarding the XFEM, reference is also made to Karihaloo and Xiao (2002).

In the following chapters a number of the central aspects of the XFEM will be discussed in more detail in connection with the development of XFEM elements for modeling of cohesive crack growth in concrete.

Chapter 4

Fully Cracked XFEM Elements

In Chapter 2 the theory of fracture mechanics was discussed in the context of modeling of fracture in concrete and it appeared that the fictitious crack model by Hillerborg et al. (1976) was an appropriate model for fracture of concrete. The outcome of the discussion of computational methods for modeling of fracture in concrete in Chapter 3 was that the XFEM is a preferable choice for modeling of localized, mesh independent fracture. This chapter deals with the modeling of fracture in concrete applying fully cracked XFEM elements - i.e. elements that are capable of being either uncracked or fully cracked. The fictitious crack model is applied for the constitutive relation in the crack. Focus will be on the chosen enrichment scheme, the variational formulation for the XFEM element and aspects of implementation in relation to crack propagation. The suggested XFEM scheme fits within the context of standard FE code and it is applied to the 3-node constant strain triangle (CST) and the 6-node linear strain triangle element (LST). The performance of the scheme is illustrated by modeling of fracture in concrete benchmark tests such as the three point beam bending test (TPBT) and the four point shear beam test (FPSB). For all details regarding the implementation and the performed tests, reference is made to the appended *Paper I*.

4.1 Enrichment of The Displacement Field

4.1.1 Enrichment Strategies

Considering linear elastic fracture mechanics (Belytschko and Black, 1999; Moës et al., 1999; Stolarska et al., 2001) nodes in elements, fully cut by the discontinuity, were enriched by the step function. The tip element (the element holding the crack tip is referred to as the tip element) was enriched with an asymptotic field. In cohesive crack models, cohesive stresses act near the crack tip and it is assumed that no singularity is present at the crack tip. However, considering partly cracked elements for cohesive crack growth Moës and Belytschko (2002) enriched the crack tip element with a set of nonsingular branch functions to model the displacement field around the tip of the discontinuity. Wells and Sluys (2001) considered fully cracked elements and applied the Heaviside step function as the only enrichment of nodes with a supporting side cut by the discontinuity. Applying the Heaviside step function as in Wells and Sluys (2001) the nodal enrichment influences the displacement field, not only in the elements cut by the discontinuity, but

also in the elements sharing the enriched nodes. In this case the enrichments typically influences all elements in a band three elements wide along the line of the discontinuity. Zi and Belytschko (2003) proposed an enrichment of the crack tip element for the case of partly cracked elements in which the shifted sign function was applied. The application of the shifted sign function to a 1D example is illustrated in Figure 4.1(b). As shown the enrichment only influences elements cut by the discontinuity. In (Mergheim et al., 2005) a dual node strategy was applied and the displacement field was not decomposed into a continuous and discontinuous part in the same way as in the "standard" XFEM. However, even though the basis for the shape functions is different, the scheme in Mergheim et al. (2005) is able to model the same variation in the displacement field as in the scheme by Zi and Belytschko (2003). The enrichment as applied by Mergheim et al. (2005) is illustrated in Figure 4.1(c). Although the authors in Mergheim et al. (2005) distinct their approach from the XFEM it is essentially based on the same concept.

In *Paper I* a direct XFEM scheme for modeling of cohesive crack growth is developed using the Heaviside step function and limiting the discontinuous displacement field to elements cut by the crack. The XFEM formulation follows the concepts proposed in Asferg et al. (2004). The Heaviside step function, H, is applied as the only enrichment of elements cut by the discontinuity, c.f. Figure 4.1(a).

Figure 4.1 illustrates how a displacement jump of a magnitude of one may be modeled applying the three different approaches discussed above. For the present approach and the approach by Zi and Belytschko (2003) the two upper sketches illustrate the continuous displacement fields for node 1, respectively node 2, while sketch 3 and 4 illustrate the discontinuous displacement fields. Regarding the approach by Mergheim et al. (2005) the two upper figures illustrate the displacement field for the two "original" nodes 1 and 2, while figure 3 and 4 depict the displacement fields for the dual nodes 1^* and 2^*. Finally, the lower sketch in each row depicts an example of a displacement field containing a jump of the magnitude of one. From Figure 4.1 it is evident that the difference between the three approaches is a question about the applied basis for modeling the displacement field. Compared to the enrichment by the shifted sign function in Zi and Belytschko (2003) and the enrichment in Mergheim et al. (2005), the proposed enrichment is more straight forward, but essentially the three formulations model the same discontinuous field.

4.1.2 The Applied Enrichment

As discussed in Section 3.4 and illustrated in Figure 4.1 the displacement field for a cracked element can be formulated as the sum of the continuous and the discontinuous displacement field, c.f. Eq. (3.6). The enriched displacement field applied in the present work is given by:

$$\mathbf{u}\left(x,y\right) = \mathbf{N}^c(x,y)\mathbf{v}^c + \mathbf{N}^d(x,y)\mathbf{v}^d \tag{4.1}$$

where $\mathbf{v}^c$ and $\mathbf{v}^d$ are the degree of freedom (dof) vectors while $\mathbf{N}^c$ and $\mathbf{N}^d$ are the interpolation matrices. The superscript c refers to continuous and d to discontinuous.

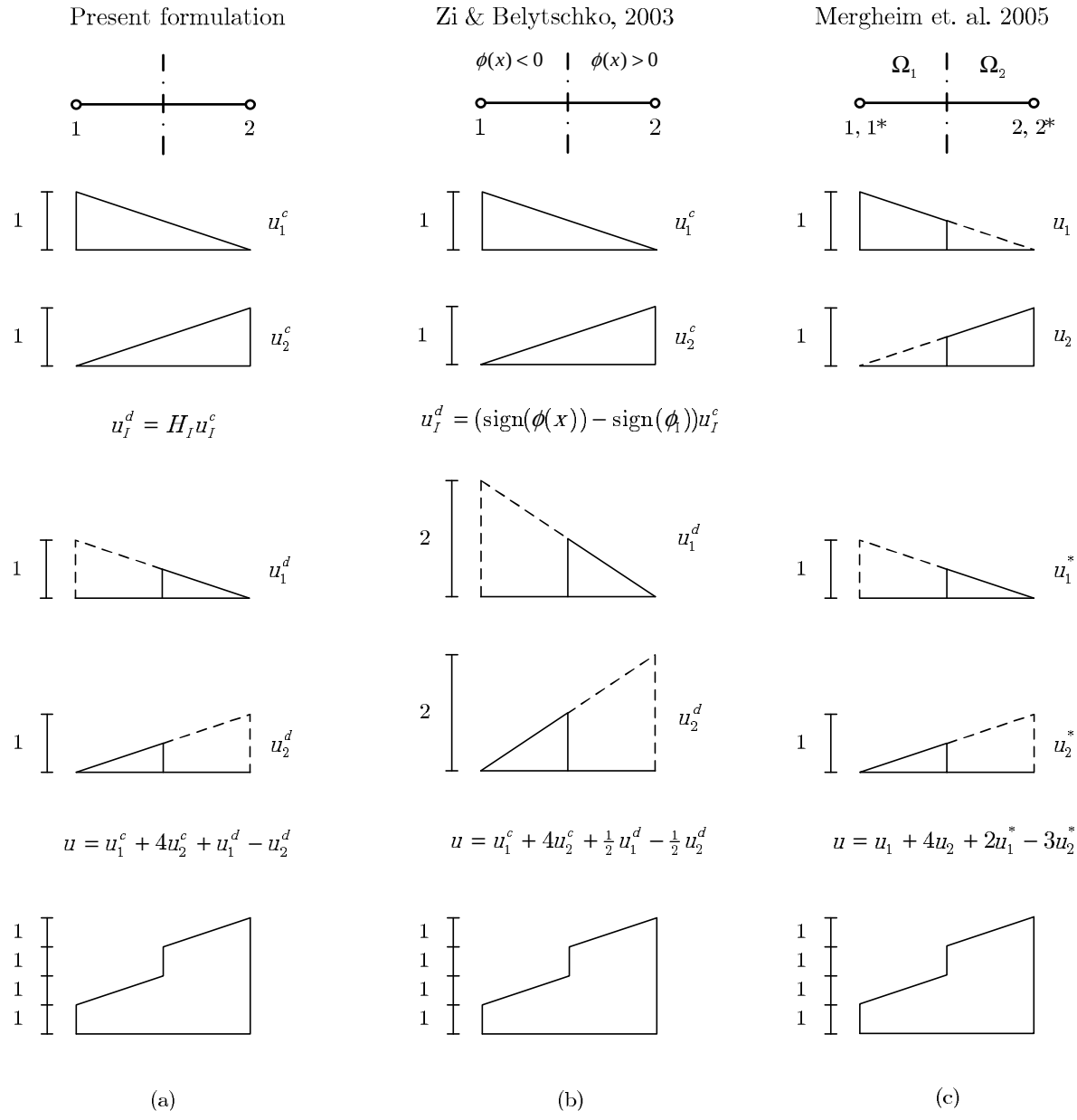

Figure 4.1 *Comparison of different enrichments of the displacement field: (a) Present formulation, (b) Zi and Belytschko (2003), (c) Mergheim et al. (2005). For the present formulation and the formulation by Zi and Belytschko (2003) the two upper figures illustrate the continuous displacement fields and the following two figures illustrate the discontinuous displacement field. Regarding the formulation by Mergheim et al. (2005) the two upper figures illustrate the displacement field for the two "original" nodes 1 and 2 while figure 3 and 4 depict the displacement fields for the dual nodes 1^* and 2^*. The lower figure in each column illustrates how a displacement jump of magnitude one may be modeled by the different formulations.*

Here the element discontinuity interpolation matrix, $\mathbf{N}^d$, is chosen as

$$\mathbf{N}^d(x,y) = \sum_I H_I(x,y)\mathbf{N}_I^c(x,y) \tag{4.2}$$

where $H_I(x,y)$ is the 2D Heaviside step function for node I. The step function $H_I(x,y)$ is 0 on the same side of the discontinuity as node I and 1 on the other side. It is noted that in this work the expression for the location of the discontinuity is not included explicitly in the expression for the Heaviside step function. In line width the standard applied in the XFEM literature it is implied that the Heaviside step function is defined in relation to the line of discontinuity.

Figure 4.2 illustrates a discontinuous displacement field for a CST element cut by a crack while Figure 4.3 illustrates two of the discontinuous displacement fields for a LST element. The left most subfigure in each figure shows the crack geometry, coordinates to the start and the endpoints are given in area coordinates. The remaining subfigures depicts individual nodal discontinuous displacement fields.

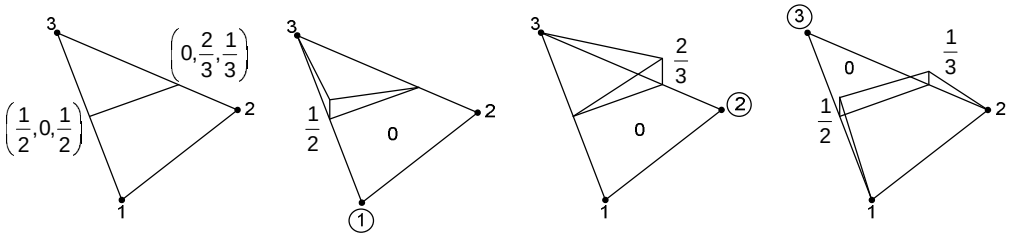

(a) (b) (c) (d)

Figure 4.2 *Example of the enrichment of the displacement field for a cracked CST element. (a) Crack geometry, (b), (c), (d) Displacement fields for discontinuity dof's in node 1, 2 and 3*

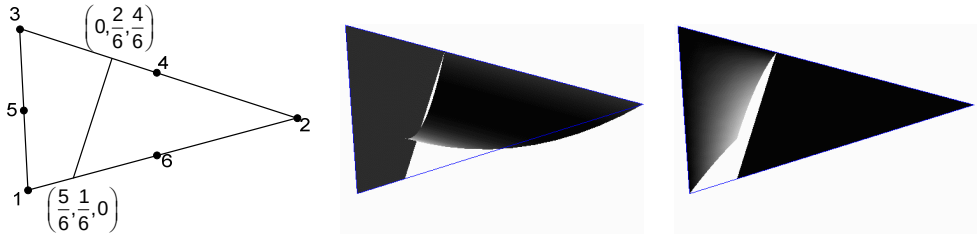

(a) (b) (c)

Figure 4.3 *Example of the enrichment of the displacement field for a cracked LST element.(a) Crack geometry, (b) and (c) Discontinuous displacement field for discontinuity dof's in node 1 respectively node 6.*

From Figure 4.2 and Figure 4.3 it is seen that the choice of interpolation for the discontinuous displacement field ensures that the discontinuous contribution to the displacement

field vanishes at all element edges not cut by the crack. The discontinuous displacement field only has to be included in elements cut by the crack.

Figure 4.4 illustrates the enrichment at system level. Only nodes for which the support is cut by the discontinuity are enriched. The discontinuity dof's located at the element edge where the crack tip is located have to be set to zero to ensure that the discontinuity at that edge is zero.

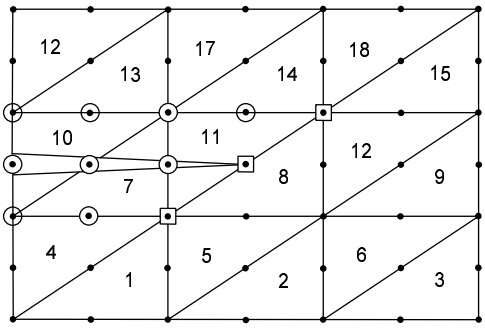

Figure 4.4 *Enrichment at system level for a mesh with LST elements. Nodes marked with a circle or a square are enriched. Discontinuity dof's in nodes marked with a square are set to zero.*

4.2 Variational Formulation

As the onset for deriving the variational formulation for the XFEM element consider a cohesive crack in a structure in a state of plane stress or plane strain described in a Cartesian coordinate system x,y (cf. Figure 4.5), the arc length along the crack is termed s, and n,s is a curve linear coordinate system, n being normal to the crack face. The positive direction of s is seen in Figure 4.5. The orientation of n determines the positive side of the crack. The stress state in the crack may be defined by the normal stress σ_n and the shear stress τ_{ns}, while work conjugated generalized strains are the opening of the crack, $\Delta u_n = u_n^+ - u_n^-$ and the slip in the crack, $\Delta u_s = u_s^+ - u_s^-$. A small strain / small displacement static theory is used and the material outside the crack is assumed linear elastic.

Let $[\![\ \ ]\!]$ denote a jump, then the stress increments $d\boldsymbol{\sigma}^{cr}$ across the crack surfaces are related to the increments in the displacement jump, $d[\![\boldsymbol{u}]\!]$, - i.e. the separation of the crack surfaces - through the tangential material stiffness matrix $\mathbf{D}_T^{cr}$ (se also Eq. (3.1)).

$$\boldsymbol{\sigma}^{cr}\left([\![\boldsymbol{u}]\!]\right) = \begin{bmatrix} \sigma_n\left([\![\boldsymbol{u}]\!]\right) \\ \tau_{ns}\left([\![\boldsymbol{u}]\!]\right) \end{bmatrix} \qquad [\![\boldsymbol{u}]\!] = \begin{bmatrix} \Delta u_n \\ \Delta u_s \end{bmatrix} \qquad d\boldsymbol{\sigma}^{cr}\left([\![\boldsymbol{u}]\!]\right) = \mathbf{D}_T^{cr}\left([\![\boldsymbol{u}]\!]\right) d[\![\boldsymbol{u}]\!] \quad (4.3)$$

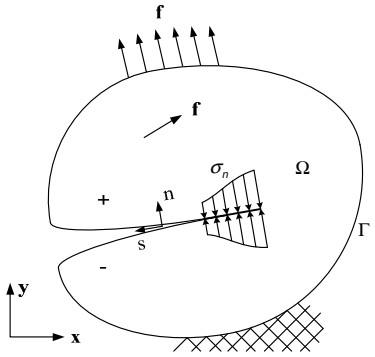

Figure 4.5 *Cohesive crack in two dimensional domain with f representing both domain load and boundary load*

For the uncracked part of the structure, the stress vector $\boldsymbol{\sigma}^T = [\sigma_x \quad \sigma_y \quad \tau_{xy}]$ and the strain vector $\boldsymbol{\epsilon}^T = [\epsilon_x \quad \epsilon_y \quad \gamma_{xy}]$, $(\gamma_{xy} = 2\epsilon_{xy})$ are defined as usual and related through the standard material stiffness matrix $\mathbf{D}$, specified below for an isotropic material in plane stress.

$$d\boldsymbol{\sigma} = \mathbf{D}d\boldsymbol{\epsilon} \qquad , \qquad \boldsymbol{D} = \frac{E}{1-\nu^2}\begin{bmatrix} 1 & \nu & 0 \\ \nu & 1 & 0 \\ 0 & 0 & \frac{1-\nu}{2} \end{bmatrix} \tag{4.4}$$

The virtual internal work-per-unit length of the crack δW^i_{cr} and the virtual internal work-per-unit area of the uncracked part of the structure δW^i_c may now be written, δ referring to a virtual quantity

$$\begin{aligned} \delta W^i_{cr} &= \delta[\![\boldsymbol{u}]\!]^T \boldsymbol{\sigma}^{cr} = \sigma_n \delta\Delta u_n + \tau_{ns}\delta\Delta u_s \\ \delta W^i_c &= \delta\boldsymbol{\epsilon}^T\boldsymbol{\sigma} = \sigma_x\delta\epsilon_x + \sigma_y\delta\epsilon_y + \tau_{xy}\delta\gamma_{xy} \end{aligned} \tag{4.5}$$

For the entire structure the virtual internal and external work becomes

$$\begin{aligned} \delta W^i &= \textstyle\int_\Omega \delta\boldsymbol{\epsilon}^T\boldsymbol{\sigma}d\Omega + \int_\Gamma \delta[\![\boldsymbol{u}]\!]^T\boldsymbol{\sigma}^{cr}d\Gamma \\ \delta W^e &= \textstyle\int_\Omega \delta\mathbf{u}^T\mathbf{f}d\Omega + \int_\Gamma \delta\mathbf{u}^T\mathbf{f}d\Gamma \end{aligned} \tag{4.6}$$

where $\mathbf{f}$ is the load on the structure.

By applying incremental quantities, the incremental stiffness relation, can obtained.

$$\mathbf{K}_T\Delta\mathbf{V} = \int_\Omega \mathbf{N}^T\Delta\mathbf{f}d\Omega + \int_\Gamma \mathbf{N}^T\Delta\mathbf{f}d\Gamma \tag{4.7}$$

Where $\mathbf{V}$ is the system DOF vector and Δ refers to an incremental quantity.

Special attention must be paid to the internal work, because the contribution from each element to the tangential stiffness matrix $\mathbf{K}_T$ depends on whether the element is cracked or not. The element tangential stiffness matrix, $\mathbf{k}_T$, for a cracked element is found by the following procedure. From (4.1) and (5.1) the strain vector in a cracked element, except in the crack itself, is obtained

$$\boldsymbol{\epsilon} = \mathbf{B}^c\mathbf{v}^c + \sum H_I\mathbf{B}_I^c\mathbf{v}_I^d = \mathbf{B}^c\mathbf{v}^c + \mathbf{B}^d\mathbf{v}^d \tag{4.8}$$

Where $\mathbf{B}^c$ and $\mathbf{B}^d$ are the generalized strain distribution matrixes corresponding to the interpolation matrix $\mathbf{N}^c$ respectively $\mathbf{N}^d$.

Due to the displacement field from the first terms in (4.1) being continuous, the strains in the crack itself may be written as

$$[\![\boldsymbol{u}]\!](s) = \mathbf{T}\left(\mathbf{N}_+^d(s) - \mathbf{N}_-^d(s)\right)\mathbf{v}^d = \mathbf{B}^{cr}\mathbf{v}^d \tag{4.9}$$

Here, $\mathbf{B}^{cr}$ is the strain distribution matrix in the crack, $\mathbf{T}$ is the transformation matrix between the (x, y) and (n, s) coordinate systems, while $\mathbf{N}_+^d$ and $\mathbf{N}_-^d$ are the discontinuous interpolation matrices on the positive and negative sides of the crack respectively.

Applying the strain relations in Eq. (4.8) and Eq. (4.9) when formulating the virtual incremental internal work, Eq. (4.6), the outcome is:

$$\begin{aligned}
\delta W^i &= \int_\Omega \left(\begin{bmatrix}\mathbf{B}^c & \mathbf{B}^d\end{bmatrix}\begin{bmatrix}\delta\mathbf{v}^c\\ \delta\mathbf{v}^d\end{bmatrix}\right)^T \mathbf{D}\begin{bmatrix}\mathbf{B}^c & \mathbf{B}^d\end{bmatrix}\begin{bmatrix}\mathbf{v}^c\\ \mathbf{v}^d\end{bmatrix} d\Omega \\
&+ \int_\Gamma \left(\mathbf{B}^{cr}\delta\mathbf{v}^d\right)^T \mathbf{D}^{cr}\mathbf{B}^{cr}\mathbf{v}^d d\Gamma \\
&= \begin{bmatrix}\delta\mathbf{v}^c\\ \delta\mathbf{v}^d\end{bmatrix}\begin{bmatrix}\int \mathbf{B}^{cT}\mathbf{D}\mathbf{B}^c & \int \mathbf{B}^{cT}\mathbf{D}\mathbf{B}^d \\ \int \mathbf{B}^{dT}\mathbf{D}\mathbf{B}^c & \int \mathbf{B}^{dT}\mathbf{D}\mathbf{B}^d + \int_{cr}\mathbf{B}^{crT}\mathbf{D}^{cr}\mathbf{B}^{cr}\end{bmatrix}\begin{bmatrix}\mathbf{v}^c\\ \mathbf{v}^d\end{bmatrix}
\end{aligned} \tag{4.10}$$

Defining $\mathbf{k}_T$ by $\delta W^i = \delta\mathbf{v}^T\mathbf{k}_T\Delta\mathbf{v}$, where $\mathbf{v}^{\mathbf{T}} = [\mathbf{v}^{cT} \quad \mathbf{v}^{dT}]$, $\mathbf{k}_T$ is:

$$\begin{aligned}
\mathbf{k}_T &= \begin{bmatrix}\int \mathbf{B}^{cT}\mathbf{D}\mathbf{B}^c & \int \mathbf{B}^{cT}\mathbf{D}\mathbf{B}^d \\ \int \mathbf{B}^{dT}\mathbf{D}\mathbf{B}^c & \int \mathbf{B}^{dT}\mathbf{D}\mathbf{B}^d + \int_{cr}\mathbf{B}^{crT}\mathbf{D}^{cr}\mathbf{B}^{cr}\end{bmatrix} \\
&= \begin{bmatrix}\mathbf{k}^{cc} & \mathbf{k}^{cd} \\ \mathbf{k}^{dc} & \mathbf{k}^{dd} + \mathbf{k}_T^{cr}\end{bmatrix}
\end{aligned} \tag{4.11}$$

Due to a constant D-matrix outside the crack the stiffness contribution from the areas outside the crack are constant and thus only the stiffness contribution from the crack itself is non-linear. This is an important property of the element stiffness matrix in relation to the following derivation of the expression for the element nodal forces.

The element nodal forces, $\mathbf{q}$, depend, like $\mathbf{k}_T$, on the crack opening and are determined analogous to $\mathbf{k}_T$. The contributions to $\mathbf{q}$ from the crack, $\mathbf{q}^{cr}$, are found from the stresses in the crack. The stresses in the crack are related to the displacement jump across the crack according to Eq. (4.3) and in general depends on the applied softening law. Thereby $\mathbf{q}^{cr}$ also depends on the applied softening law. Adding this contribution to the contribution from the part of the element outside the crack, $\mathbf{q}$ is obtained as

$$\mathbf{q} = \begin{bmatrix} \mathbf{k}^{cc} & \mathbf{k}^{cd} \\ \mathbf{k}^{dc} & \mathbf{k}^{dd} \end{bmatrix} \begin{bmatrix} \mathbf{v}^{c} \\ \mathbf{v}^{d} \end{bmatrix} + \mathbf{q}^{cr} \qquad \text{where} \qquad \mathbf{q}^{cr} = \int_{cr} \mathbf{B}^{crT} \begin{Bmatrix} \sigma_n \\ \tau_{ns} \end{Bmatrix} \tag{4.12}$$

4.3 Aspects of Implementation

This section deals with some of the aspects of the implementation of the XFEM scheme. Focus is on the condition for smooth crack closure and the criteria for crack propagation. For details regarding the applied integration scheme and the choice of the algorithm to solve the non-linear equations reference is made to *Paper I*

4.3.1 Conditions for Smooth Crack Closure

In a cohesive crack tractions act at the crack surfaces near the tip as illustrated in Figure 4.5 causing the crack to close smoothly. For an opening crack the tensile stresses at the crack tip will be equal to the tensile material strength, corresponding to vanishing stress intensity factors at the crack tip. Therefore, criterions for smooth closure may be imposed in terms of either a stress criterion or an equivalent stress intensity factor criterion. Investigations using interface cohesive crack elements by Stang et al. (2006a) show that smooth crack closure is automatically achieved in a finite element formulation with a stress criterion when a sufficient numbers of elements are applied. In the case considered where the elements are either uncracked or fully cracked, it is ensured that the stresses in the element next to the crack-tip element do not exceed the tensile strength. This approximately ensures smooth crack closure as well.

4.3.2 Crack Growth

In the case of fully cracked elements a discontinuity is introduced in the element, when the principal stress in the element exceeds the tensile strength of the material. The discontinuity is a straight line through the element originating from the point where the discontinuity ended in the previous cracked element and hereby a continuous discontinuity is assured.

Concerning the crack growth direction, different approaches have been considered. The first and simplest approach is local and rely only upon the stresses in the element that is located next to the tip-element (the element to become the next tip-element, element 8 in Figure 4.6) for the determination of the crack growth direction. The discontinuity is grown perpendicular to the principal stress direction.

Several authors state that the local stresses in the next tip element can not be relied upon for computation of the crack growth direction and different nonlocal approaches are suggested. In Wells and Sluys (2001) the principal stress direction in the next tip element is computed from a non-local stress tensor calculated as a weighted average of stresses using a Gaussian weight function. Stresses in integration points within a radius of three times the typical element size are taken into account. In Moës and Belytschko (2002) the maximum hoop stress criterion is applied. The requirement for considering stresses in more than one element when computing the crack growth direction is clear when recalling the discontinuous displacement field in a cracked CST tip element, c.f. Figure 4.6. Due to the discontinuous degrees of freedom in the nodes located on the crack tip edge being set equal to zero, the crack tip element is not able to model the case, where equal stresses are present at both sides of the discontinuity. This lack of capability to model correct stresses in the tip element influences the stresses in the next tip elements and may call for more elements to be relied on for the computation of crack growth direction. The problem is of course most pronounced when CST elements are considered.

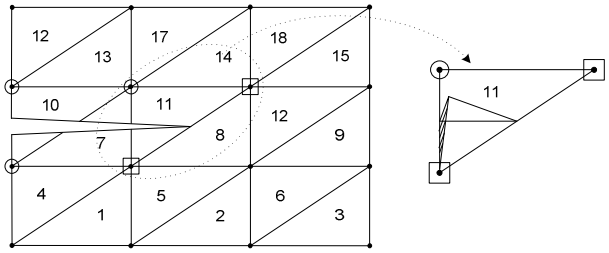

Figure 4.6 *Discontinuous displacement field in CST "tip" element.*

When a non-local stress tensor is applied in this work (only for CST elements), average nodal stresses are computed from element stresses in the elements sharing a given node - c.f. Eq. (4.13). All elements are assigned the same weight except previously cracked elements that are disregarded in the computation of the average nodal stresses, due to the above illustrated limited quality of the stress field in the crack tip element. From the average nodal stresses a non-local stress tensor at the crack tip is interpolated c.f., Eq. (4.14), and used for the determination of the crack growth direction. In Eq. (4.14) $(\zeta_1, \zeta_2, \zeta_3)$ are the area coordinates to the crack tip.

$$\boldsymbol{\sigma}_{node}^{ave} = \left(\sum_{i=1}^{n_{el}^{uncr}} \boldsymbol{\sigma_i} \right) / n_{el}^{uncr} \tag{4.13}$$

$$\sigma_{tip}^{NL} = \begin{bmatrix} \sigma_x^{no1} & \sigma_x^{no2} & \sigma_x^{no3} \\ \sigma_y^{no1} & \sigma_y^{no2} & \sigma_y^{no3} \\ \tau_{xy}^{no1} & \tau_{xy}^{no2} & \tau_{xy}^{no3} \end{bmatrix} \begin{bmatrix} \zeta_1 \\ \zeta_2 \\ \zeta_3 \end{bmatrix} \tag{4.14}$$

4.4 Numerical Examples

To illustrate the capability of the suggested XFEM scheme two fracture mechanical benchmark tests, the TPBT and the FPSB, are considered. Results will be given for the TPBT applying CST as well as LST elements while only results applying LST elements will be given for the FPSB. Applying CST elements for the the TPBT specimen, local as well as nonlocal determination of crack growth direction will be considered and discussed.

4.4.1 Three Point Beam Bending Test

The geometry of the TPBT specimen considered is in accordance with the RILEM recommendations (Vandervalle, 2000). The geometry is depicted in Figure 4.7(a), the cross section of the beam being a square. For the material parameters standard values for a good quality concrete were chosen, c.f. Table 4.1.

Concerning the stress-crack-opening relationship it was chosen to apply the simplest option - i.e. a linear softening curve for the normal stress in the crack as illustrated in Figure 4.7(b). A linear softening curve is a relative crude approximation to the true behavior of concrete, and a softening curve determined on the basis of experimental results would be a better match to reality. However, in this case the results obtained by the XFEM scheme are compared against computational results obtained by modeling of fracture in the TPBT specimen applying standard 6-node cohesive interface elements in the commercial code DIANA, and the choice of softening curve is therefore less important for illustrating the performance of the XFEM scheme. Utilizing the DIANA results as reference for XFEM computations is justified by the modeling of a symmetric problem like the TPBT for which the DIANA interface elements have proven to produce reliable results when comparison is made to experimental results - se e.g. Østergaard (2003). A softening curve based on the experimental results by Østergaard and Olesen (2004) and fitted by the method suggested by Hordijk (1991) was applied in modeling of the TPBT specimen with the proposed XFEM scheme in Asferg et al. (2004).

Considering a pure Mode-I problem the shear stiffness and the mixed mode stiffness terms for the crack were all set equal to zero - i.e. the tangential discontinuous material stiffness matrix, Eq. (4.15), only holds one term different from zero.

$$\mathbf{D}_{cr}^{T} = \begin{bmatrix} \frac{-f_t}{\Delta u_{n,ult}^{cr}} & 0 \\ 0 & 0 \end{bmatrix} \tag{4.15}$$

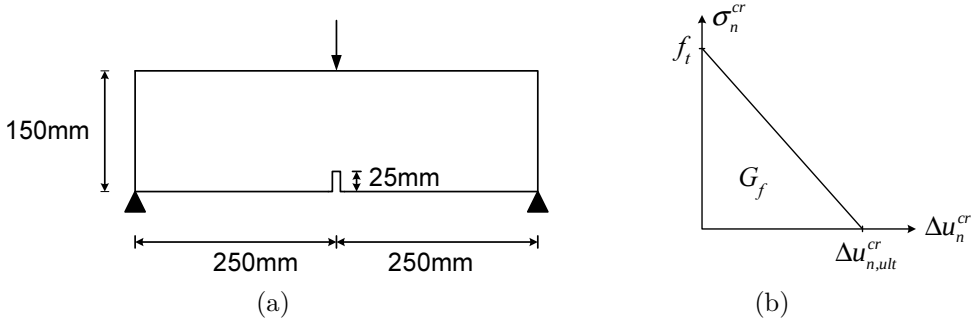

Figure 4.7 *(a) Geometry of TPBT specimen. (b) Applied linear softening curve.*

Table 4.1 *Constitutive parameters TPBT*

Parameter	Value
Young's modulus, E_c	37400MPa
Poisson's ratio, ν_c	0.2
Tensile strength, f_t	3.5MPa
Fracture energy, G_f	160 N/m

Applying CST Elements to Model TPBT

Modeling the TPBT specimen applying CST elements structured as well as unstructured meshes are considered. Results are given for two structured meshes, a 21 by 12 element, c.f. Figure 4.8(a), and a 25 by 24 element mesh. For both structured meshes results for local as well as non-local computation of crack growth direction are given. The unstructured mesh, c.f. Figure 4.8(b), consisted of 709 elements and results are only given for the non-local crack growth computation. Note that for the structured meshes the notch is modeled as a predefined stress free discontinuity while in the unstructured mesh the notch is defined by the geometry of the mesh.

Regarding the reference computations applying standard interface elements along a predefined crack path in the commercial code DIANA, two meshes holding 24, respectively, 48 elements over the beam height were considered.

Figure 4.9 shows the load-deformation-response for the five XFEM computations and the two reference DIANA computations. The deformation is computed as the difference between the vertical displacement of the center point of the beam and the average vertical

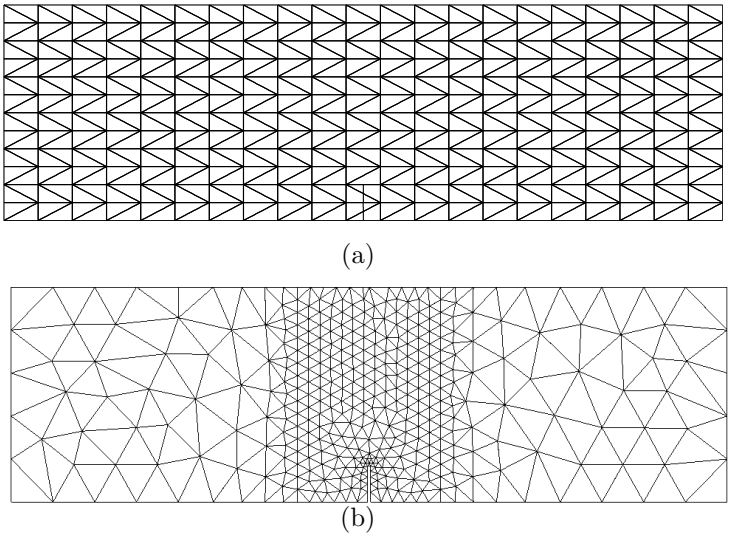

Figure 4.8 *(a) Structured mesh. (b) Unstructured mesh.*

displacement of the mid points of the beam ends. Figure 4.10(a) shows the predicted crack path for the 25 by 24 mesh applying local computation of the crack growth direction while 4.10(b) shows the prediction achieved applying a non-local approach for the 25 by 24 mesh. 4.10(c) depicts the predicted crack path for the unstructured mesh applying the local approach.

From the load-deformation-responses it is seen that the coarse structured mesh over predicts the load carrying capacity of the TPBT specimen with about 20% while the finer structured mesh overestimates the load carrying capacity with about 8%. The unstructured mesh predicts the maximum load carrying capacity well. Applying the local approach for the crack growth direction, only the first part of the post peak response corresponding to the crack having propagated approximately through 2/3 of the beam hight may be obtained. Applying the non-local approach, the full load-deformation response may almost be obtained - in Figure 4.10(b) the crack has almost reached the top of the beam. The main reason for the bad prediction of the crack growth direction applying the local approach is the bad reproduction of the stresses in the tip element discussed in Section 4.3.2. The difference in stability of the determination of crack growth direction for the local versus the non-local approach is also evident from Figure 4.10 (a) and (b). The non-local approach smoothes the crack path considerably compared to the local approach. The unstructured mesh captures the load carrying capacity well but is not able to reproduce the full load deformation response for the TPBT specimen with the applied non-local computation scheme. The use of a non-local criteria for determination of crack growth direction is, however, seen as less appealing due to the required user interaction for determination of interaction radius that e.g. depends on the chosen element size and the actual structure considered. Furthermore, the use of a non local criterion somewhat

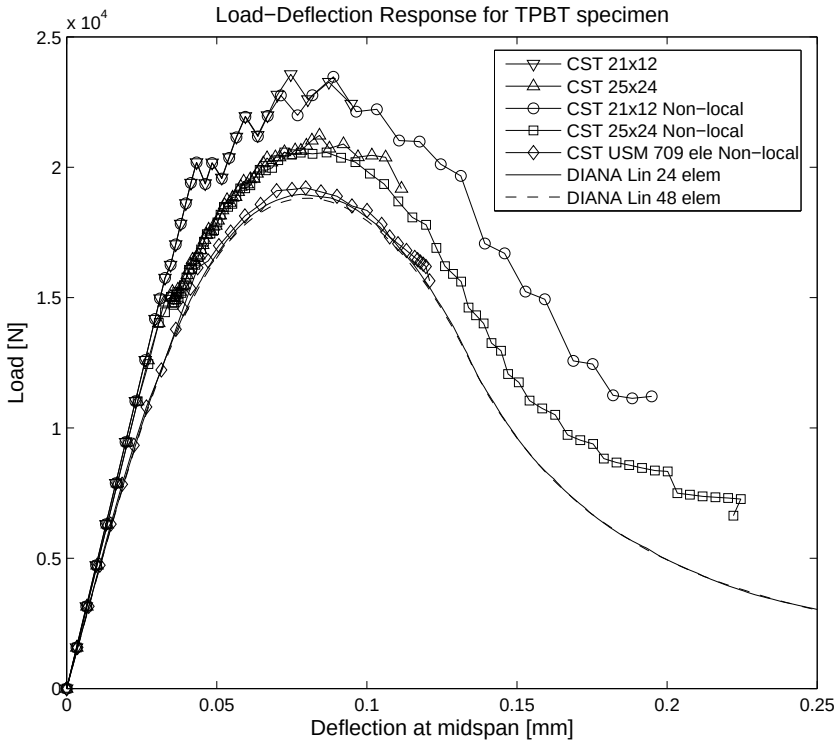

Figure 4.9 *Load-deformation-response for TPBT specimen modelled applying fully cracked CST elements.*

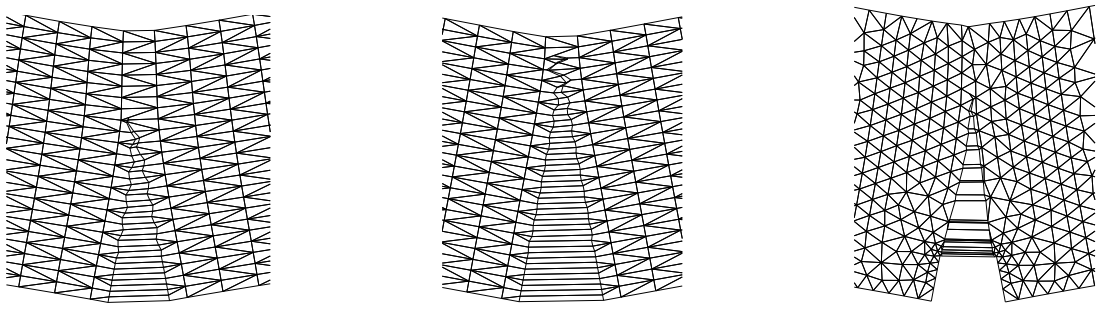

(a) (b) (c)

Figure 4.10 *Predicted crack path for: (a) 25 by 24 Mesh, local computation of crack growth direction. (b) 25 by 24 Mesh, non-local computation of crack growth direction (c) Unstructured mesh, non-local computation of crack growth direction.*

violates the element local approach of the XFEM where everything is handled element locally.

Applying LST Elements to Model TPBT

Applying LST elements results are given for four structured meshes - a 11 by 6, a 15 by 9, the 21 by 12 and the 25 by 24 mesh. Only local computation of crack growth direction is considered. In Figure 4.11 the load-deformation responses from the XFEM LST computations are compared with the DIANA computations while Figure 4.12 depicts the predicted crack patterns for the 21 by 12 and the 25 by 24 mesh.

From the load-deformation response it is seen that applying LST elements the overall behavior is predicted well by the 21 by 12 and the 25 by 24 mesh while the two coarsest meshes have trouble capturing the post peak response. Looking at the predicted crack paths it is seen that applying LST elements, and hereby having more active discontinuity dof's, a more smooth crack path is achieved than for CST elements. However when the crack reaches the top of the beam and only a few elements remain uncracked the quality of the determined stress near the crack tip becomes low, and hence, influences the crack growth direction causing increasing tortuosity of the crack path. The conclusion is, however, that applying LST a sufficient accuracy concerning the crack growth direction is obtained applying the local approach.

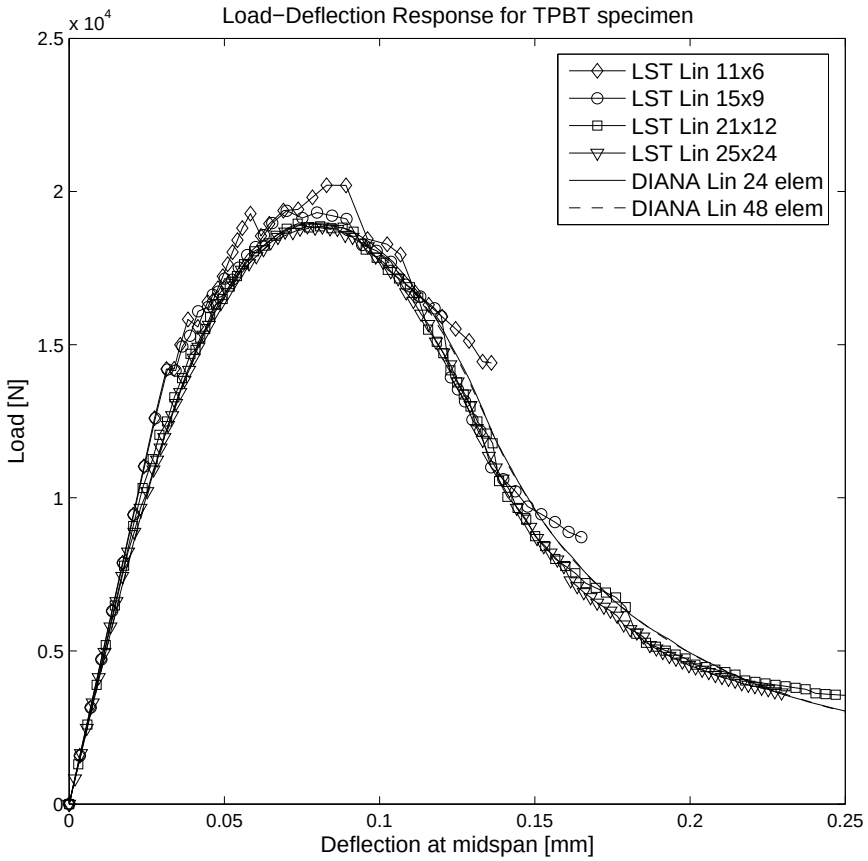

Figure 4.11 *Load-deformation-response for TPBT specimen modelled applying fully cracked LST elements.*

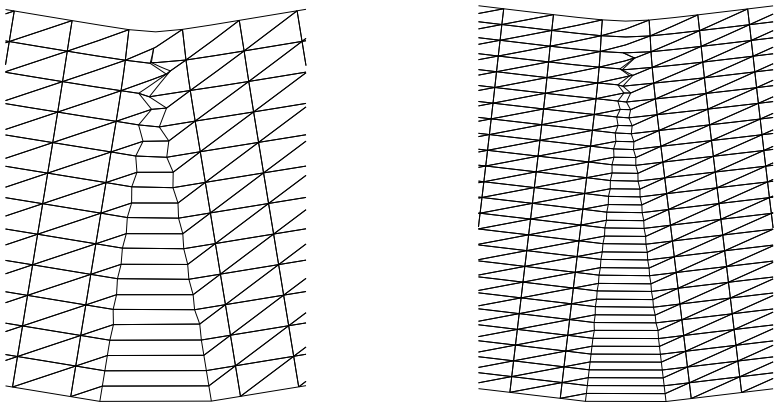

(a) (b)

Figure 4.12 *Predicted crack path for LST computations of TPBT: (a) 21 by 12 Mesh. (b) 25 by 24 Mesh.*

4.4.2 Four Point Shear Beam

The four point shear beam serves to illustrate the capability of the suggested XFEM scheme to model curved cracks. The geometry of the four point shear beam (FPSB) - or the "double-edge notched specimen subjected to four point shear" is equivalent to the one investigated experimentally by Carpinteri et al. (1992). Here it is concluded that the FPSB may be modeled considering only mode I fracture - i.e. the shear stiffness in the crack may be ignored. Therefore the FPSB in this study is also modeled considering only mode-I fracture. However it has to be emphasized that the XFEM scheme is general and is capable of handling Mode-I, Mode-II and mixed mode loading if the required constitutive relations are supplied, c.f. the discussion in section 2.4. The FPSB specimen was analyzed by XFEM in Moës and Belytschko (2002) and the results obtained are also compared to their findings. The geometry of the test setup is shown in Figure 4.13, while constitutive parameters are given in Table 4.2. As for the TPBT specimen a linear softening curve (Figure 4.7(b)) was applied.

A fairly coarse structured LST mesh, depicted in Figure 4.14, consisting of 1222 elements and 2549 nodes was used for the XFEM computation.

Table 4.2 *Constitutive parameters FPSB*

Parameter	Value
E_c	28000MPa
ν_c	0.1
f_t	2.4MPa
G_f	$145N/m$

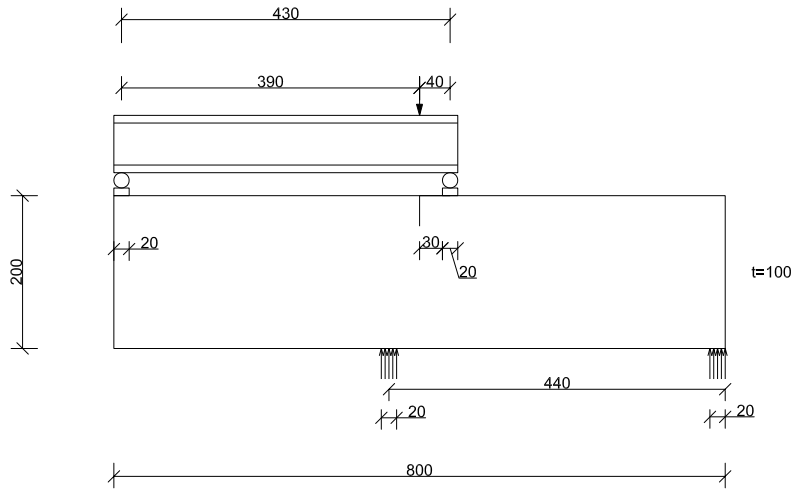

Figure 4.13 *Geometry of four point shear beam, all measures in mm*

Figure 4.14 depicts the computed crack path. The crack path is in good agrement with the experimental findings in Carpinteri et al. (1992). In Figure 5.16 the computed load-deflection response is compared to the experimental determined response obtained by Carpinteri et al. (1992) and to the XFEM response computed by Moës and Belytschko (2002). It is seen that the obtained results correlate well with the experimental results whereas there are some deviations compared to the results obtained in Moës and Belytschko (2002). Applying the XFEM scheme, the somewhat surprising conclusion drawn by Carpinteri et al. (1992), regarding the influence of Mode-II fracture on the structural response of the FPSB, is supported: Crack propagation in the FPSB specimen seams to be governed by Mode-I fracture. The Mode-II energy dissipation does not seems to be "missing" in the global response for the fracture of the FPSB.

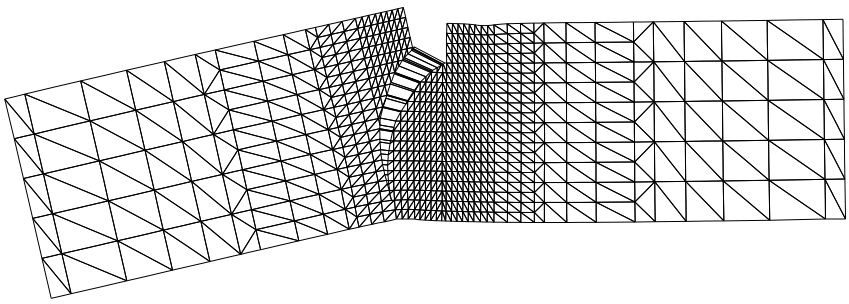

Figure 4.14 *Predicted crack path for FPSB specimen.*

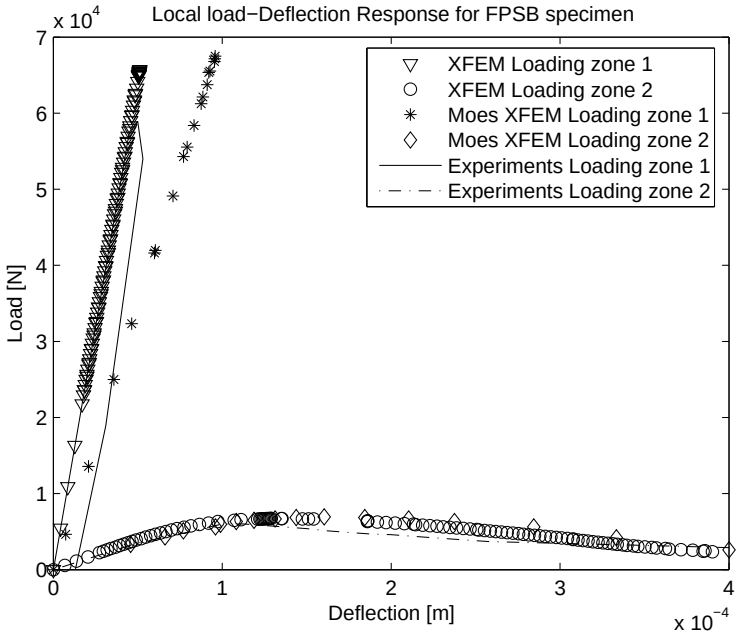

Figure 4.15 *Comparison of load-displacement response for FPSB obtained by present XFEM model, XFEM results by Moës and Belytschko (2002) and by experiments Carpinteri et al. (1992). Loading zone 2 refers to the loading zone to the left in Figure 4.13, while loading zone 1 refers to the right.*

4.5 Conclusions Regarding Fully Cracked Elements

Applying the direct enrichment of the displacement field an XFEM scheme that fits directly in the framework of standard finite element has been developed. The XFEM scheme has been implemented for the CST element and the LST element. Considering the CST element it was found necessary to implement a nonlocal computation of crack growth direction to obtain good prediction of the crack path, while for the LST element the crack path computation could be based on element local computations. Considering three point bending and four point shear, the efficiency of the suggested scheme was illustrated and it was found that even for relatively coarse meshes the scheme produces good results. Regarding the FPSB the XFEM results confirm the conclusion drawn by Carpinteri et al. (1992); the global response of the FPSB may be modeled considering only Mode-I fracture.

Chapter 5

A Consistent Partly Cracked XFEM Element

In the previous chapter fully cracked elements were considered and fairly good results were obtained when modeling fracture in the two benchmark tests: three point bending and four point shear. Referring to the load-displacements response for the tests some tortuosity was, however, observed.

Applying elements that may only be fully cracked does not allow for all possible load-displacement states to be computed, as, is normally required in a general solution of a non-linear problem. Therefore the application of elements that are not allowed to be partly cracked may not only lead to a erroneous load-deformation response for a crack propagating through a given structure, but may also be the reason for numerical problems when solving the non-linear equations. An element that can be partly cracked is therefore preferable. Previously proposed partly cracked elements include the ones by Moës and Belytschko (2002) and Zi and Belytschko (2003). These elements were discussed in Chapter 4 from the enrichment point of view.

Using the enrichment strategy implemented in Wells and Sluys (2001),Zi and Belytschko (2003) and Asferg et al. (2007b) the crack tip element can not model equal stresses on both sides of the crack as assumed in the cohesive model. Recalling the discussion regarding the need for nonlocal procedures for determination of crack growth direction in Chapter 4, the problem was illustrated in Figure 4.6, and for convenience repeated in Figure 5.1(a). The figures show the displacement field that may be modeled in the element holding the crack tip on its boundary applying the enrichment suggested in *Paper I*. Figure 5.1(b) depicts the enriched displacement field in the partly cracked element proposed by Zi and Belytschko (2003). To ensure the continuity of the displacement field at the crack tip, the discontinuity degrees of freedom in nodes located at the crack tip element boundary must be set to zero and this means that only one set of discontinuity degrees of freedom is available in the tip element. Various nonlocal approaches have been applied to compensate for the inability of the tip element to model equal stresses on both sides of the discontinuity, especially when 3-node constant strain triangle elements (CST) are considered. In Wells and Sluys (2001) and Asferg et al. (2007b) a non-local computation

of the stresses in the near tip area was used to determine the principal stress direction at the tip, while the maximum hoop stress criterion utilizing stress intensity factors was applied in Zi and Belytschko (2003). Recently Xiao and Karihaloo have extended their element local statically admissible stress recovery scheme (Xiao and Karihaloo (2005)) to cohesive cracks (Xiao and Karihaloo (2006)) and obtained good results for fairly dense meshes of higher order elements.

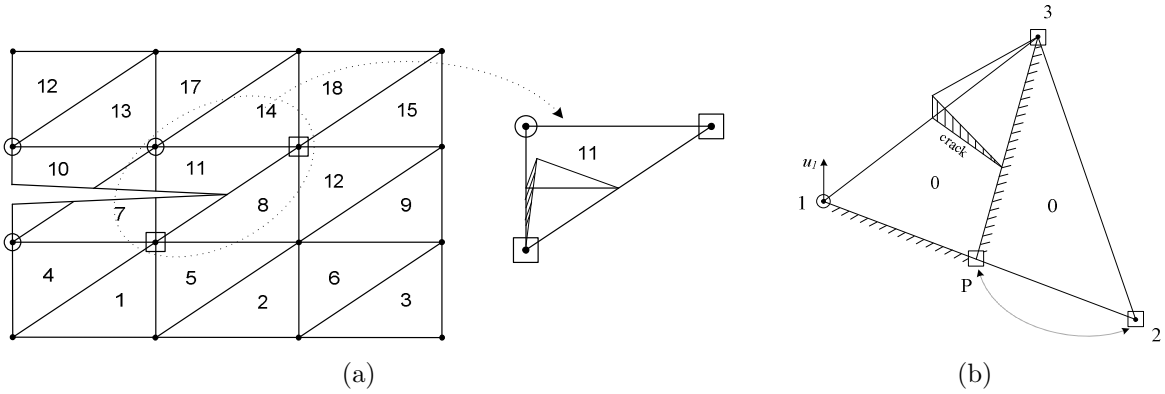

Figure 5.1 *Displacement fields in XFEM crack-tip elements. (a) Fully cracked element (Asferg et al., 2007b) (b) Partly cracked element by Zi and Belytschko (2003).*

A more direct way to obtain a better stress distribution on both sides of the crack in cohesive crack growth would be to formulate a tip element with the capability of modeling variations in the discontinuous displacement field on both sides of the discontinuity. *Paper II* presents such a consistent approach to obtain a more correct stress distribution in a partly cracked tip element. The new enrichment scheme is based on additional enrichment of the cracked elements. The extra enrichment is constructed as a superposition of the standard nodal shape functions and standard nodal step functions created for a sub-area of the cracked element. The suggested enrichment may be seen as a natural extension of the enrichments applied in Wells and Sluys (2001); Zi and Belytschko (2003); Asferg et al. (2004). The extra enrichment allows the element to model equal stresses on both sides of the crack tip. Whereas only fully cracked elements are considered in Wells and Sluys (2001); Asferg et al. (2006), the new enrichment scheme has been implemented so that the discontinuity in the crack tip element may have any length.

In this chapter focus will be on the development of the new enrichment scheme and the special features of implementation related to the extra discontinuity degrees of freedom. The numerical examples that were used to show the performance of the fully cracked elements will also serve to illustrate the performance of the consistent partly cracked element. The variational formulation applied for the partially cracked element is essentially the same as for the fully cracked element and reference is made to Section 4.2 or to *Paper II* for details regarding the variational formulation. In general the reader is referred to *Paper II* regarding the details of the partly cracked element.

5.1 Development of the Enrichment

Compared to the enrichment of the fully cracked element and the approximation for the displacement field given in Eq. (4.1) the new development is related to the element discontinuity interpolation matrix, $\boldsymbol{N}_d$, that is chosen as

$$\mathbf{N}^d(x,y) = \sum_I H_I(x,y)\mathbf{N}_I^*(x,y) \tag{5.1}$$

where $H_I(x,y)$ is the 2D Heaviside step function for node I and the set I is the number of enriched nodes. The step function $H_I(x,y)$ is 0 on the same side of the discontinuity as node I and 1 on the other side. $\mathbf{N}_I^*$ is the part of $\mathbf{N}^*$ from node *I*. In the standard case, $\mathbf{N}^*$ is chosen as $\mathbf{N}^c$, but for the proposed element $\mathbf{N}^*$ is more general but able to describe the same variations as $\mathbf{N}^c$. Figure 4.2 shows an example of the standard discontinuous displacement field for a CST element completely cut by a crack. The special enrichment applied in this work was developed from these standard enrichments.

The requirement for the new partly cracked tip element is that it must be able to model equal stresses on both sides of the discontinuity, i.e. the element must be able to perform as shown in Figure 5.2

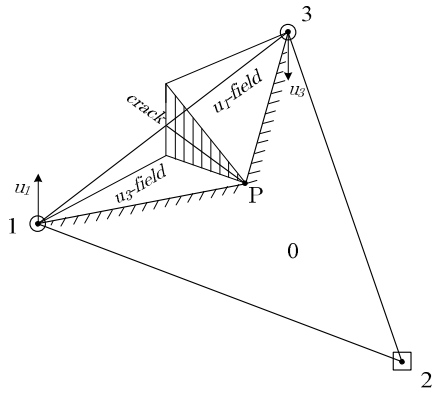

Figure 5.2 *New XFEM crack tip element.*

From Figure 5.2, it can be seen that an internal pseudo-node P, located at the crack tip, has been introduced. The pseudo-node does not hold any DOFs; it is just a point at which the discontinuous displacement field vanishes. Activating the enrichment of both nodes 1 and 3 allows for variations in the displacement fields on both sides of the crack as shown in the figure. This means that the element becomes capable of modeling the case where equal stresses are present on both sides of the crack. But the introduction of the pseudo-node defining the sub-displacement field 1-P-3 requires extra attention to the propagation of the crack from one element to another. Figure 5.3 illustrates the situation just before and just after the crack has crossed an element boundary. When the crack

propagates within one element (upper part of Figure 5.3), the contribution to the displacement field from the discontinuity DOFs in node 3 can have a value. When the crack just has passed an element edge and starts to propagate into a new element (lower part of Figure 5.3), the contribution from the discontinuity DOFs in node 3 must increase from a value of 0. To deal with this discrepancy in the value of the DOFs, the nodes connected to the element edge cut just before the crack propagates into a new element are enriched with extra discontinuity DOFs - c.f. Figure 5.4 (c) and (d). As long as an element is acting as a crack-tip element, only the discontinuity DOF's corresponding to (a) and (b) will be active. When the crack propagates into the next element, the discontinuity DOF's corresponding to (c) and (d) become active in the element which is now the previous crack-tip element. The extra set of discontinuity DOFs can model a displacement field in the neighbor crack-tip element that is equal to the displacement field along the edge 2-3 in the lower figure in Figure 5.3, whereby the desired continuity across the element boundary is achieved.

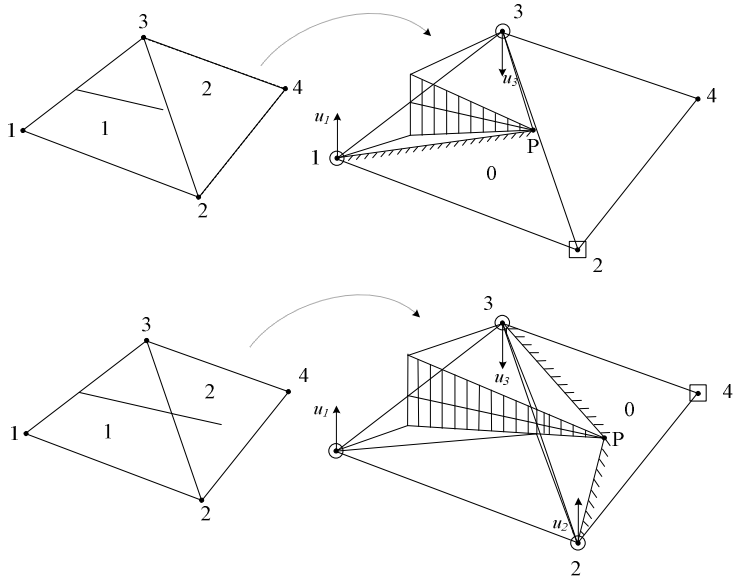

Figure 5.3 *Propagation of a crack across an element boundary. The upper figures illustrate the situation just before the crack reaches the element boundary, while the lower figures illustrate the case where a crack continues into a new element.*

The discontinuous displacement field in node 3 in relation to the tip edge (Figure 5.4(c)) is found by the superposition of the standard discontinuous displacement field in node 3 and a standard nodal displacement field for node 3 taking into account the sub-triangle 1-P-3 in Figure 5.2. The superposition is illustrated in Figure 5.5.

So far the two enrichments in node 3 have just been referred to as $u_{3,1}$ and $u_{3,2}$, however, it is evident from the figures, especially Figure 5.5 that the discontinuous DOFs in node 3 are element side local - $u_{3,1}$ refers to the "entrance" side where the crack propagates into the element while $u_{3,2}$ refers to the "exit" side where the crack leaves the element, and the element becomes fully cracked.

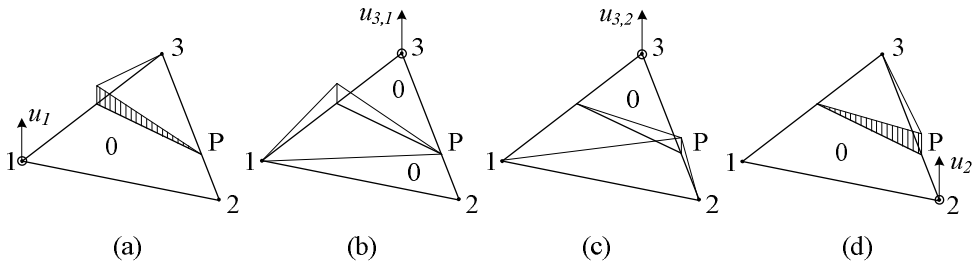

Figure 5.4 *Nodal discontinuous displacement fields for the new crack tip element. (a) field corresponding to node number 1, (b) field for node 3 referring to the "entrance" side of the element, (c) field for node 3 referring to the "exit" side of the element, (d) field for node 2.*

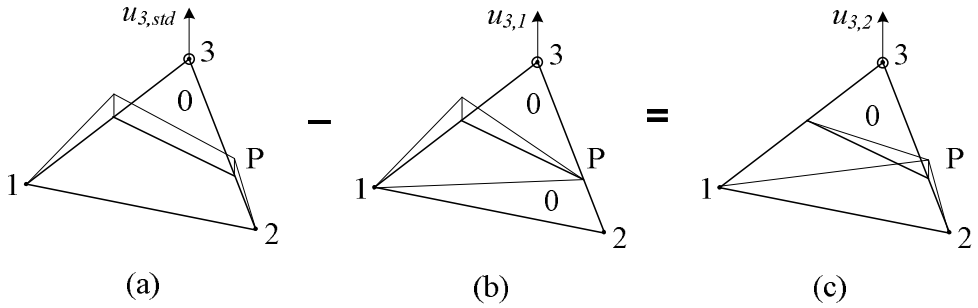

Figure 5.5 *Construction of discontinuous displacement field $u_{3,2}$ by superposition.*

The enrichment of a node in an element where two element sides are cut by the discontinuity may now be summarized by writing out the elements of the interpolation matrix, N^*, for the element. With reference to Figures 5.4 and 5.5, the local element coordinates in terms of area coordinates for the entire element (1-2-3) are termed $(\zeta_1, \zeta_2, \zeta_3)$, while the area coordinates for the sub-triangle (1-P-3) are termed $(\tilde{\zeta}_1, \tilde{\zeta}_2, \tilde{\zeta}_3)$. In line with the previously introduced notation, $N^*_{3,1}$ refers to the entrance side of the element and $N^*_{3,2}$ to the exit side of the element.

$$\begin{aligned} N^*_1 &= \zeta_1 \\ N^*_2 &= \zeta_2 \\ N^*_{3,1} &= \tilde{\zeta}_3 \\ N^*_{3,2} &= \zeta_3 - \tilde{\zeta}_3 \end{aligned} \tag{5.2}$$

At the system level, the enrichment is limited to nodes whose support is cut by the discontinuity. In the above discussed case where focus was on the crack propagating from one element to another, one extra set of discontinuity DOFs were added to the node that is common for the element sides cut by the discontinuity. However, in the general case where several element sides cut by the discontinuity all share a given node, there will be

as many active sets of discontinuity DOFs in that node as the number of element sides cut by the discontinuity sharing that node. The enrichment at system level is illustrated in Figure 5.6 where some nodes have one set of active discontinuity DOFs, some nodes have two active sets, and one node has three active sets.

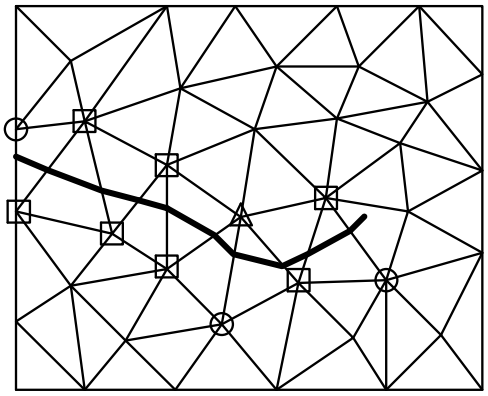

Figure 5.6 *Enrichment at system level. Nodes marked with a circle have one set of discontinuity DOFs, nodes marked with a square have two sets, while the node marked with a triangle has three sets.*

However, the storage of a variable number of degrees of freedoms in the nodes is seen as less favorable due to the handling of the DOFs at system level. The enrichments are, therefore stored side-locally, depending on whether they belong to the "entrance" or the "exit" side of the element. This will be discussed in detail in the next section.

5.2 Aspects of Implementation

Special features of the implementation of the partly cracked element will be discussed in this section. Storage of the discontinuity degrees of freedom (d-DOFs), criteria for crack growth and smooth closure as well as some comments regarding the procedure for solving the non-linear equations will be discussed. For further details reference is made to *Paper II*.

5.2.1 Storage of Discontinuity Degrees of Freedom

The additional discontinuous degrees of freedom requires extra bookkeeping hence the affiliation of discontinuous DOFs to the element edges discussed in the previous section. Therefore, for storage purposes only, the discontinuous degrees of freedom are related to the element edges, as illustrated in Figure 5.7. Figure 5.7(a) illustrates how the two active sets of discontinuous DOFs are stored when an element acts as a partly cracked tip element, while Figure 5.7(b) illustrates the storage of the four sets of discontinuous DOFs for a fully cracked non-tip element.

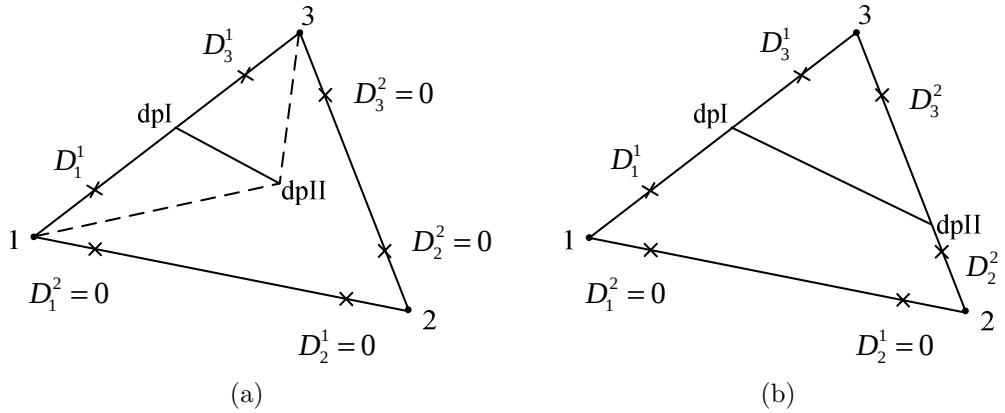

Figure 5.7 *Element side local storage of discontinuous DOFs in (a) a partly cracked element, and (b) a fully cracked non-tip element.* D^1_{NO} *refers to discontinuity DOFs related to the "entry" side of the element in node* NO *while* D^2_{NO} *refers to discontinuity DOFs related to the "exit" side of the element in node* NO.

5.2.2 Criteria for Crack Growth and Smooth Closure

A CST element is by default only able to model constant stresses in the element. Therefore there is a need to construct a stress interpolation through the element when the element acts as a partly cracked tip element where stresses equal to the tensile strength are to be found at the tip. Furthermore it is important to ensure a smooth transition when an element changes status from being uncracked to partly cracked and later changes status to being fully cracked. The smooth transition is of major importance for the capability of the element to model all possible crack lengths and for the stability of the iterative procedure.

A stress interpolation is created from the average nodal stresses computed by weighting the contribution from each element to a given node with the area of that element - c.f. (5.3).

$$\boldsymbol{\sigma}_{no}^{ave} = \left(\sum_{i=1}^{n_{el}^{no}} \boldsymbol{\sigma_i} A_i \right) / \sum_{i=1}^{n_{el}^{no}} A_i \tag{5.3}$$

Where σ_{no}^{ave} is the average nodal stress, n_{el}^{no} is the number of elements sharing a given node, σ_i is the stress in element i and A_i is the area of element i.

The contribution from fully cracked or partly cracked elements is weighted by using the relevant sub-areas when taking into account the contribution from the discontinuous displacement field. By weighting the stress contribution from the discontinuous field with the corresponding sub-areas in the partly cracked element, stress continuity across the element boundary is ensured when the discontinuity propagates from one element to another. From the nodal stresses, a linear interpolation is used for computation of the tip-stresses.

Several strategies can be applied for the determination of crack growth direction and computation of initial crack length increment in each load step. In this work, the crack propagates when the tensile strength of the material is exceeded in the crack tip, and the crack is propagated in the normal direction for the principal stress direction in the crack tip. The crack may be incremented either in pre-specified increments or it may be propagated to the point where the continuous field yields tensile stresses equal to the tensile strength for a given load increment. The crack length is then kept constant in the load step for the following iterations. To keep the crack length constant in each load step, the iteration procedure has to ensure stresses equal to the tensile strength in the crack tip. This issue will be returned to below, when the algorithm used for solving the non-linear equations is discussed.

As discussed in Section 4.3 smooth crack closure is automatically achieved in a finite element formulation with a stress criterion when a sufficient numbers of elements are applied for the cohesive zone, thus no additional criterion for smooth closure is needed.

5.2.3 Algorithm

To remain within the framework of traditional FEM code, a general procedure, the orthogonal residual algorithm Krenk (1995), was adopted for the XFEM scheme to solve the non-linear equations in Asferg et al. (2006). The algorithm proved to be efficient for fully cracked elements and it was therefore also used here. In the present case, the algorithm is supplemented with a stress criterion for smooth crack closure - i.e. the iterative procedures ensures stresses equal to the tensile strength in the crack tip. The algorithm is summarized in Table 5.1. The focus in this work was on the development and the performance of the new crack-tip element and the procedure for ensuring stresses equal to the material tensile strength at the crack-tip was chosen as the simplest and most robust possible. In terms of speed the algorithm could be improved by applying a more sophisticated strategy for the crack-tip stress iterations - e.g. an algorithm that iterates simultaneously on the global equilibrium and the crack length.

As a convergence criterion, an energy criterion was applied, and the elastic energy in the initial elastic load step was used as reference energy, E_{ref}. Furthermore it will be noticed that it was decided to implement the orthogonal residual algorithm in a Newton-Raphson style, where the tangential stiffness matrix was updated in each iteration to take into account changes in crack opening and thus also changes in the contributions from the enriched nodes during the iterations.

Table 5.1 *Orthogonal residual algorithm for XFEM*

initial state: $\mathbf{u}_0, \mathbf{f}_0, \Delta\mathbf{u}_0 = 0, E_{ref}, \Delta\boldsymbol{f}_0$

load increments n=1,2...,n_{max}

$\Delta\mathbf{u}_1 = \mathbf{K}_{T,n-1}^{-1}\Delta\mathbf{f}_n$

$\Delta\mathbf{u} = min\left(1, u_{max}/\|\Delta\mathbf{u}\|\right)\Delta\mathbf{u}$

$\Delta\mathbf{u}_0^T\Delta\mathbf{u} < 0$ *then* $\Delta\mathbf{u} = -\Delta\mathbf{u}$,$\Delta\mathbf{f} = -\Delta\mathbf{f}$

$j = 1$

Iterations i=1,2,...i_{max}

$\Delta\mathbf{q} = \mathbf{q}\left(\mathbf{u} + \Delta\mathbf{u}\right) - \mathbf{f}_{n-1}$

$\zeta = \mathbf{q}^T\mathbf{u}/\mathbf{f}_n^T\Delta\mathbf{u}$ — ζ *is the optimal load scaling factor*

$\mathbf{r} = \zeta\Delta\mathbf{f}_n - \Delta\mathbf{q}$ — $\mathbf{r}$ *is the unbalanced force vector*

$\mathbf{K}_{T,n} = \mathbf{K}_T\left(\mathbf{u} + \Delta\mathbf{u}\right)$

$\delta\mathbf{u} = \mathbf{K}_{T,n}^{-1}\mathbf{r}$ — $\delta\mathbf{u}$ *is the displacement correction*

$\delta\mathbf{u} = min\left(1, u_{max}/\|\delta\mathbf{u}\|\right)\delta\mathbf{u}$

$E_i = \mathbf{r}^T\delta\mathbf{u}$ — E_i *is the residual energy*

$\varepsilon_i = E_i/E_{ref}$

$\Delta\mathbf{u} = \Delta\mathbf{u} + \delta\mathbf{u}$

if $\varepsilon_i \leq$ *stop value*

$\Delta\sigma_{tip} = f_t - \sigma_{tip}$

if $\Delta\sigma_{tip} > \gamma f_t$ — γ *is the tolerance on* σ_{tip}

if $j = 1$

if $\Delta\sigma_{tip} > 0$

$\Delta\mathbf{f}_n = \Delta\mathbf{f} + \beta\Delta\mathbf{f}_0$ — β *is a load scaling factor*

if $\Delta\sigma_{tip} < 0$

$\Delta\mathbf{f}_n = \Delta\mathbf{f} - \beta\Delta\mathbf{f}_0$

end

else

$\delta\mathbf{f}_n = (f_t - \sigma_{tip})\frac{\Delta\mathbf{f}(j) - \Delta\mathbf{f}(j-1)}{\sigma_{tip}(j) - \sigma_{tip}(j-1)}$

$\Delta\mathbf{f}_n = \Delta\mathbf{f}_n - \phi\delta\mathbf{f}$ — ϕ *is a numerical damping factor*

end

$j = j+1, \quad \Delta\mathbf{u} = \mathbf{K}_{T,n}^{-1}\Delta\mathbf{f}_n, \quad \varepsilon_i = 1$

end

end

stop iteration when $\varepsilon_i \leq$ *stop value*

$\mathbf{u}_n = \mathbf{u}_{n-1} + \Delta\mathbf{u}_n$

$\mathbf{f}_n = \mathbf{f}_{n-1} + \zeta\Delta\mathbf{f}_n$

$\Delta\mathbf{u}_0 = \Delta\mathbf{u}$

stop load increments when $\|\mathbf{u}_n\| > u_{max}^{check}$

5.3 Numerical Examples

The performance of the new crack tip element was tested by modeling of fracture in the TPBT specimen and in the FPSB also considered for the fully cracked elements in Section 4.4. The results will be compared to those obtained applying fully cracked elements. For the TPBT-specimen the results are also compared to the results of a model applying standard interface elements in the commercial code DIANA. With regard to the FPSB, the XFEM results will also be compared to the experimental results obtained by Carpinteri et al. (1992).

The geometry of the considered test specimens and constitutive parameters for the concrete was given in Section 4.4 and reference is made to this section or to *Paper II*.

5.3.1 Three Point Beam Bending Test

For the TBTP specimen, both the structured mesh of 25 by 24 elements (24 elements over the beam height - 20 elements from the notch to the top of the beam) as well as an unstructured mesh of 709 elements holding 25 elements of varying size over the beam height were considered. The structured mesh is depicted in Figure 5.8, which shows the fractured beam, while the unstructured mesh is depicted in Figure 5.9. In both cases, the crack path was achieved by propagating the crack half the way through one element in each step. For the structured mesh, the notch was modeled as a predefined stress-free discontinuity. In the unstructured mesh, the notch was geometrically modeled, resulting in fairly small elements present just next to the tip of the notch. In both cases, the tolerance on the crack tip stress (γ in Table 5.1) was set to 1% of the material tensile strength. In the last three steps for each mesh, slightly higher tolerance on the tip stress was allowed - for the structured mesh up to 2.6% error and for the unstructured mesh up to 4% error.

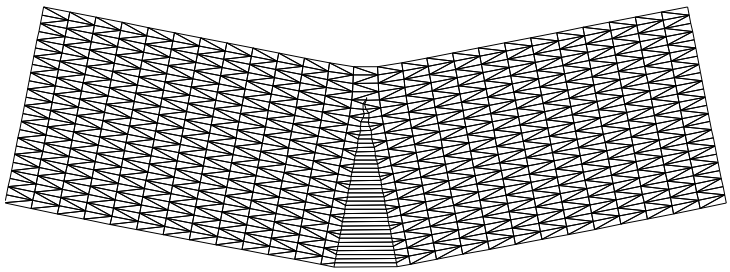

Figure 5.8 *Crack path for TPBT specimen modeled applying partly cracked elements in a structured mesh of 25 by 24 elements. The crack was propagated half an element length in each step.*

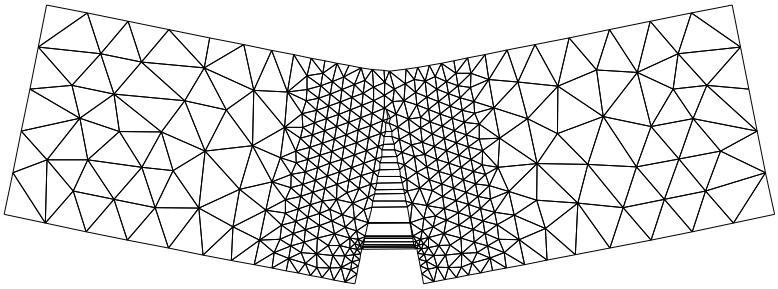

Figure 5.9 *Crack path for TPBT specimen modeled applying partly cracked elements in a unstructured mesh of 709 elements. The crack was propagated half an element length in each step.*

The load-displacement responses for the two models are depicted in Figure 5.10 and Figure 5.11. In both figures the results obtained applying partly cracked CST elements are compared to the results obtained applying fully cracked CST elements. The results are also compared to the results obtained applying 48 standard 3-node cohesive interface elements over the beam hight in the commercial code DIANA.

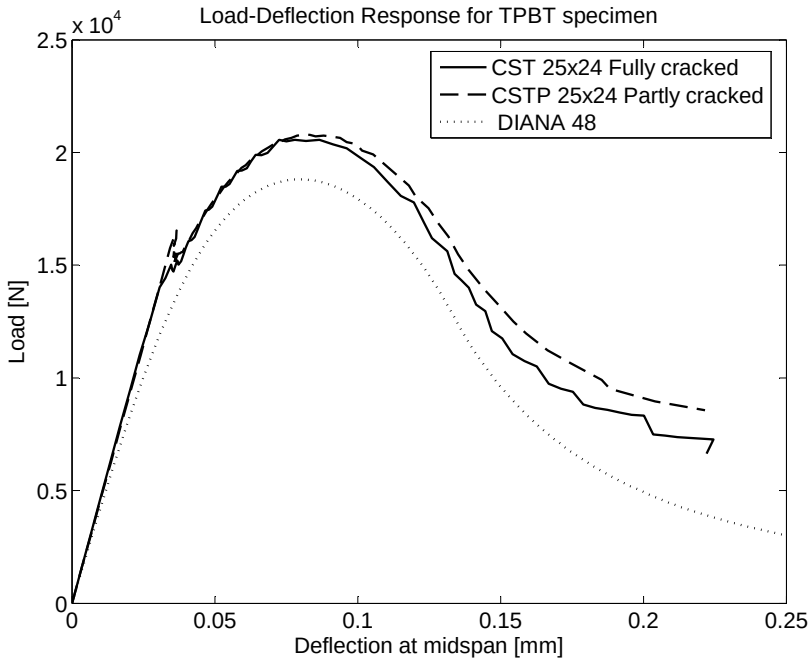

Figure 5.10 *Crack path for TPBT specimen modeled applying partly cracked elements in a structured mesh of 25 by 24 elements. The crack was propagated half an element length in each step.*

In both cases, the application of the new partly cracked tip-element produces a significantly smoother response than was obtained using fully cracked elements. The character-

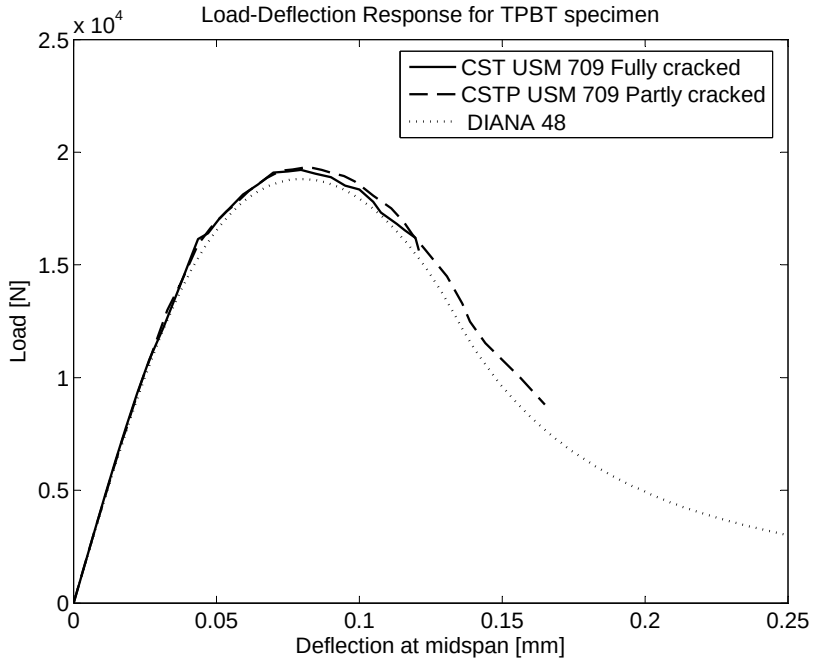

Figure 5.11 *Crack path for TPBT specimen modeled applying partly cracked elements in a unstructured mesh of 709 elements. The crack was propagated half an element length in each step.*

istics in terms of maximum load-carrying capacity and the overall shape of the response are, as expected, seen to be almost the same for fully cracked and partly cracked elements. With regard to the maximum load-carrying capacity, the structured mesh overestimates the load-carrying capacity by about 8%, while the unstructured mesh captures the maximum load-carrying capacity well. With regard to the post-peak response, the major part is captured well for both meshes. The difference in the determined load level for the last part of the post-peak response between the computations applying fully cracked and partly cracked elements is partly due to the fact that, when applying fully cracked elements, stresses equal to the material tensile strength are not assured in the crack-tip. Another reason is that for fully cracked elements, the criteria for crack growth is based on element local stresses, while in the partly cracked case, crack growth is based on average nodal stresses. The difference compared with the DIANA computations is partly due to the difference in the applied numbers of elements, the different order of applied elements, and partly to the tortuosity of the last part of the XFEM crack path. When there are about four elements left between the crack tip and the top of the beam, the limited capability of CST elements does not allow for a reasonable stress variation across the remaining elements, and solutions where the tip-stresses are equal to the material tensile stress may not be obtained.

From the load deformation responses - in particular for the structured mesh - a sudden drop in the load carrying capacity may be noted when the first element cracks. This non-smooth start of the non-linear response is due to the inability of one cracked CST element

to produce a smooth closing crack and thus reproduce the required cohesive crack profile. About three elements are required to model the smooth closure and thus the nature of a cohesive crack. The smooth closure of the cohesive crack can also be seen in Figure 5.12 which shows different stages of the crack propagation in the structured mesh. From Figure 5.12 it may also be noticed that the tortuosity of the crack increases as the crack approaches the top of the beam. This is due to the difficulties of modeling the true stress distribution with only a few un-cracked elements available. With regard to the cohesive stresses across the crack, it should also be mentioned that the crack in the element next to the notch becomes stress-free when the load has decreased to the level of the crack initiation (∼15kN) on the post-peak response.

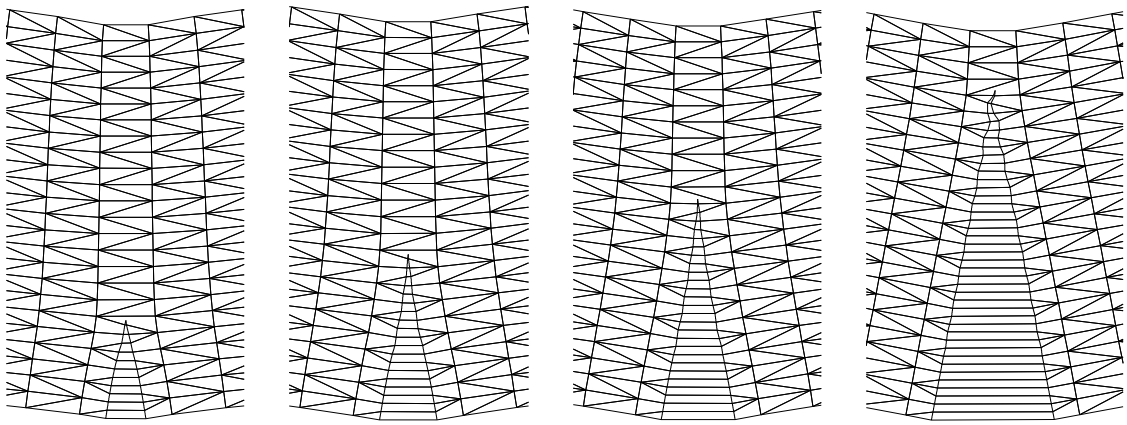

Figure 5.12 *Propagation of crack in structured mesh. (a) P=15.3kN, scaling factor 1140, (b) P=18.9kN, scaling factor 762, (c) P=20.8kN (max load), scaling factor 526, (d) P=8.6kN, scaling factor 208,*

In the application of partly cracked elements, it is interesting to study the behavior of the structural response when the crack propagates through a single element in more steps. In Figure 5.13, the load-deformation response is plotted for three different crack-length increments for a crack propagating through one element - in the present case when the crack is propagating through the element next to the tip-element in Figure 5.12(b). The plots are obtained prescribing a tolerance on the tip-stress of 0.01% of the tensile strength. From the figure, it can be seen that the deformation response depends only slightly on the size of the crack length increment. If an even lower tolerance on the tip-stresses is specified, even better results can be obtained. The Figure also reveals that a very smooth response is obtained when the crack propagates through an element in several increments. The importance of a smooth response was discussed in the introduction and when discussing the criteria for crack growth. The ability of the proposed partly cracked element in principle to model all possible load deformation states, and therefore to produce a smooth response for varying crack increments, represents a major improvement compared with elements only able to be fully cracked.

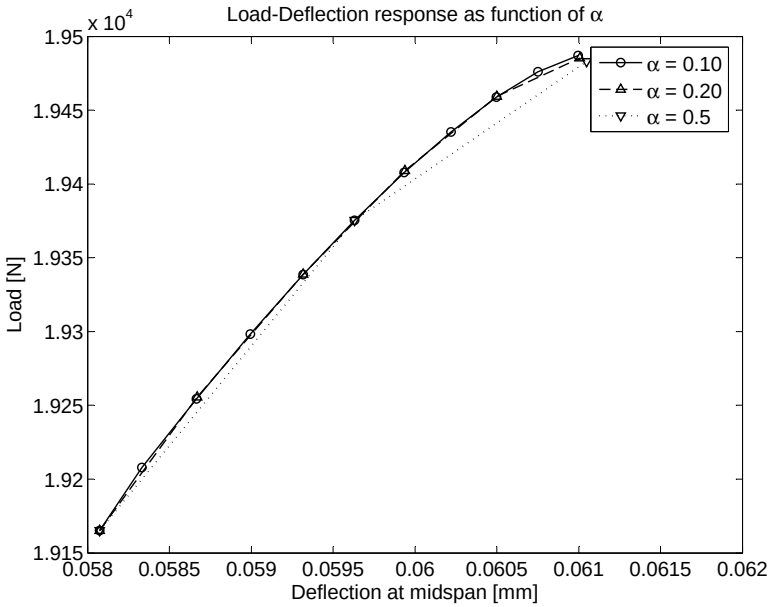

Figure 5.13 *Load deformation response as function of crack length increment when crack propagates through one element (the element next to the tip-element in 5.12(b)). α is the relative crack length increment. $\alpha = 1$ corresponds to the element being fully cracked.*

5.3.2 Four Point Shear Beam

As for the fully cracked elements a fairly coarse structured mesh of 1222 elements and 2549 nodes was considered for the XFEM computation. The mesh can be seen in Figure 5.14, which shows the crack path for the FPSB specimen. The results presented were obtained by propagating the crack in two increments across each element. This made it possible to test the modeling of a great variety of finite crack increments. In some cases, only a "corner" of an element was cut, while in other cases the crack followed close to the longest possible path through the element.

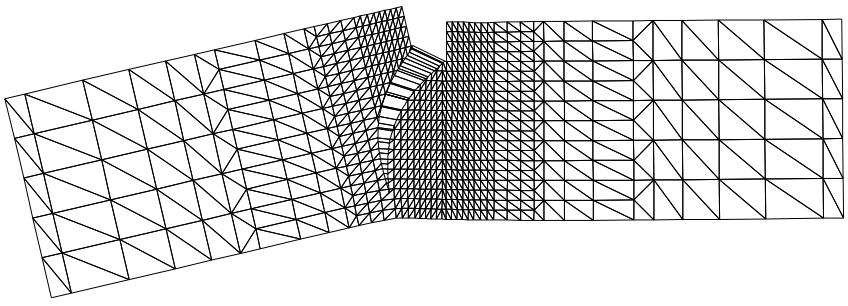

Figure 5.14 *Crack path for fracture in the FPSB specimen*

Figure 5.15 shows different stages of the developing crack. In Figure 5.16 the load deformation response obtained when applying the new partly cracked XFEM element is compared with the experimental results of Carpinteri et. al Carpinteri et al. (1992) and with the results obtained when applying fully cracked XFEM LST elements.

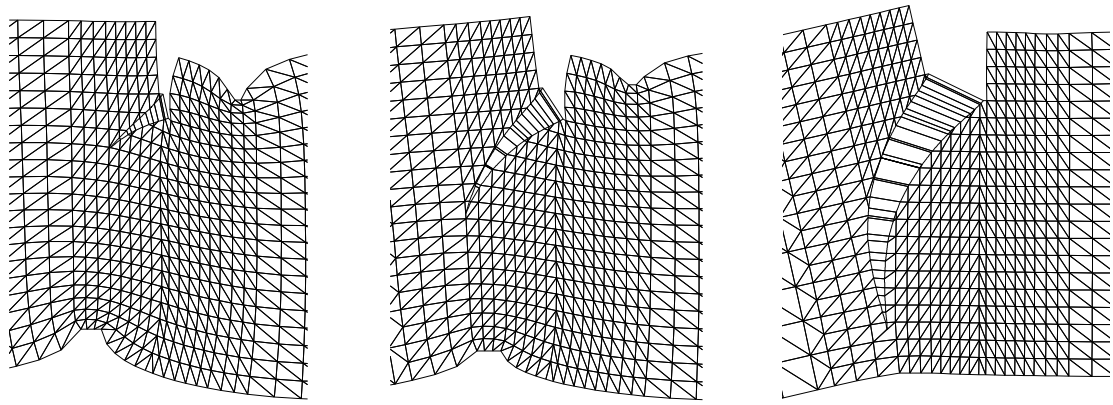

Figure 5.15 *Propagation of crack in FPSB. (a) P=62.6kN, scaling factor 973, (b) P=73.8kN, (Max load) scaling factor 581, (c) P=21.2kN, scaling factor 154.*

From Figure 5.14 and Figure 5.15, it can be seen that when applying the proposed partly cracked XFEM element, a nice smooth crack path is obtained that correlates well with what is observed in experiments. From the load-deformation response, it can also be seen that the results correlates well with the experimental results as well as with the previously obtained XFEM results for higher order elements.

5.4 Conclusion: Partly Cracked XFEM Elements

A new XFEM cohesive crack-tip element for cohesive cracking has been developed by the introduction of element-side local enrichment of elements cut by the discontinuity. The new enrichment was developed by the superposition of the standard nodal shape functions and standard nodal shape functions for a sub-triangle of the cracked element. When the suggested enrichment is applied, the tip element becomes capable of modeling the situation where equal stresses are present on both sides of the crack. The enrichment was implemented for the three-node triangular constant-strain triangle (CST) element. Based on average nodal stresses for the crack-tip element, a stress interpolation was computed through the tip element and the ability of the tip element to hold the crack-tip at different positions through the element was illustrated. The performance of the element in fracture mechanical benchmark tests was illustrated by modeling fracture in the notched three-point beam bending test and in the four-point shear beam test. The numerical examples show the element performs well even for fairly coarse meshes.

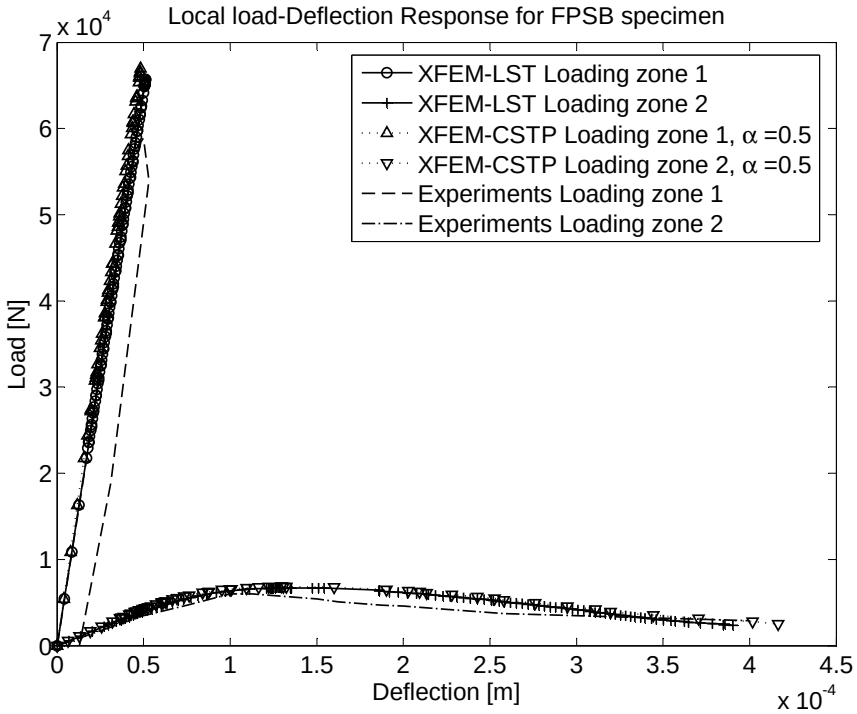

Figure 5.16 *Comparison of load-displacement response for FPSB obtained by the new XFEM model, XFEM results obtained by applying fully cracked LST elements, and experimental results from Carpinteri et al. (1992). Loading zone 1 refers to the loading zone to the left in Figure 4.13, while loading zone 2 refers to the loading zone to the right. Only every 5th data point in each XFEM series has been marked on the graphs.*

Further developments may include the extension of the scheme to higher order elements and optimization of the algorithm, outlined in Table 5.1, for solving the non-linear equations.

Chapter 6

Partly Cracked XFEM Interface Element

In the previous chapters focus has been on the modeling of crack propagation in the bulk concrete. However, the interaction between the bulk concrete and the reinforcement is the governing factor for the load carrying capacity of RC structures. A complete model for RC structures must be capable of modeling this interaction properly. Confining pressure on the reinforcement, mainly due to dilation caused by the ribs on the reinforcement, is of major importance for the stress transfer between concrete and reinforcement and a proper model must be capable of including this. Furthermore the model must be able to handle combined separation and sliding between reinforcement and concrete. To be operational it would be beneficial if all the effects could be modeled in a "super" element modeling the overall physical behavior of the interaction between reinforcement and concrete. Hereby the cumbersome individual meshing of reinforcement, bond zone and bulk concrete applied in earlier applications by e.g. Lundgren (1999) and Østergaard (2003) could be avoided. The basis for a super element may be a cohesive XFEM interface element for the bond zone. The XFEM interface element must be capable of handling intersecting cracks - longitudinal cracking along the reinforcement is initiated by cracks crossing the reinforcement as depicted in Figure 6.1. Furthermore the interface element must be capable of being partly cracked. Bond between concrete and reinforcement is a 3D phenomenon, however, initially the XFEM interface is considered in a plane version.

In this chapter a cohesive interface element that allows longitudinal cracking is developed. The interface element is formulated as a partly cracked element. At present the element is not able to model intersecting cracks.

Following the approach in the previous chapters this chapter opens with the development of the applied enrichment for the interface element. The basis for the element is a 6 node element with a quadratic interpolation in its longitudinal direction and a linear interpolation across the thickness. The applied variational formulation is equivalent to the one applied for the previously developed XFEM elements and reference is made to Chapter 4.2 or to *Paper III* for further details regarding the variational formulation. After discussing aspects of the implementation the performance of the interface element

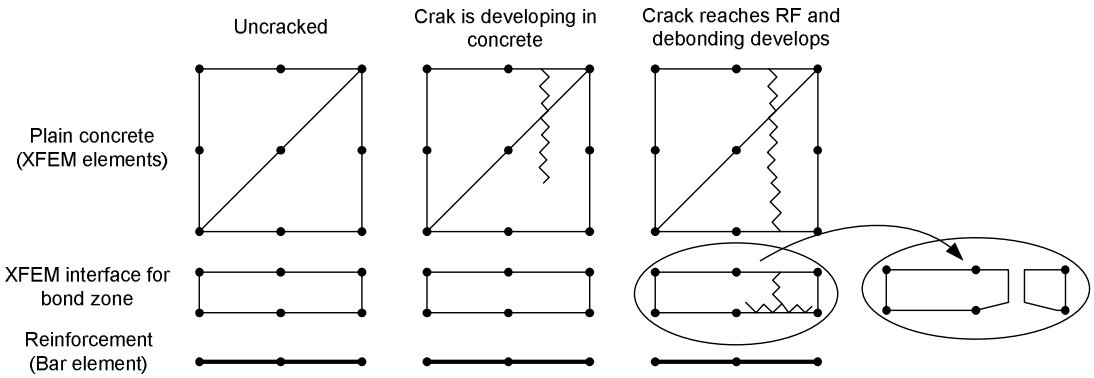

Figure 6.1 *Development of crack in interface between concrete and reinforcement*

is illustrated by modeling of crack propagation in the TPBT specimen also considered in Chapter 4 and 5. For details regarding the interface element reference is made to *Paper III*.

6.1 Enrichment of the Displacement Field

The enrichment of the displacement field is developed following the approach applied for the other XFEM elements proposed in this thesis. It is based on a true local partition of unity. The discontinuous interpolation matrix, $\mathbf{N}^d$, is chosen in line with the choice for the partly cracked element introduced in Chapter 5.

$$\mathbf{N}^d(x,y) = \sum_I H_I(x,y)\mathbf{N^*}_I(x,y) \tag{6.1}$$

where $H_I(x,y)$ is the 2D Heaviside step function for node I. The step function $H_I(x,y)$ is 0 on the same side of the discontinuity as node I and 1 on the other side. $\mathbf{N}^*_I$ is the part of $\mathbf{N}^*$ from node *I*. In the standard case $\mathbf{N}^*$ is chosen as $\mathbf{N}^c$, however, for the proposed element $\mathbf{N}^*$ is more general but able to describe the same variations as $\mathbf{N}^c$ if $\mathbf{N}^*$ and $\mathbf{N}^c$ are applied to the same domain. It has to be emphasized that $\mathbf{N}^*$ applied for the interface element is not the same as the $\mathbf{N}^*$ applied for the partly cracked element in Chapter 5. $\mathbf{N}^*$ for the interface element is developed below.

Referring to Figure 6.2, $\mathbf{N}^*$ is formulated in terms of the standard shape functions introducing the relative crack length $\alpha \in [0,1]$ as additional variable. The element may be interpreted as two superimposed elements, the first with a continuous field as shown in Figure 6.2(B), the second with a discontinuous field defined on $-1 < \zeta < -1 + 2\alpha$, $-1 \leq \eta \leq 1$, c.f. Figure 6.2(C). The element is not isoparametric, so ζ and η are scaled coordinates of a rectangle. The enrichment of the displacement field refers only to the cracked part of the element. It has to be emphasized that Figure 6.2(C) only serves to illustrate the interpretation of the enrichment; no extra nodes are added to the element,

the discontinuous degrees of freedom are stored in the standard nodes c.f. Figure 6.2(A). For completeness the shape functions $\mathbf{N}^*$ are written out in (6.2).

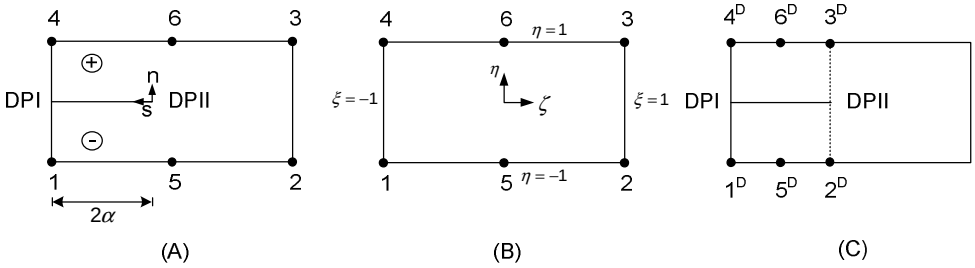

Figure 6.2 *Topology of interface element. (A) Topology of partly cracked interface element. (B) Standard element coordinates. (C) "Discontinuity" nodes in partly cracked interface element.*

$$
\begin{aligned}
N_1^* &= \tfrac{-1}{4\alpha^2}\,(\zeta+1-\alpha)\,(\zeta+1-2\alpha)\,(\eta-1)\\
N_2^* &= \tfrac{-1}{4\alpha^2}\,(\zeta+1)\,(\zeta+1-\alpha)\,(\eta-1)\\
N_3^* &= \tfrac{1}{4\alpha^2}\,(\zeta+1)\,(\zeta+1-\alpha)\,(\eta+1)\\
N_4^* &= \tfrac{1}{4\alpha^2}\,(\zeta+1-\alpha)\,(\zeta+1-2\alpha)\,(\eta+1)\\
N_5^* &= \tfrac{1}{2\alpha^2}\,(\zeta+1)\,(\zeta+1-2\alpha)\,(\eta-1)\\
N_6^* &= \tfrac{-1}{2\alpha^2}\,(\zeta+1)\,(\zeta+1-2\alpha)\,(\eta+1)
\end{aligned}
\tag{6.2}
$$

where α is shown in Figure 6.2(A)

The enrichment above is applied only to elements cut by the discontinuity; the enrichment is purely local. Therefore, the discontinuous displacement field will always be zero on edges where elements, not cut by the discontinuity, join the enriched element. To ensure that the crack closes at the tip, the discontinuity dofs corresponding to the tip are set to zero. Figure 6.3 illustrates a possible discontinuous displacement field modeled by applying the discontinuous shape functions in Eq. (6.2). Notice the capability to model smooth closure of the crack.

6.2 Aspects of Implementation

The implementation of the interface element follows to a large extend the approach applied for the XFEM elements previously developed in this thesis. However, the applied integration scheme for the interface element is slightly different compared to the scheme applied for the previous developed elements, and some comments will be given regarding this. Crack growth and the condition for smooth crack closure is also discussed in this section.

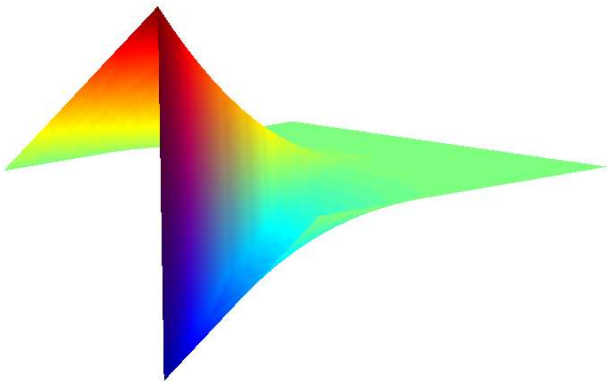

Figure 6.3 *Discontinuous displacement field for partly cracked interface element*

6.2.1 Integration of Enriched Elements

In elements cut by the discontinuity integration must be performed independently on each side of the discontinuity to ensure sufficient accuracy of the strain field. For the elements previously considered in this thesis the integration has been carried out applying the same sub-domain for the continuous and the discontinuous field. Here the integration of the continuous field is carried out by considering the entire area of the element. For the discontinuous field the area cut by the discontinuity is divided into two parts and individual integration performed on those sub-domains. For the three sub-domains a standard seven point Gauss integration scheme is applied. Concerning the line of discontinuity three point point integration is applied for the traction forces across the discontinuity. Figure 6.4 illustrates the integration scheme.

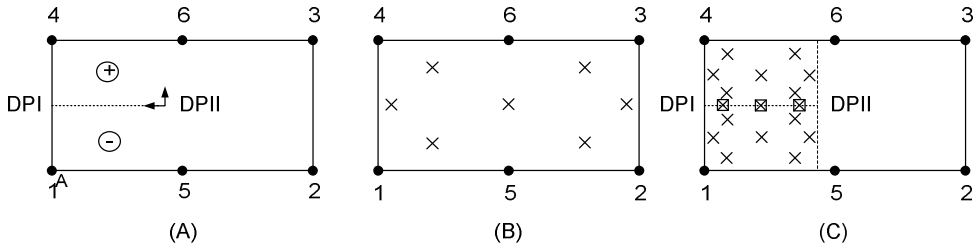

Figure 6.4 *Applied integration scheme. (A) Element partly cut by discontinuity. (B) Integration point for continuous field. (C) Integration point for discontinuous field, crosses mark integration points i continuum, crossed squares mark integration point in discontinuity.*

6.2.2 Criteria for Crack Growth and Smooth Closure

Determination of the crack growth direction is not an issue for an interface element. The interface element limits the crack growth to the longitudinal direction of the interface

element; the crack propagates along the centerline of the element. When the element is applied to practical modeling problems, the thickness of the element is chosen to be small compared to the element length.

As for the partly cracked element in Chapter 5 the crack is propagated when the material tensile strength is exceeded in the crack tip. The crack may either be incremented in fixed increments or to the location where the continuous displacement field yields stresses equal to the material tensile strength. Independently of the chosen strategy for incrementing the crack, the iteration scheme, equivalent to the one applied for the partly cracked element, c.f. Table 5.1, ensures stresses equal to the tensile strength in the crack tip. Hereby smooth crack closure is achieved when a sufficient number of elements are applied for the cohesive zone.

For the partly cracked CST element a linear stress interpolation based on average nodal stresses was applied for the crack-tip stress iterations. For the interface element it was expected that the displacement field would yield acceptable stresses for this purpose. However, when carrying out the initial test computations the stresses in the crack-tip element were found to be of insufficient quality. Therefore it was chosen to base the computation of the stresses applied for the crack-tip stress iterations on the nodal stresses in the neighboring elements.

6.3 Numerical Example

To illustrate the performance of the interface element the TPBT specimen also considered in Chapter 4 and 5 is modeled applying a narrow band of interface elements along the midsection of the beam. For further reference regarding the geometry and the material parameters for the TPBT specimen reference is made to Section 4.4 or to *Paper III*. In the example in *Paper III*, 6-node rectangular elements were applied for the modeling of the concrete outside the midsection of the beam. Here LST elements are applied for this purpose. Two meshes are considered - one holding 12 elements over the beam hight (2 of the 12 elements are pre-cracked, modeling the notch). The other mesh holds 24 elements over the beam height (of which 4 are modeling the notch). The DIANA computation utilizing 48 standard cohesive interface elements over the beam height serves as a reference. Results will be given for computations where the crack is propagated element by element, half the way or one fourth the way through an element in each load step. The tolerance on the crack-tip stress is set to 1% of the tensile strength of the concrete.

The results are given in terms of the load-displacement response in Figure 6.5 (12 elements over the beam hight) and in Figure 6.6 (24 elements over the beam hight).

From Figure 6.5 and 6.6 it is seen that the overall shape of the load deformation response is captured well for both meshes when propagating the crack element by element (the blue curves). As expected a more smooth response is obtained when more elements are applied. When the crack is propagated through an element in more steps (the red and green curves), the load steps representing the situation where the crack-tip is in the inte-

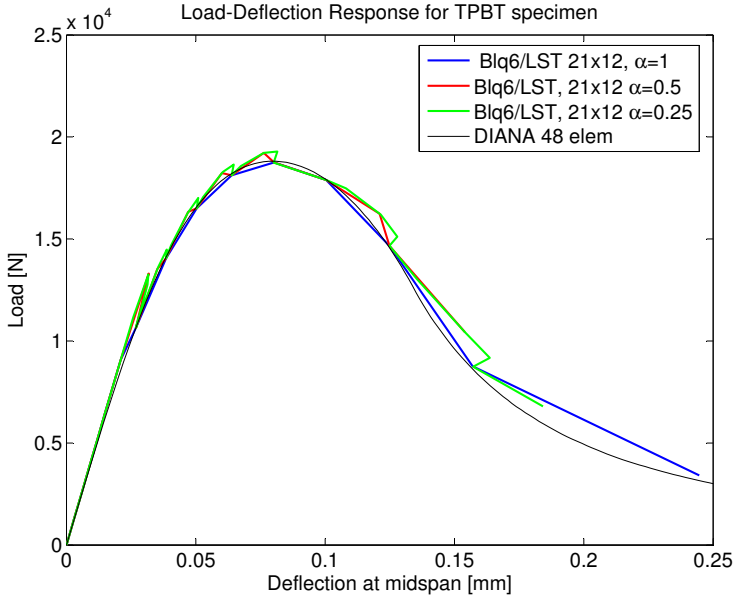

Figure 6.5 *Load deformation responses for TPBT specimen modeled applying 12 XFEM interface elements over the beam height. The figure depict results for propagating the crack in different increments, α refers to the crack size of the increments and for $\alpha = 1$ the crack is propagated element by element.*

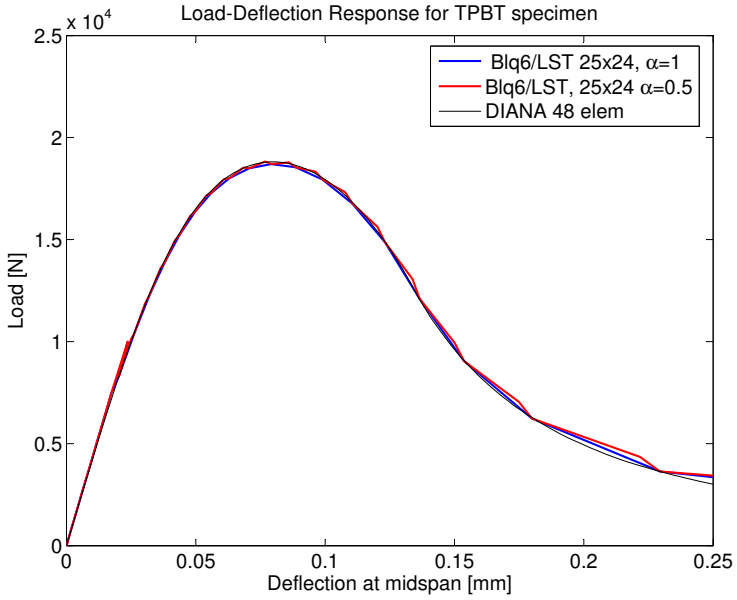

Figure 6.6 *Load deformation responses for TPBT specimen modeled applying 24 XFEM interface elements over the beam height. The figure depict results for propagating the crack in different increments; α refers to the crack size of the increments and for $\alpha = 1$ the crack is propagated element by element.*

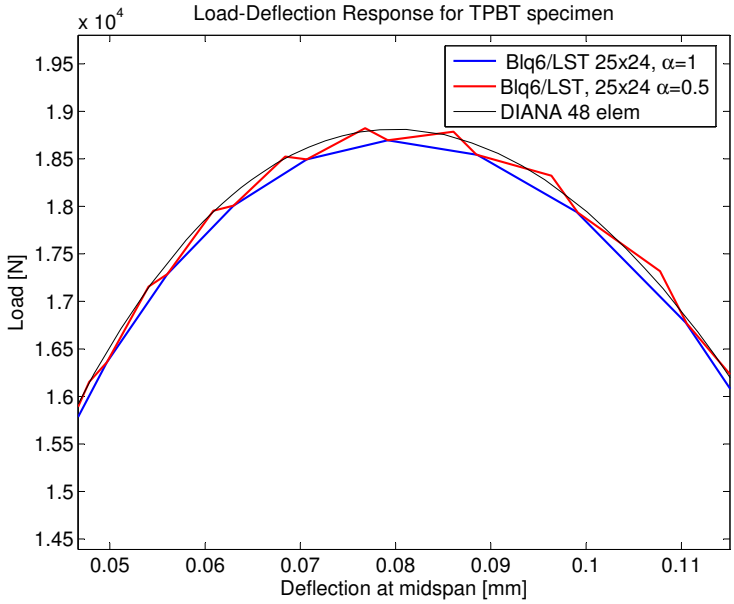

Figure 6.7 *Zoom on load deformation responses for TPBT specimen modeled applying 24 XFEM interface elements over the beam hight.*

rior of an element do not reproduce the expected load-deformation response. Figure 6.7 depicts a zoom of the peak load area of the load-deformation response given in Figure 6.6. Propagating the crack through the element in two steps, each representing the same increment in crack length, the expectation would be a smooth curve where the points representing the partly cracked state would be place approximately equally spaced between the points corresponding to the element being uncracked, respectively, fully cracked. The behavior observed for the partly cracked CST element and depicted in Figure 5.13 would be expected. It may be assumed that the deviation from the expected may be reduced by specifying a smaller tolerance on the convergence criterion for the crack-tip stresses. Specifying a tolerance that is a factor 10 lower than the one applied for the computations illustrated in Figure 6.5-6.7 does, however, not change the position of the points corresponding to the crack-tip element being partly cracked. It is assumed that the odd spacing is related to the stress interpolation when the XFEM interface element is partly cracked. It is therefore assumed that improvement of the basis for the stresses computation in the partly cracked element may reduce the observed problems.

Figure 6.8 depicts different stages of the propagating crack. Notice the smooth closure of the crack.

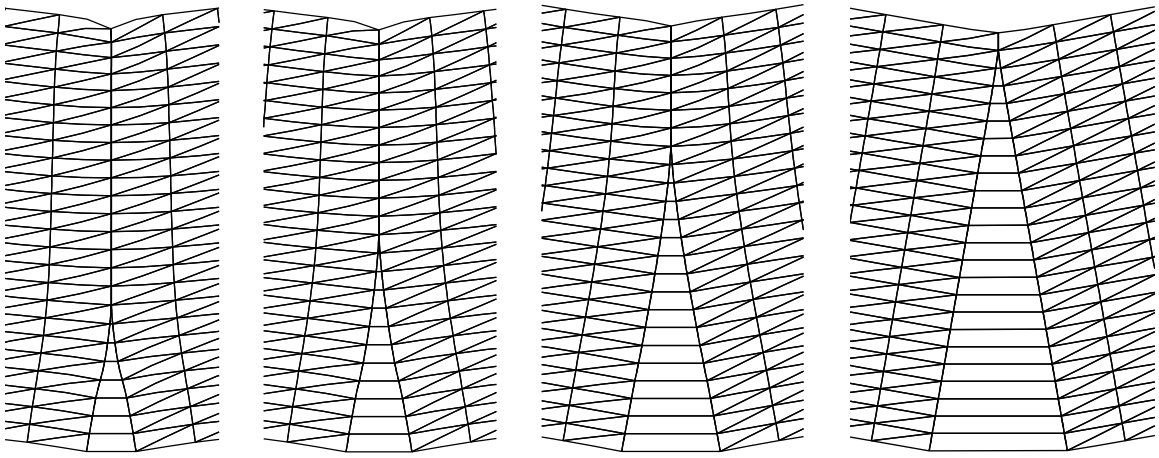

Figure 6.8 *Propagation of crack in XFEM interface elements. (a) P=13.9kN, scaling factor 988, (b) P=18.0kN, scaling factor 641, (c) P=16.7kN, scaling factor 409, (d) P=1.4kN, scaling factor 111.*

6.4 Conclusion on XFEM Interface Element

A cohesive XFEM interface element for modeling of the bond zone between concrete and reinforcement has been proposed. The interface element is capable of being partly cracked. By modeling of crack growth in a notched three point bending beam the performance of the element has been illustrated. Good results are obtained when the crack is propagated element by element trough a fairly coarse meshes. A smooth closing crack profile is achieved. When the crack-tip element is partly cracked some deviations from the expected are observed. The deviations are assumed related to the capability of the element to reproduce the correct stresses when the element is partly cracked. It is assumed that by improving the basis for the stress calculations the observed deviations may be minimized. To increase the computational speed the iteration scheme may be optimized. More demanding improvements of the interface element include the capability of the element to handle intersecting cracks as depicted in Figure 6.1.

Chapter 7

Conclusion

Existing methods for modeling of concrete structures are often not capable of predicting the development in crack patterns and crack widths and hence are not able to predict developments in structural properties such as e.g. the stiffness of concrete structures in the serviceability state.

This thesis contributes to the development of more proper numerical models for modeling of concrete structures by proposing a number of elements for modeling of crack growth in concrete within the framework of the eXtended Finite Element Method, XFEM. The fictitious crack model is implemented. By modeling of fracture mechanical benchmark tests the capabilities of the proposed XFEM elements for modeling of crack growth in concrete have been demonstrated.

The significant contribution in Chapter 4/*Paper I* is a direct enrichment scheme proposed for fully cracked elements. The enrichment scheme is able to model the same variation in the displacement field as the enrichment schemes suggested by other authors. However, the proposed enrichment scheme is more straightforward and easily implemented. The enrichment scheme was implemented for the 3-node CST element and for the 6-node LST element. The performance of the XFEM elements was illustrated by modeling of fracture in concrete benchmark tests such as the notched three point bending beam (TPBT) and the notched four point shear beam (FPSB). It was found necessary to apply a nonlocal strategy for determining the crack growth direction when considering CST elements whereas the crack growth direction could be based on element local stresses when LST elements were applied. The results obtained for the TPBT specimen were compared with results obtained by modeling of fracture in the TPBT applying standard cohesive interface elements in a commercial FEM code. The results for the FPSB was compared with experimental results and previously obtained XFEM results. Keeping in mind that the long time perspective is the capability to model real size civil structures investigations were carried out applying fairly coarse meshes. For the TPBT specimen reasonable results were obtained applying 24 CST elements over the beam hight. Applying LST elements good results were obtained applying only 12 elements over the beam hight. Modeling of fracture in the FPSB illustrated the capability to model a curved crack applying fully cracked LST elements. Good results were obtained in terms of predicted crack path as well as predicted

load-deformation response. Regarding the capability to model the entire load deformation response, the crack may be propagated until three elements remains uncracked in TPBT specimen when CST elements are applied - i.e. the major part of the post peak response may be modeled. Applying LST elements the crack may be propagated slightly closer to the top of the beam and hence a larger part of the post peak response may be captured.

The important contribution in Chapter 5/*Paper II* is a partly cracked tip element that is capable of modeling equal stresses at each side of the crack in the crack-tip element. Applying the enrichment proposed in *Paper I* or the enrichments found in the literature, the crack-tip element is not capable of modeling equal stresses at each side of the crack. This lack of capability was identified as one of the reasons for the requirement for a non-local procedure for determining the crack growth direction when applying fully cracked elements. Furthermore applying elements that are not capable of holding the crack tip within the interior of the element does not allow computation of all possible load-displacement states as it is normally required in a general non-linear procedure. Therefore a consistent XFEM element, capable of modeling equal stresses at each side of the crack in the tip-element, and capable of holding the crack tip at any point inside the element, was proposed in Chapter 5/*Paper II*. The capability to model equal stresses at each side of the crack in the tip-element was achieved by addition of extra enrichments to elements cut by the discontinuity. The extra enrichments are, like the enrichment applied for the fully cracked elements, based on a local partition of unity and influence only elements cut by the crack. The new enrichment scheme was applied to the CST element. The performance of the partly cracked element was illustrated by modeling of fracture in the previously considered TPBT specimen as well as in the FPSB specimen. For the TPBT specimen the partly cracked element yields a more smooth load-deformation response than obtained applying fully cracked elements and the crack path becomes less tortious. Considering different crack length increments for the crack propagating through one element it was illustrated that the computed load-deformation response is independent of the crack length increments. From the analysis of the TPBT specimen it was concluded that about three elements are required to model smooth closure of the crack. The improved capability of the partly cracked CST element was also illustrated by modeling of fracture in the FPSB specimen that was previously modeled applying fully cracked LST elements. It was found that in the case of the FPSB the partly cracked CST elements produce a smoother crack path than the fully cracked LST elements. Only negligible differences was found with regard to the load-deformation response.

The major finding in Chapter 6/*Paper III* is a new cohesive XFEM interface element. The element may be seen as a first step towards a super element for modeling of the bond zone between concrete and reinforcement. The proposed 6-node cohesive interface element is capable of being partly cracked. The performance of the interface element is illustrated by modeling of fracture in the previously considered TPBT specimen. The interface element yields a nice smooth crack closing profile. With respect to the load-deformation response the interface elements yield the best results when the crack tip is located on an element boundary. A better basis for computing stresses in the interface crack-tip element is assumed to improve the performance of the element when the element is partly cracked.

7.1 Further Work

The examples considered in this thesis illustrate the capabilities of the proposed XFEM elements. However, these examples only consider one propagating crack whereas the fracture of real RC structures involves the development of several localized cracks. In the long time perspective the XFEM scheme therefore needs to be extended so it may handle multiple cracking in the bulk concrete.

As expected and illustrated for fully cracked elements higher order elements yield better results than lower order elements. Therefore the good results obtained applying the low order partly cracked element may be further improved extending the enrichment scheme suggested in Chapter 5/*Paper II* to higher order elements. The extension to higher order elements - e.g. LST elements - may at first be seen as counterintuitive to the aim of being able to model real size civil structures. However, higher order elements may be justified by the fact that fewer elements will be required across the beam hight for modeling of e.g. bending. In total the outcome of applying higher order elements may therefore maybe a reduced number of degrees of freedom in the system considered. Also with regard to the partly cracked element the computational efficiency may be improved by optimizing the algorithm for solving the non-linear equations.

Focus in this thesis has been on problems where the crack is propagated in Mode I. However, the XFEM scheme is general, and it would be interesting to investigate e.g. problems with pronounced mixed mode crack opening applying the XFEM scheme together with a proper constitutive model for mixed-mode fracture of concrete.

With respect to the interface element a number of challenges still need to be met. First and foremost the stress representation needs to be improved. Hereby it is assumed that the performance of the interface elements, when being partly cracked, will improve. As it was discussed in the introduction to the interface element one of the requirements to the interface element is that it must be able to handle intersecting cracks. Therefore this capability also needs to be implemented in the interface element. Also a proper physical bond law capable of including the effects of the confining pressure needs to be identified before a super element modeling the overall behavior of the interaction between concrete and reinforcement may be formulated.

Bibliography

ABAQUS (2004a). *Analysis Users Manual, Volume III: Materials.* USA, 6.5 edition.

ABAQUS (2004b). *Analysis Users Manual, Volume IV: Elements.* USA, 6.5 edition.

ACI Committe 446 (1992). *ACI 446.1R-91, Fracture Mechanics of Concrete: Concepts, Models and Determination of Material Properties.* American Concrete Institute. Chairman of the Committee: Z.P. Bažant.

ACI Committee 318 (2002). *Building Code Requirements for Structural Concrete.* American Concrete Institute.

Areias, P. M. A. and Belytschko, T. (2005a). Analysis of three-dimensional crack initiation and propagation using the extended finite element method. *International Journal for Numerical Methods in Engineering*, 63:760–788.

Areias, P. M. A. and Belytschko, T. (2005b). Non-linear analysis of shels with arbitrary evolving cracks using XFEM. *International Journal for Numerical Methods in Engineering*, 62:384–415.

Arya, C. and Ofori-Darko, F. K. (1996). Influence of crack frequency on reinforcement corrosion in concrete. *Cement and Concrete Research*, 26(3):345–353.

Asferg, J. L., Poulsen, P. N., and Nielsen, L. O. (2004). Modeling of Cohesive Crack Applying XFEM. In Walraven, J., Blauwendraad, J., Scarpas, T., and Snijder, B., editors, *5th international PhD symposium in Civil Engineering*, pages 1261–1269. Balkema Publishers.

Asferg, J. L., Poulsen, P. N., and Nielsen, L. O. (2006). Modeling of crack propagation in concrete applying the XFEM. In Meshke, G., de Borst, R., Mang, H., and Bićanić, N., editors, *Computational Modeling of Concrete Structures*, pages 33–42. Taylor & Francis Group, London.

Asferg, J. L., Poulsen, P. N., and Nielsen, L. O. (2007a). A consistent partly cracked XFEM element for cohesive crack growth. *Submitted to International Journal for Numerical Methods in Engineering*, Available online /In press.

Asferg, J. L., Poulsen, P. N., and Nielsen, L. O. (2007b). A direct XFEM formulation for modelling of cohesive crack growth in concrete. *Computers and Concrete*, 4(2):83–100.

Bao, G. and Suo, Z. (1992). Remarks on crack-bridging concepts. *Applied Mehanics Review*, 45(8):355–366.

Barenblatt, G. I. (1962). The mathematical theory of equlibirum of cracks in britle fracture. *Advances in Applied Mechanics*, 7:55–129.

Bažant, Z. P. and Cedolin, L. (1979a). Blunt crack band propagation in finite element analysis. *Journal of the Engineering Mechanics Division, ASCE*, 105(EM2):297–315.

Bažant, Z. P. and Cedolin, L. (1979b). Fracture mechanics of reinforced concrete. *Journal of the Engineering Mechanics Division, ASCE*, 106(EM6):1287–1306.

Bažant, Z. P. and Cedolin, L. (1983). Finite element propagation of crack band propagation. *Journal of Structural Engineering, ASCE*, 109(ST2):69–82.

Bažant, Z. P. and Oh, B. H. (1983). Crack band theory for fracture of concrete. *Materials and structures, RILEM*, 16 (93):155–177.

Beeby, A. W. (1978). Cracking: what are crack width limits for? *Concrete*, pages 31–33.

Belytschko, T. and Black, T. (1999). Elastic crack growth in finite elements with minimal remeshing. *International Journal for Numerical Methods in Engineering*, 45 (5):601–620.

Belytschko, T., Fish, J., and Engelmann, B. E. (1988). A finite element with embeded localization zones. *Computer Methods in Applied Mechanics and Engineering*, 70:247–256.

Belytschko, T., Krongauz, Y., Organ, D., Fleming, M., and Krysl, P. (1996). Meshless methods: an overview and recent developments. *Computer Methods in Applied Mechanics and Engineering*, 139:3–47.

Brühwiler, E. and Wittmann, F. H. (1990). The wedge splitting test, a new method of performing stable fracture mechanics tests. *Engineering Fracture Mechanics*, 35(1/2/3):117–125.

Carol, I., López, C. M., and Roa, O. (2001). Micromechanical analyis of quasi-brittle materials using fracture-based interface elements. *International Journal for Numerical Methods in Engineering*, 52:193–215.

Carol, I., Prat, P. C., and Lopez, C. M. (1997). Normal/shear cracking model: Application to discrete crack analysis. *ASCE Journal of Engineering Mechanics*, 123(8):765–773.

Carpinteri, A., Valente, S., Ferrara, G., and Melchiorri, G. (1992). Is mode II fracture energy a real material property? *Computers and Structures*, 48 (3):397–413.

Christiansen, M. B. (2000). *Serviceability limit state analysis of reinforced concrete*. Department of Structural Engineering and Materials, The Technical University of Denmark.

Christiansen, M. B. and Nielsen, M. P. (2001). Plane stress tension stiffening effects in reinforced concrete. *Magazine of concrete Research*, 53(6):357–365.

Cox, B. and Marshall, D. (1991). Stable and unstable solutions for bridged cracks in various specimens. *Acta Metallurgica et Materialia*, 39(4):579–589.

Damkilde, L. and Kirk, J. (1981). Ruptus - a program for rupture analysis (in danish). Report 8115, ADB-udvalget.

Damkilde, L. and Krenk, S. (1997). Limits - a system for limit state analysis and material layout. *Computers and Structures*, 64(1-4):709–718.

Daux, C., Moës, N., Dolbow, J., Sukumar, N., and Belytschko, T. (2000). Arbitrary branched and intersecting cracks with the extended finite element method. *International Journal for Numerical Methods in Engineering*, 48:1741–1760.

de Borst, R. and Nauta, P. (1985). Non-orthogonal cracks in a smeared finite element model. *Engineering Computations*, 2:35–46.

Diana User Manual (2003a). *DIANA User Manual, Element Libary*. TNO Building and Construction Research, P.O. Box 49, 2600 AA Delft, The Netherlands, 8.1 edition.

Diana User Manual (2003b). *DIANA User Manual, Material Libary*. TNO Building and Construction Research, P.O. Box 49, 2600 AA Delft, The Netherlands, 8.1 edition.

Dick-Nielsen, L., Stang, H., and Poulsen, P. N. (2006). Simulation of strain-hardening in ECC uniaxial test specimen by use of a damage mechanics formulation. In Meschke, de Borst, Mang, and Bićanić, editors, *Computational Modelling of Concrete Structures*, pages 319–328. Taylor & Francis Group, London.

DS 411 (1999). *Code of Practice for the structural use of concrete*. Dansk Standard. eds. E. Skettrup, B. Feddersen, G. Heshe, H.S. Nielsen, J. Westh, M.E. Andersen and F. Bach.

Dugdale, D. S. (1960). Yielding of steel sheets containing slits. *Journal of the Mechanics and Physics of Solids*, 8:100–104.

Dvorkin, E. N., Cuitiño, A. M., and Gioia, G. (1990). Finite elements with displacement interpolated embedded localization lines insensitive to mesh size and distortions. *Computer Methods in Applied Mechanics and Engineering*, 90:829–844.

Ferro, G. (2002). Mulitlevel bridge crack model for high-performance concretes. *Theoretical and Applied Fracture Mechanics*, 38(2):177–190.

Gálvez, J. C., Červenka, J., Cendón, D. A., and Saouma, V. (2002). A discrete approach to normal/shear cracking of concrete. *Cement and Concrete Research*, 32:1567–1585.

Griffith, A. A. (1921). The phenomena of rupture and flows in solids. *Philosophical Transactions of the Royal Society of London. Series A, Containing Papers of a Mathematical or Physical Character*, 221:163–198.

Gupta, A. K. and Akbar, H. (1984). Cracking in reinforced concrete analysis. *Journal of Structural Engineering, ASCE*, 110(8):1735–1746.

Hassanzadeh, M. (1991). *Behaviour of fracture process zones in concrete influenced by simultaneously applied normal and shear displacements*. PhD thesis, Division of Building Materials at the Lund Institute of Technology, Lund, Sweden.

Hawkins, N. M. (1985). The role of fracture mechanics in conventional reinforced concrete design. In Shah, S. P., editor, *Application of Fracture to Cementitious Composites, NATO Advanced Research Workshop, Evanston, IL, USA, 1984*, pages 639–666. Matinus Nijhoff Publishers, Dordrecht.

Hillerborg, A., Moder, M., and Peterson, P.-E. (1976). Analysis of crack formation and crack growth in concrete by means of fracture mechanics and finite elements. *Cement and Concrete Research*, 6:773–782.

Hordijk, D. A. (1991). *Local Approach to Fatigue of Concrete,*. PhD thesis, Delft University of Technology.

Irwin, G. R. (1957). Analysis of stresses and strain near the end of a crack traversing a plate. *ASME Journal of Applied Mechanics*, 24:361–364.

Jirásek, M. (2000). Comparative study on finite elements with embedded discontinuities. *Computer Methods in Applied Mechanics and Engineering*, 188:307–330.

Jirásek, M. (2004). *Modelling of Localized Inelastic Deformation, Lecture Notes*. Czech Technical University.

Jirásek, M. and Belytschko, T. (2002). Computational resolution of strong discontinuities. In Mang, H. A., Rammerstorfer, F. G., and Eberhardsyeiner, J., editors, *Proceedings of Fifth World Congress on Computational Mechanics*. Vienna, Austria.

Jirásek, M. and Zimmermann, T. (1998a). Analysis of rotating crack model. *ASCE Journal of Engineering Mechanics*, 124:842–851.

Jirásek, M. and Zimmermann, T. (1998b). Rotating crack model with trasistion to scalar damage. *ASCE Journal of Engineering Mechanics*, 124:277–284.

Jirásek, M. and Zimmermann, T. (2001). Embedded crack model: Part I, basic formulation, Part II combination with smeared cracks. *International Journal for Numerical Methods in Engineering*, 50:1269–1305.

Karihaloo, B. L. (1995). *Fracture mechanics and structural concrete*. Longman Scientific and Technical.

Karihaloo, B. L. and Xiao, Q. Z. (2002). Modelling of stationary and growing cracks in FE framework without remeshing: a state-of-the-art review. *Computers and Structures*, 81:119–129.

Krabbenhoft, K. and Damkilde, L. (2002). Lower bound limit analysis of slabs with nonlinear yield criteria. *Computers and Structures*, 80:2043–2057.

Krenk, S. (1995). An orthogonal residual procedure for nonlinear finite element equations. *International Journal for Numerical Methods in Engineering*, 38:823–839.

Li, V. C. and Maalej, M. (1996). Toughening in cement based composites. Part I: cement, mortar and concrete. *Cement and Concrete Composites*, 18:223–237.

Linsbauer, H. N. and Tschegg, E. K. (1986). Fracture energy determination of concrete with cube shaped specimens (in german). *Zement und Beton*, 31:38–40.

Lotfi, H. R. and Shing, P. B. (1995). Embedded representation of fracture in concrete with mixed finite elements. *International Journal for Numerical Methods in Engineering*, 38:1307–1325.

Lundgren, K. (1999). *Three-Dimensional Modeling of Bond in Reinforced Concrete.* PhD thesis, Division of Concrete Structures, Department of Structural Engineering, Chalmers University of Technology.

Mellenk, J. M. and Babuška, I. (1996). The partion of unity finite element method: basic theory and application. *Computer Methods in Applied Mechanics and Engineering*, 139:289–314.

Mergheim, J., Kuhl, E., and Steinmann, P. (2005). A finite element method for the computational modelling of cohesive cracks. *International Journal for Numerical Methods in Engineering*, 63:276–289.

Moës, N. and Belytschko, T. (2002). Extended finite element method for cohesive crack growth. *Engineering Fracture Mechanics*, 69:813–833.

Moës, N., Dolbow, J., and Belytschko, T. (1999). A finite element method for crack growth without remeshing. *International Journal for Numerical Methods in Engineering*, 46:131–150.

Mohammed, T. U., Otsuki, N., Hisada, M., and Shibata, T. (2001). Effect of crack width and bar types on corrosion of steel in concrete. *Journal of Materials in Civil Engineering*, 13:194–201.

Needlemann, A. (1990). An analysis of tensile decohesion along an interface. *Journal of the Mechanics and Physics of Solids*, 38:289–324.

Ngo, D. and Scordelis, C. (1967). Finite element analysis of reinforced concrete beams. *ACI Journal*, 64:152–163.

Nielsen, M. P. (1999). *Limit analysis and concrete plasticity.* CRC Press, second edition.

Nooru-Mohamed, M. B. (1992). *Mixed-mode fracture of concrete: an experimental approach.* PhD thesis, Delft University of Technology, The Netherlands.

Ohgishi, S., Ono, H., Takatsu, M., and Tanahashi, I. (1986). Influence of test conditions on fracture toughness of cement paste and mortar. In Wittmann, F. H., editor, *Fracture Toughness and Fracture Energy of Concrete*, pages 281–290. Elsevier Science Publishers B.V., Amsterdam.

Olesen, J. F. (2001). Fictitious crack propagation in fiber-reinforced concrete beams. *ASCE Journal of Engineering Mechanics*, 127(3):272–280.

Oliver, J. (1996). Modelling strong discontinuities in solid mechanics via strain softening constitutive equations. Part 1: Fundamentals. Part 2: Numerical simulation. *International Journal for Numerical Methods in Engineering*, 39:3575–3623.

Ortiz, M., Leroy, Y., and Needlemann, A. (1987). A finite element method for localized failure analysis. *Computer Methods in Applied Mechanics and Engineering*, 61:189–214.

Østergaard, L. (2003). *Early-Age Fracture Mechanics and Cracking of Concrete, Experiments and Modelling*. PhD thesis, The Technical University of Denmark.

Østergaard, L. and Olesen, J. F. (2004). Comparative study of fracture mechanical test methods for concrete. In Li, V. C., Leung, C. K. Y., Willam, K. J., and Billington, S. L., editors, *Fracture Mechanics of Concrete Structures*, pages 455–462. Ia-FraMCos.

Poulsen, P. N. and Damkilde, L. (2000). Limite state analysis of reinforced concrete plates subjected to in-plane forces. *International Journal of Solids and Structures*, 37:6011–6029.

Prasad, M. V. K. V. and Krishnamoorthy, C. (2002). Computational model for discrete crack growth in plain and reinforced concrete. *Computer Methods in Applied Mechanics and Engineering*, 191:2699–2725.

Rashid, Y. R. (1968). Ultimate strength analysis of prestressed concrete pressure vessels. *Nuclear Engineering and Design*, 7:334–344.

RILEM (1985). Determination of the fracture energy of mortar and concrete by means of three-point bend tests on notched beams. *Materials and Structures*, 18(106):99–101. Prepared by TC50-FMC.

Rots, J. G. (1988). *Computational modeling of concrete fracture*. PhD thesis, Delft University of Technology, Delft, The Netherlands.

Schießl, P. and Raupach, M. (1997). Laboratoty studies and calculations on the influence of crack width of chloride-induced corrosion of steel in concrete. *ACI Materials Journal*, 94(1):56–62.

Shah, S. P., Stuart, E. S., and Ouyang, C. (1995). *Fracture Mechanics of Concrete*. John Wiley and Sons, Inc.

Sluys, L. J. and Berends, A. H. (1998). 2D/3D modelling of crack propagation with embeded discontinuity elements. In R. de Borst, N. Bićanić, H. M., editor, *Computational Modeling of Concrete Structures*, pages 291–300. Balkema, Rotterdam.

Stang, H., Olesen, J., Poulsen, P., and Nielsen, L. (2006a). Application of the cohesive crack in cementitious material modeling. In Meschke, G., de Borst, R., Mang, H., and Bićanić, N., editors, *Computational Modelling of Concrete Structures*, pages 443–449. Taylor & Francis.

Stang, H., Olesen, J. F., Poulsen, P. N., and Nielsen, L. D. (2006b). On the applications of cohesive crack modeling in cementitious materials. *Materials and Structures*, Accepted for publication.

Stankowski, T., Runesson, K., and Sture, S. (1993). Fracture and slip of interfaces in cementitious composites. I: Characteristics, and II: Implementation. *ASCE Journal of Engineering Mechanics*, 119:292–327.

Stolarska, M., Chopp, D., Moës, N., and Belytschko, T. (2001). Modeling crack growth by level sets in the extended finite element method. *International Journal for Numerical Methods in Engineering*, 51:943–960.

Sukumar, N., Moës, N., Moran, B., and Belytschko, T. (2000). Extended finite element method for three-dimensional crack modeling. *International Journal for Numerical Methods in Engineering*, 48:1549–1570.

Tada, H., Paris, P., and Irwin, G. (1985). *The Stress Analysis of Cracks Handbook*. Paris Productions Incorporated, St. Louise, Missouri, USA.

Vandervalle, L. (2000). Test and design methods for steel fiber reinforced concrete. Recommendations for bending test. *Materials and Structures*, 33:3–5.

Walter, R. (2005). *Cement-Based Overlay for Orthotropic Steel Bridge Decks*. PhD thesis, Department of Civil Engineering, the Technical University of Denmark.

Walter, R. and Olesen, J. F. (2006). Cohesive mixed mode fracture modelling and experiments. *Journal of Engineering Fracture Mechanics*. Sumbitted for publication.

Wells, G. N. and Sluys, L. (2001). A new method for modeling of cohesive cracks using finite elements. *International Journal for Numerical Methods in Engineering*, 50 (12):2667–2682.

Williams, M. L. (1952). Stress singularities resulting from various equations for certain plane crack problems. *ASME Journal of Applied Mechanics*, 19:526–528.

Xiao, Q. Z. and Karihaloo, B. L. (2005). Improving the accuracy of XFEM crack tip fields using higher order quadrature and statically admissible stress recovery. *International Journal for Numerical Methods in Engineering*, 66:1378–1410.

Xiao, Q. Z. and Karihaloo, B. L. (2006). Asymptotic fields at frictionless and frictional cohesive crack tips in quasi-brittle materials. *Journal of Mechanics of Materials and Structures*, 1:881–910.

Yang, Z. and Chen, J. (2004). Fully automatic modelling of cohesive discrete crack propagation in concrete beams using local arc-length methods. *International Journal of Solids and Structures*, 41:801–826.

Yang, Z. J. and Chen, J. (2005). Finite element modeling of mulitple cohesive discrete crack propagation in reinforced concrete beams. *Engineering Fracture Mechanics*, 72:2280–2297.

Zi, G. and Belytschko, T. (2003). New crack-tip elements for XFEM and applications to cohesive cracks. *International Journal for Numerical Methods in Engineering*, 57:2221–2240.

Zienkiewicz, O. C. and Taylor, R. L. (2000). *The Finite Element Method, Volume 1, The Basis*. Butterworth-Heinemann.

List of Figures

List of Tables

Part II

Appended Papers

Paper I

A direct XFEM formulation for modeling of cohesive crack growth in concrete

Computers and Concrete, Vol 4, No 2 (2007) 83-100

A direct XFEM formulation for modeling of cohesive crack growth in concrete

J. L. Asferg[†], P. N. Poulsen[‡] and L. O. Nielsen[‡†]

Department of Civil Engineering, Technical University of Denmark, DK-2800 Kgs. Lyngby, Denmark

(Received August 17, 2006, Accepted February 5, 2007)

Abstract. Applying a direct formulation for the enrichment of the displacement field an extended finite element (XFEM) scheme for modeling of cohesive crack growth is developed. Only elements cut by the crack is enriched and the scheme fits within the framework of standard FEM code. The scheme is implemented for the 3-node constant strain triangle (CST) and the 6-node linear strain triangle (LST). Modeling of standard concrete test cases such as fracture in the notched three point beam bending test (TPBT) and in the four point shear beam test (FPSB) illustrates the performance. The XFEM results show good agreement with results obtained by applying standard interface elements in FEM and with experimental results. In conjunction with criteria for crack growth local versus nonlocal computation of the crack growth direction is discussed.

Keywords: extended finite elements-XFEM; fracture mechanics; cohesive crack growth.

1. Introduction

Throughout the last century research has been carried out regarding methods to determine the ultimate strength of reinforced concrete structures. Today well-documented methods are available for estimating the ultimate strength of most reinforced concrete (RC) structures and the theory of rigid plasticity is highly developed (e.g. Nielsen 1999). However, most of these methods require the use of empirical factors and do not consider phenomena such as size effects and reinforcement arrangement in a fully consistent way. Regarding RC structures in the serviceability limit state the predictive capability of existing methods of analysis is limited. Predictions regarding the development in e.g., stiffness due to cracking, development in crack widths and the deformations at ultimate loading for RC structures are often based on empiric rules.

A consistent model for modeling of RC structures may be obtained if the model is able to predict the cracking that takes places long before the ultimate capacity of RC structures is reached. Cracking influences structural properties and is one of the governing factors in relation to durability and service life prediction. A consistent approach for modeling of concrete may be based on the concept of fracture mechanics and the capability to model localized crack growth. Aiming at the capability to model real size RC structures with complex shapes it would be beneficial if the model fits within the concept of the finite element method (FEM) and that the method do not require to

†Corresponding Author, E-mail: jla@byg.dtu.dk
‡E-mail: pnp@byg.dtu.dk
‡†E-mail: lon@byg.dtu.dk

dense FEM meshes.

Concrete belongs to the group of materials that are classified as being quasi-brittle (e.g. Karihaloo 1995) and a suitable model for crack propagation in concrete is the fictitious crack model by Hillerborg, *et al*. (1976) that models the crack propagation within the framework of cohesive cracking (Barenblatt 1962, Dugdale 1960).

Today several commercial FEM codes have interface elements suitable for modeling of discrete cohesive cracks. The use of interface elements however requires the crack path to be known beforehand and is therefore less relevant when the aim is to predict crack patterns. Several programs also have elements for smeared cracking that are based on the concept of a crack band (Bažant and Oh 1983) however the smeared approach is not well-suited for modeling of localized crack growth.

Remeshing has been used as a tool when modeling crack growth, (Bouchard, *et al.* 2000, 2002, Patzák and Jirásek 2004). Remeshing is however cumbersome hence it requires projection of variables between different meshes. Three methods: the element free Galerkin method (Belytschko, *et al.* 1996), the embedded crack methods (e.g. Jirásek 2000) and the extended finite element method (XFEM) (Belytschko and Black 1999) allow modeling of crack growth without remeshing. While the element free Galerkin method deviates in its principal structure from the structure of commercial FEM codes, embedded cracks and the XFEM fits well in the structure of commercial FEM codes. The XFEM is however preferable to the concept of embedded cracks hence in the XFEM the strains are independent in the separated parts of the elements whereas they are partly coupled in the embedded concept (Jirásek and Belytschko 2000).

In the extended finite element method the displacement field consists of two parts, a continuous and a discontinuous part. The continuous part is the standard displacement field corresponding to the situation without any cracks. The discontinuous displacement field is based on local partitions of unity (Melenk and Babuška 1996) and enables the element to include a discontinuity, in the present case a cohesive crack.

XFEM has been applied to different problems within the area of fracture mechanics. While it was first developed for linear elastic fracture mechanics (Belytschko and Black 1999, Moës, *et al.* 1999, Stolarska, *et al*. 2001) it has now been applied to different problems such as cohesive cracking (Wells and Sluys 2001, Moës and Belytschko 2002, Zi and Belytschko 2003, Mergheim, *et al*. 2005) arbitrary branched and intersecting cracks (Daux, *et al*. 2000) and three dimensional crack propagation (Sukumar, *et al.* 2000). Reference is also made to Karihaloo and Xiao (2002) for an overview of the earlier works regarding the XFEM.

Considering linear elastic fracture mechanics (Belytschko and Black 1999, Moës, *et al.,* 1999, Stolarska, *et al*. 2001) nodes in elements fully cut by the discontinuity was enriched by the step function while the tip element was enriched with an asymptotic field. In cohesive crack models, cohesive stresses act near the crack tip and it is assumed that no singularity is present at the crack tip. However, considering partly cracked elements for cohesive crack growth Moës and Belytschko (2002) enriched the crack tip element with a set of nonsingular branch functions to model the displacement field around the tip of the discontinuity. Wells and Sluys (2001) considered fully cracked elements and applied the Heaviside step function as the only enrichment of nodes with a supporting side cut by the discontinuity. Applying the Heaviside step function as in Wells and Sluys (2001) the nodal enrichment influences not only the displacement field in the elements cut by the discontinuity but also in the elements sharing the enriched nodes, i.e., the enrichments typically have to be dealt with in a band of three elements along the line of the discontinuity.

Zi and Belytschko (2003) proposed an enrichment of the crack tip element for the case of partly

cracked elements in which the shifted sign function was applied. The application of the shifted sign function to a 1D example is illustrated in Fig. 1(b). As shown the enrichment only influences elements cut by the discontinuity. In Mergheim, *et al*. (2005) a dual node strategy was applied and the displacement field was not decomposed into a continuous and discontinuous part in the same way as in the approach by Wells and Sluys (2001) and Zi and Belytschko (2003). However even though the basis for the shape functions is different the scheme in Mergheim, *et al. (*2005) is able to model the same variation in the displacement field as in the scheme by Zi and Belytschko (2003). The enrichment as applied by Mergheim, *et al*. (2005) is illustrated in Fig. 1(c). Although the authors in Mergheim, *et al.* (2005) distinct their approach from the XFEM it is essentially based on the same concept.

In the present paper a direct XFEM scheme for modeling of cohesive crack growth is developed using the Heaviside step function and limiting the discontinuous displacement field to elements cut by the crack. The XFEM formulation follows the concepts proposed in Asferg, *et al.* (2004). The Heaviside step function, H, is applied as the only enrichment of elements cut by the discontinuity c.f. Fig. 1(a).

Fig. 1 illustrates how a displacement jump of the magnitude of one may be modeled applying the three different approaches discussed above. For the present approach and the approach by Zi and Belytschko (2003) the two upper sketches illustrate the continuous displacement fields for node 1 respectively node 2 while sketch 3 and 4 illustrate the discontinuous displacement fields. Regarding the approach by Mergheim, *et al*. (2005) the two upper figures illustrate the displacement field for the two "original" nodes 1 and 2 while Figs. 3 and 4 depict the displacement fields for the dual nodes 1* and 2*. Finally the lower sketch in each row depicts an example of a displacement field containing a jump of the magnitude of one. From Fig. 1 it is evident that the difference between the three approaches is a question about the applied basis for modeling the displacement field. Compared to the enrichment by the shifted sign function in Zi and Belytschko (2003) and the enrichment in Mergheim, *et al*. (2005) the proposed enrichment is more straight forward but essential the three formulations models the same discontinuous field.

Common for the approaches in Wells and Sluys (2001), Moës and Belytschko (2002), Zi and Belytschko (2003), Mergheim, *et al.* (2005) is that they all adopt a nonlocal approach for the determination of the crack growth direction. A nonlocal approach is required because of the lack of capability of the tip element to model equal stresses at both sides of the discontinuity which is most pronounced when CST elements are considered.

The suggested XFEM scheme fits in the context of standard FEM code and it is applied to the 3-node constant strain triangle elements (CST) and the 6-node linear strain triangle elements (LST). The performance of the scheme is illustrated by modeling of fracture in concrete benchmark tests such as the three point beam bending test (TPBT) and the four point shear beam test (FPSB). In the present work only elements completely cut by a crack have been considered, i.e., the crack extends element by element and the crack tip will always be located on an element edge.

In section two the enrichment of the displacement field will be introduced and the discontinuous displacement fields developed and illustrated for CST and LST elements. Section three concerns the variational formulation while matters of the implementation is discussed in section four. Section five shows the numerical examples.

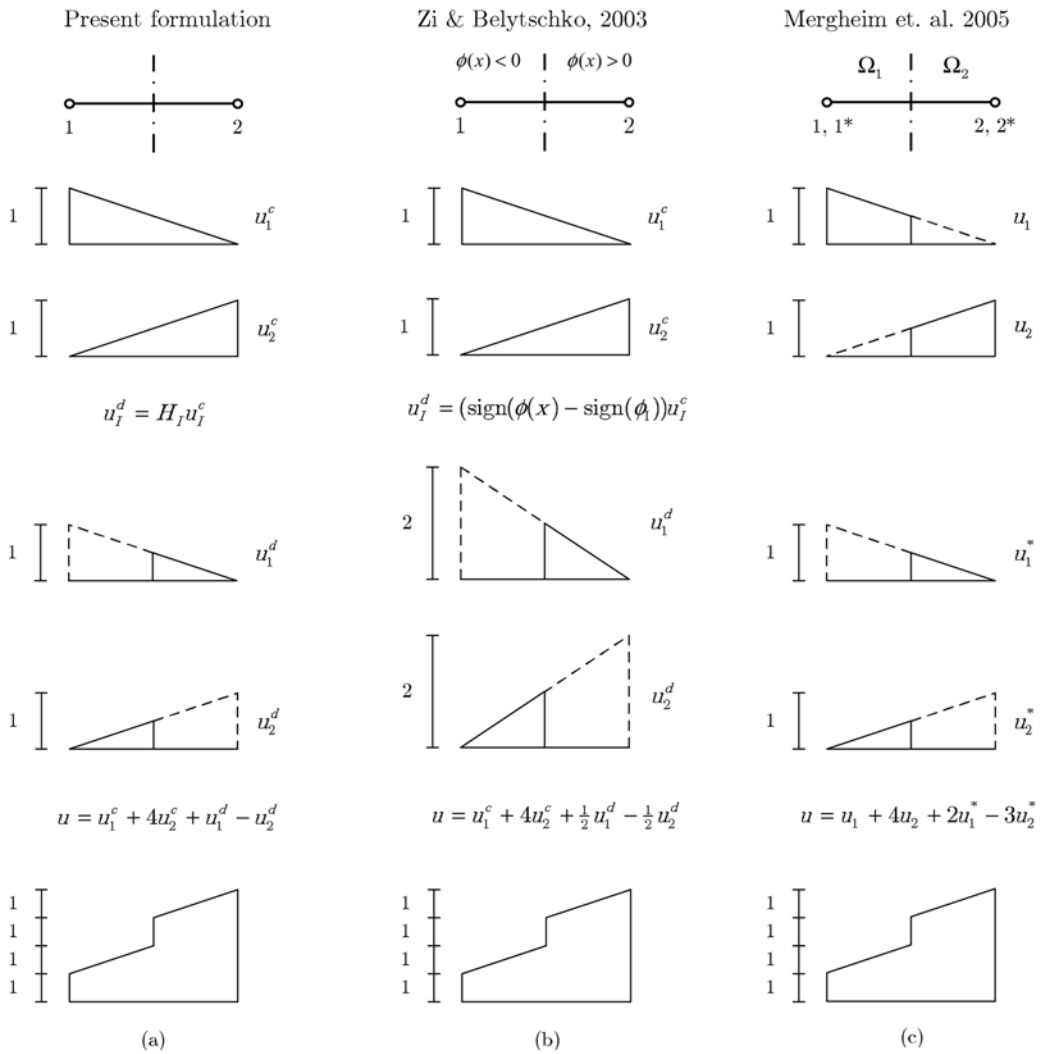

Fig. 1 Comparison of different enrichments of the displacement field: (a) Present formulation, (b) Zi and Belytschko (2003), (c) Mergheim, *et al.* (2005). For the present formulation and the formulation by Zi and Belytschko (2003) the two upper figures illustrate the continuous displacement fields and the following two figures illustrate the discontinuou displacement field. Regarding the formulation by Mergheim, *et al*. (2005) the two upper figures illustrate the displacement field for the two "original" nodes 1 and 2 while figure 3 and 4 depict the displacement fields for the dual nodes 1* and 2*. The lower figure in each column illustrates how a displacement jump of magnitude one may be modeled by the different formulations

2. Enrichment of displacement field

The displacement field for a cracked element can be formulated as the sum of the continuous and the discontinuous displacement field as already illustrated in Fig. 1. The continuous displacement field is defined equally to the displacement field for an uncracked element, i.e., the displacement

field may be written

$$\mathbf{u}(x,y) = \mathbf{N}^c(x,y)\mathbf{v}^c + \mathbf{N}^d(x,y)\mathbf{v}^d \tag{1}$$

where $\mathbf{v}^c$ and $\mathbf{v}^d$ are the degree of freedom (dof) vectors while $\mathbf{N}^c$ and $\mathbf{N}^d$ are the interpolation matrices. c refers to continuous and d to discontinuous.

The element discontinuity interpolation matrix, $\mathbf{N}^d$, is chosen as suggested in Asferg, *et al.* (2004).

$$\mathbf{N}^d(x,\ y) = \sum_I H_I(x,\ y)\mathbf{N}_I^c(x,\ y) \tag{2}$$

where $H_I(x,\ y)$ is the 2D Heaviside step function for node I. The step function $H_I(x,\ y)$ is 0 on the same side of the discontinuity as node I and 1 on the other side.

Fig. 2 illustrates a discontinuous displacement field for a CST element cut by a crack while Fig. 3 illustrates two of the discontinuous displacement fields for a LST element. The left most subfigure in each figure shows the crack geometry, coordinates to the start and the endpoints are given in area coordinates, while the remaining subfigures show individual nodal discontinuous displacement fields.

From Fig. 2 and Fig. 3 it is seen that the choice of interpolation for the discontinuous displacement field ensures that the discontinuous contribution to the displacement field vanish at all element edges not cut by the discontinuity implying the discontinuous displacement field to be included only in elements cut by the crack.

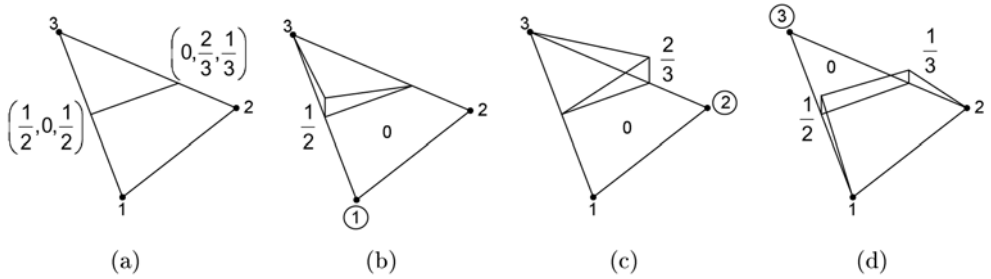

Fig. 2 Example of the enrichment of the displacement field for cracked CST element. (a) Crack geometry, (b), (c), (d) discontinuous displacement field for discontinuity dof's in node 1, 2 and 3

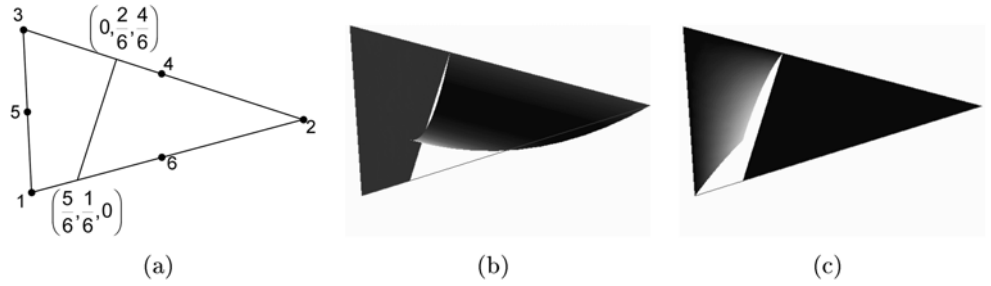

Fig. 3 Example of the enrichment of the displacement field for cracked LST element. (a) Crack geometry, (b) and (c) discontinuous displacement field for discontinuity dof's in node 1 respectively node 6

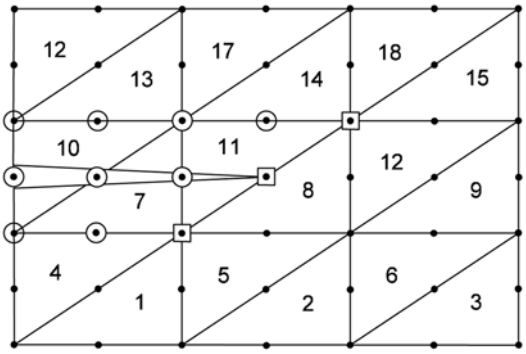

Fig. 4 Enrichment at system level for a mesh with LST elements. Nodes marked with a circle or a square are enriched. Discontinuity dof's in nodes marked with a square are set to zero

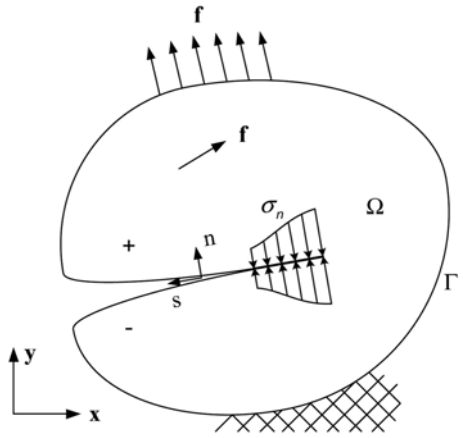

Fig. 5 Cohesive crack in a two dimensional domain with f representing both domain load and boundary load

Fig. 4 illustrates the enrichment at system level. Only nodes who's support is cut by the discontinuity are enriched. The discontinuity dof's located at the element edge where the crack tip is located have to be set to zero to ensure that the discontinuity at that edge is zero.

3. Variational formulation

Given a cohesive crack in a structure in a state of plane stress or plane strain described in a Cartesian coordinate system x,y (cf. Fig. 5), the arc length along the crack is termed s, and n,s is a curve linear coordinate system, n being normal to the crack face. The positive direction of s is seen on Fig. 5. The orientation of n determines the positive side of the crack. The stress state in the crack may be defined by the normal stress σ_n and the shear stress τ_{ns} while work-conjugated generalized strains are the opening of the crack, $\Delta u_n = u_n^+ - u_n^-$ and the slip in the crack, $\Delta u_s = u_s^+ - u_s^-$. A small strain / small displacement static theory is used and the material outside the crack is assumed linear elastic.

Let $[\![\ ]\!]$ denote a jump, then the stress increments $d\boldsymbol{\sigma}^{cr}$ across the crack surfaces are related to the increments in the displacement jump, $d[\![\mathbf{u}]\!]$, i.e., the separation of the crack surfaces through the tangential material stifiness matrix $\mathbf{D}_T^{cr}$.

$$\boldsymbol{\sigma}^{cr}([\![\mathbf{u}]\!]) = \begin{bmatrix} \sigma_n\ ([\![\mathbf{u}]\!]) \\ \tau_{ns}\ ([\![\mathbf{u}]\!]) \end{bmatrix} \qquad [\![\mathbf{u}]\!] = \begin{bmatrix} \Delta u_n \\ \Delta u_s \end{bmatrix} \qquad d\boldsymbol{\sigma}^{cr}([\![\mathbf{u}]\!]) = \mathbf{D}_T^{cr}([\![\mathbf{u}]\!])\, d[\![\mathbf{u}]\!] \tag{3}$$

For the uncracked part of the structure, the stress vector $\boldsymbol{\sigma}^T = \begin{bmatrix} \sigma_x\ \sigma_y\ \tau_{xy} \end{bmatrix}$ and the strain vector $\varepsilon^T = \begin{bmatrix} \varepsilon_x\ \varepsilon_y\ \gamma_{xy} \end{bmatrix}$, $(\gamma_{xy} = 2\varepsilon_{xy})$ are defined as usual and related through the standard material stiffness matrix $\mathbf{D}$, specified below for an isotropic material in plane stress.

$$d\boldsymbol{\sigma} = \mathbf{D}d\boldsymbol{\varepsilon}, \qquad \mathbf{D} = \frac{E}{1-\nu^2}\begin{bmatrix} 1 & \nu & 0 \\ \nu & 1 & 0 \\ 0 & 0 & \dfrac{1-\nu}{2} \end{bmatrix} \tag{4}$$

The virtual internal work-per-unit length of the crack δW^i_{cr} and the virtual internal work-per-unit area of the uncracked part of the structure δW^i_c may now be written, δ referring to a virtual quantity

$$\delta W^i_{cr} = \delta [\![\mathbf{u}]\!]^T \boldsymbol{\sigma}^{cr} = \sigma_n \delta \Delta u_n + \tau_{ns} \delta \Delta u_s$$

$$\delta W^i_c = \delta \boldsymbol{\varepsilon}^T \boldsymbol{\sigma} = \sigma_x \delta \varepsilon_x + \sigma_y \delta \varepsilon_y + \tau_{xy} \delta \gamma_{xy} \tag{5}$$

For the entire structure the virtual internal and external work becomes

$$\begin{aligned} \delta W^i &= \int_\Omega \delta \boldsymbol{\varepsilon}^T \boldsymbol{\sigma} d\Omega + \int_\Gamma \delta [\![\mathbf{u}]\!]^T \boldsymbol{\sigma}^{cr} d\Gamma \\ \delta W^e &= \int_\Omega \delta \mathbf{u}^T \mathbf{f} d\Omega + \int_\Gamma \delta \mathbf{u}^T \mathbf{f} d\Gamma \end{aligned} \tag{6}$$

where **f** is the load on the structure.
By applying incremental quantities, the incremental stiffness relation, can obtained by:

$$\mathbf{K}_T \Delta \mathbf{V} = \int_\Omega \mathbf{N}^T \Delta \mathbf{f} d\Omega + \int_\Gamma \mathbf{N}^T \Delta \mathbf{f} d\Gamma \tag{7}$$

where **V** is the system DOF vector and Δ refers to an incremental quantity.

Special attention must be paid to the internal work, because the contribution from each element to the tangential stiffness $\mathbf{K}_T$ depends on whether the element is cracked or not. The element tangential stiffness matrix, $\mathbf{k}_T$, for a cracked element is found by the following procedure. From Eqs. (l) and (2) the strain vector in a cracked element, except in the crack itself, is obtained

$$\boldsymbol{\varepsilon} = \mathbf{B}^c \mathbf{v}^c + \sum H_I \mathbf{B}^c_I \mathbf{v}^d_I = \mathbf{B}^c \mathbf{v}^c + \mathbf{B}^d \mathbf{v}^d \tag{8}$$

where $\mathbf{B}^c$ and $\mathbf{B}^d$ are the strain distribution matrices corresponding to the interpolation matrix $\mathbf{N}^c$ respectively $\mathbf{N}^d$.

Due to the displacement field from the first term in Eq. (1) being continuous, the strains in the crack itself may be written as

$$[\![\mathbf{u}]\!](s) = \mathbf{T}(\mathbf{N}^d_+(s) - \mathbf{N}^d_-(s))\mathbf{v}^d = \mathbf{B}^{cr}\mathbf{v}^d \tag{9}$$

here, $\mathbf{B}^{cr}$ is the strain distribution matrix in the crack, **T** is the transformation matrix between the (x, y) and (n, s) coordinate systems, while $\mathbf{N}^d_+$ and $\mathbf{N}^d_-$ are the discontinuous interpolation matrices on the positive and negative sides of the crack respectively.

Applying the strain relations in Eqs. (8) and (9) when formulating the virtual incremental internal work, $\mathbf{k}_T$ defined by $\delta W^i = \delta \mathbf{v}^T \mathbf{k}_T \Delta \mathbf{v}$, where $\mathbf{v}^T = \begin{bmatrix} \mathbf{v}^{cT} & \mathbf{v}^{dT} \end{bmatrix}$, is found to be

$$\mathbf{k}_T = \begin{bmatrix} \int \mathbf{B}^{cT}\mathbf{D}\mathbf{B}^c & \int \mathbf{B}^{cT}\mathbf{D}\mathbf{B}^d \\ \int \mathbf{B}^{dT}\mathbf{D}\mathbf{B}^c & \int \mathbf{B}^{dT}\mathbf{D}\mathbf{B}^d + \int_{cr} \mathbf{B}^{crT}\mathbf{D}^{cr}\mathbf{B}^{cr} \end{bmatrix} = \begin{bmatrix} \mathbf{k}^{cc} & \mathbf{k}^{cd} \\ \mathbf{k}^{dc} & \mathbf{k}^{dd} + \mathbf{k}^{cr}_T \end{bmatrix} \tag{10}$$

Due to a constant **D**-matrix outside the crack, the stiffness contribution from the areas outside the

crack is constant and thus only the stiffness contribution from the crack itself is non-linear.

The element nodal forces, $\mathbf{q}$, depend like $\mathbf{k}_T$, on the crack opening, and they are determined analogous to $\mathbf{k}_T$. The contribution to $\mathbf{q}$ from the crack, $\mathbf{q}^{cr}$, is found from the stresses in the crack. The stresses in the crack are related to the displacement jump across the crack according to Eq. (3). By adding this contribution to the contribution from the part of the element outside the crack, $\mathbf{q}$ is obtained as

$$\mathbf{q} = \begin{bmatrix} \mathbf{k}^{cc} & \mathbf{k}^{cd} \\ \mathbf{k}^{dc} & \mathbf{k}^{dd} \end{bmatrix} \begin{bmatrix} \mathbf{v}^{c} \\ \mathbf{v}^{d} \end{bmatrix} + \mathbf{q}^{cr} \quad where \quad \mathbf{q}^{cr} = \int_{cr} \mathbf{B}^{crT} \begin{Bmatrix} \sigma_n \\ \tau_{ns} \end{Bmatrix} \tag{11}$$

4. Implementation

This section concerns the implementation of the XFEM scheme. First the condition for smooth crack closure is discussed. Hereafter the integration scheme for the enriched elements is presented. Then the criteria for the crack propagation are dealt with and finally the choice of the algorithm to solve the non-linear equations is discussed and the algorithm is given in a schematic form.

4.1. Conditions for smooth crack closure

In order to secure that the cohesive crack closes smoothly it is required that the stress intensity factors at the crack tip are vanishing (Vandewalle 2000). In Moës and Belytschko (2002) the mode I stress intensity factor, K_I, is evaluated applying a domain integral and when performing the iterations the load factor is determined such that K_I is zero at the crack tip. In the work by Zi and Belytschko (2003) it is stated that the equilibrium equations have been supplemented by a smooth crack closure condition at system level. Equivalent to the zero stress intensity factor condition, Zi and Belytschko require the stress projection in the normal direction of the crack to be equal to the tensile strength at the crack tip. However, adding an extra equation to be fulfilled at system level makes the structure of the algorithm different from the structure of most algorithms applied in commercial FEM codes. Investigations using cohesive interface crack elements by Stang, *et al*. (2006) show that smooth closure is automatically achieved in a finite element formulation with a stress criterion when a sufficient mumber of elements are applied. However, in the case considered in this paper, where the elements are either uncracked or fully cracked, it is just ensured that the stresses in the element next to the crack-tip element do not exceed the tensile strength. This approximately ensures smooth crack closure.

4.2. Integration of enriched elements

To ensure correct integration in elements cut by the discontinuity, integration must be performed independently on each side of the discontinuity. For integration purposes elements cut by the discontinuity are therefore subdivided into three triangular areas as illustrated in Fig. 6. In the case of CST elements one point Gauss quadrature is applied to each sub triangle and two integration points are used on the line of discontinuity. In the case of LST elements three point Gauss quadrature is applied in each sub triangle and three integration points are used along the line of discontinuity.

In elements not cut by the discontinuity standard Gauss quadrature is applied - one point Gauss quadrature is applied in the case of CST elements and three point Gauss quadrature is applied for LST elements.

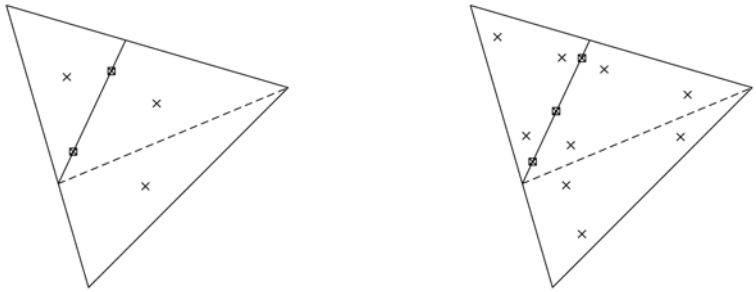

Fig. 6 Integration scheme for (a) CST and (b) LST element cut by discontinuity. Crosses marks integration point in continuum part of elements while crosses in boxes marks integration point on line of discontinuity for integration of traction forces

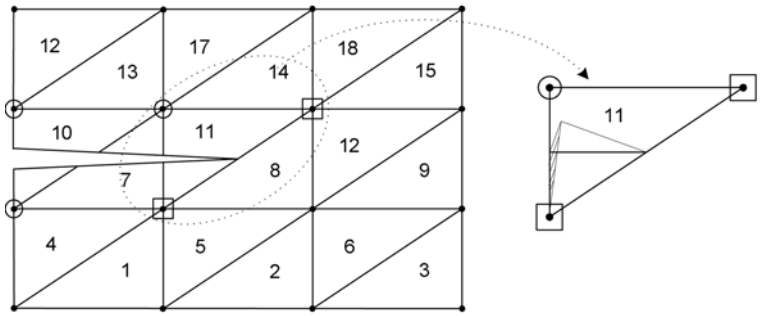

Fig. 7 Discontinuous displacement field in CST "tip" element

4.3. Crack growth

In the present work a discontinuity is introduced in the element, when the principal stress in the element exceeds the tensile strength of the material. The discontinuity is a straight line through the element originating from the point where the discontinuity ended in the previous cracked element. Hereby a continuous discontinuity is assured.

Concerning the crack growth direction different approaches have been considered. The first and simplest approach is local and rely only upon the stresses in the element that is located next to the tip-element (The element to become the next tip-element, element 8 in Fig. 7) for the determination of the crack growth direction. The discontinuity is grown perpendicular to the principal stress direction.

Several authors state that the local stresses in the next tip element can not be relied upon for computation of the crack growth direction and different nonlocal approaches are suggested. In Wells and Sluys (2001) the principal stress direction in the next tip element is computed from a non-local stress tensor calculated as a weighted average of stresses using a Gaussian weight function. Stresses in integration points within a radius of three times the typical element size are taken into account. In Moës and Belytschko (2002) the maximum hoop stress criterion is applied. The requirement for considering stresses in more than one element when computing the crack growth direction may appear when recalling the discontinuous displacement field in a cracked CST tip element c.f. Fig. 7.

Due to the discontinuous degrees of freedom in the nodes located on the crack tip edge being set equal to zero the crack tip element is not able to model the case, where equal stress are present at both sides of the discontinuity. This lack of capability to model correct stresses in the tip element influences the stresses in the next tip element and may call for more elements to be relied on for the computation of crack growth direction.

When a non-local stress tensor is applied in this work (only for CST elements), average nodal stresses are computed from element stresses in the elements sharing a given node - c.f. Eq. (12). All elements are assigned the same weight except previously cracked elements that are disregarded in the computation of the average nodal stresses due to the above illustrated bad stress field in the crack tip element. From the average nodal stresses a non-local stress tensor at the crack tip is interpolated by Eq. (13) and used for the determination of the crack growth direction. In Eq. (13)$(\zeta_1, \zeta_2, \zeta_3)$ are the area coordinates to the crack tip.

$$\boldsymbol{\sigma}_{node}^{ave} = \left(\sum_{i=1}^{n_{el}^{uncr}} \boldsymbol{\sigma}_i \right) / n_{el}^{uncr} \tag{12}$$

$$\sigma_{tip}^{NL} = \begin{bmatrix} \sigma_x^{no1} & \sigma_x^{no2} & \sigma_x^{no3} \\ \sigma_y^{no1} & \sigma_y^{no2} & \sigma_y^{no3} \\ \tau_{xy}^{no1} & \tau_{xy}^{no2} & \tau_{xy}^{no3} \end{bmatrix} \begin{bmatrix} \zeta_1 \\ \zeta_2 \\ \zeta_3 \end{bmatrix} \tag{13}$$

Applying LST elements a non local procedure for computation of the crack growth direction is not necessary. The crack growth direction is computed from the principal stresses at the start point of the crack in the element.

4.4. Algorithm

To remain within the framework of traditional FEM codes a general procedure, the orthogonal residual algorithm (Krenk 1995), was adopted for the XFEM scheme to solve the non-linear equations. The algorithm is summarized in Table 1.

As convergence criterion an energy criterion was applied and the elastic energy in the initial elastic load step was used as reference energy, E_{ref}. Further it may be noticed that it was chosen to implement the orthogonal residual algorithm in a Newton-Raphson style where the tangential stiffness matrix was updated in each iteration to take into account changes in crack opening and thereby also changes in the contribution from the enriched nodes during the iterations.

5. Numerical examples

To illustrate the capability of the suggested XFEM scheme two fracture mechanical benchmark tests, the three point beam bending test (TPBT) and the four point shear beam test (FPSB) has been considered. Results will be given for the TPBT applying CST as well as LST elements while only results applying LST elements will be given for the FPSB. Applying CST elements for the TPBT specimen local as well as nonlocal determination of crack growth direction will be considered and discussed.

Table 1 Orthogonal residual algorithm for XFEM

initial state: $\mathbf{u}_0$, $\mathbf{f}_0$, $\Delta\mathbf{u}_0 = 0$, E_{ref}, $\Delta\mathbf{f}_0$	
load increments n =1, 2..., $n_{\max}$	
$\Delta\mathbf{u}_1=\mathbf{K}_{T,n-1}^{-1}\Delta\mathbf{f}_n$	
$\Delta\mathbf{u} = \min(1, u_{\max}/\|\Delta\mathbf{u}\|)\Delta\mathbf{u}$	
$\Delta\mathbf{u}_0^T\Delta\mathbf{u}<0$ *then* $\Delta\mathbf{u}=-\Delta\mathbf{u}$, $\Delta\mathbf{f}=-\Delta\mathbf{f}$	
Iterations i=1, 2,... $i_{\max}$	
$\Delta\mathbf{q} = \mathbf{q}(\mathbf{u}+\Delta\mathbf{u})-\mathbf{f}_{n-1}$	
$\zeta = \mathbf{q}^T\mathbf{u} / \mathbf{f}_n^T\Delta\mathbf{u}$	ζ *is the optimal load scaling factor*
$\boldsymbol{r} = \zeta\Delta\mathbf{f}_n-\Delta\mathbf{q}$	$\mathbf{r}$ *in the unbalanced force vector*
$\mathbf{K}_{T,n} = \mathbf{K}_T(\mathbf{u}+\Delta\mathbf{u})$	
$\delta\mathbf{u} = \mathbf{K}_{T,n}^{-1}\mathbf{r}$	$\delta\mathbf{u}$ *is the displacement correction*
$\delta\mathbf{u} = \min(1, u_{\max}/\|\delta\mathbf{u}\|)\delta\mathbf{u}$	
$E_i = \mathbf{r}^T\delta\mathbf{u}$	E_i *is the residual energy*
$\varepsilon_i = E_i/E_{ref}$	
$\Delta\mathbf{u} = \Delta\mathbf{u}+\delta\mathbf{u}$	
stop iteration when $\varepsilon_i \leq$ *stop value*	
$\mathbf{u}_n = \mathbf{u}_{n-1}+\Delta\mathbf{u}_n$	
$\mathbf{f}_n = \mathbf{f}_{n-1}+\zeta\Delta\mathbf{f}_n$	
$\Delta\mathbf{u}_0 = \Delta\mathbf{u}$	
stop load increments when $\|\mathbf{u}_n\| > u_{\max}^{check}$	

5.1. Three point beam bending test

The geometry of the TPBT specimen considered in this case is in accordance with the RILEM recommendations (Vandewalle 2000). The geometry is depicted in Fig. 8(a), the cross section of the beam being a square. For the material parameters standard values for a good quality concrete was chosen c.f. Table 2. A linear softening law as illustrated in Fig. 8(b) was applied for the normal stress in the crack. Considering a pure mode I problem the shear stiffness and the mixed mode stiffness terms for the crack were all set equal to zero, i.e., the tangential material stiffness matrix for the crack only holds one term different from zero:

$$D_{cr}^T = \begin{bmatrix} \dfrac{-f_t}{\Delta u_{n,ult}^{cr}} & 0 \\ 0 & 0 \end{bmatrix} \tag{14}$$

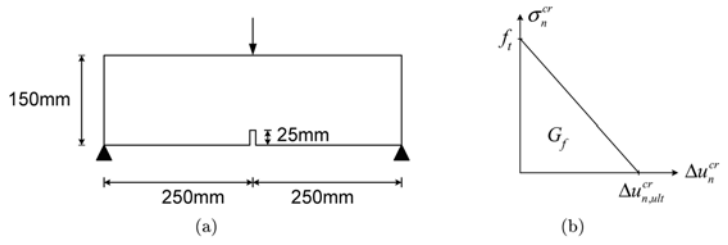

Fig. 8 (a) Geometry of TPBT specimen. (b) Applied linear softening curve

Table 2 Constitutive parameters

Parameter	Value
Young's modulus, E_c	37400MPa
Poisson's ratio, ν_c	0.2
Tensile strength, f_t	3.5MPa
Fracture energy, G_f	160 N/m

5.1.1. Applying CST elements to model TPBT

Modeling the TPBT specimen applying CST elements structured as well as unstructured meshes were considered. Results will be given for two structured meshes, a 21 by 12 element c.f. Fig. 9(a), and a 25 by 24 element mesh. For both structured meshes results for local as well as non-local computation of crack growth direction will be given. The unstructured mesh, c.f. Fig. 9(b) consisted of 709 elements and results will only be given for the non-local crack growth computation. Note that for the structured meshes the notch is modeled as a predefined stress free discontinuity while in the unstructured mesh the notch is defined by the geometry of the mesh.

As reference for the XFEM computations the TPBT specimen was also modeled applying standard interface elements along a predefined crack path in the commercial code DIANA from TNO. Two meshes holding 24 respectively 48 elements over the beam height were considered for the DIANA computation.

Fig. 10 shows the load-deformation-response for the five considered XFEM computations and the two reference DIANA computations. The deformation is computed as the difference between the vertical displacement of the center point of the beam and the average vertical displacement of the mid points of the beam ends. Fig. 11 shows the predicted crack path for the 25 by 24 mesh applying local or nonlocal computation of the crack growth direction and the predicted crack path for the unstructured mesh.

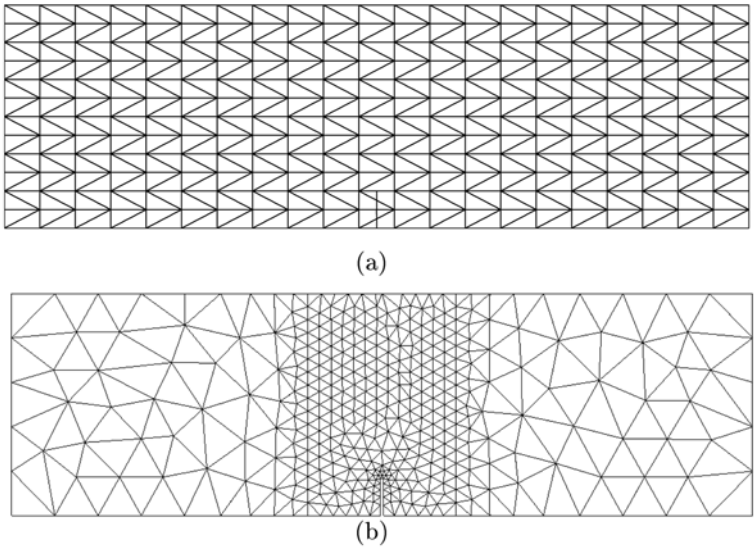

Fig. 9 (a) Structured mesh. (b) Unstructured mesh

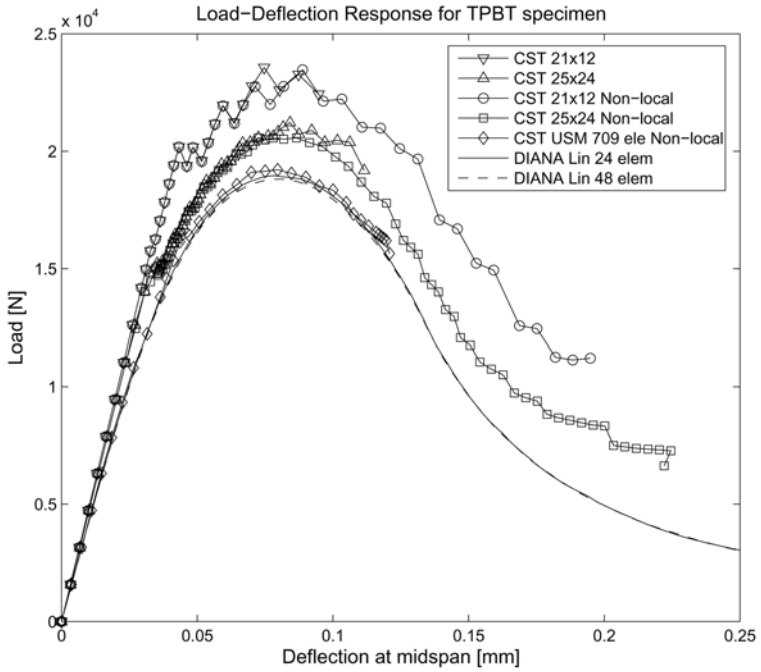

Fig. 10 Load-deformation-response for TPBT specimen modelled applying fully cracked CST elements

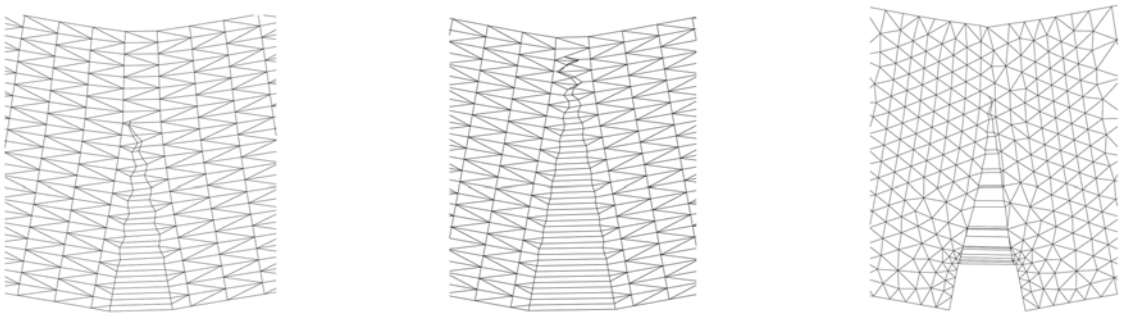

Fig. 11 Predicted crack path for: (a) 25 by 24 Mesh, local computation of crack growth direction. (b) 25 by 24 Mesh, non-local computation of crack growth direction (c) Unstructured mesh, non-local computation of crack growth direction

From the load-deformation-responses it is seen that the coarse structured mesh over predicts the load carrying capacity of the TPBT specimen with about 20% while the finer structured mesh overestimates the load carrying capacity with about 8%. The unstructured mesh predicts the maximum load carrying capacity well. Concerning the overall reproduction of the load-deformation-response it is seen that applying the local approach for the crack growth direction only the first part of the post peak response corresponding to the crack having propagated approximately through 2/3 of the beam hight may be obtained. Applying the non-local approach for determining the crack

growth direction almost the full load-deformation response may be obtained - in Fig. 11(b) the crack has almost reached the top of the beam. The main reason for the bad prediction of the crack growth direction applying the local approach is the bad reproduction of the stresses in the tip element discussed in Section 4.3. The difference in stability of the determination of crack growth direction for the local versus the non-local approach is also evident from Fig. 11 (a) and (b). The non-local approach smoothes the crack path considerably compared to the local approach. The unstructured mesh captures the load carrying capacity well but is not able to reproduce the full load deformation response for the TPBT specimen with the applied non-local computation scheme. The use of non-local criteria for determination of crack growth direction is however seen as less appealing due to the required user interaction for determination of interaction radius that e.g., depends on the chosen element size and the actual structure considered. Use of a non local criterion to some extend violates the element local approach of the XFEM where everything is handled element locally.

5.1.2. Applying LST elements to model TPBT

Considering LST elements results are given for four structured meshes - a 11 by 6, a 15 by 9, the 21 by 12 and the 25 by 24 mesh. Only local computation of crack growth direction is considered. Fig. 12 compares the load-deformation response from the XFEM LST computations with the DIANA computation while Fig. 13 depicts the predicted crack patterns for the 21 by 12 and the 25 by 24 mesh.

From the load-deformation response it is seen that applying LST elements the overall behavior is predicted well by the 21 by 12 and the 25 by 24 mesh while the two coarsest meshes have troubles capturing the post peak response. Looking at the predicted crack paths it is seen that applying LST elements and hereby having more active discontinuity dof's, a more smooth crack path is achieved than for CST elements. However when the crack reaches the top of the beam and only a few

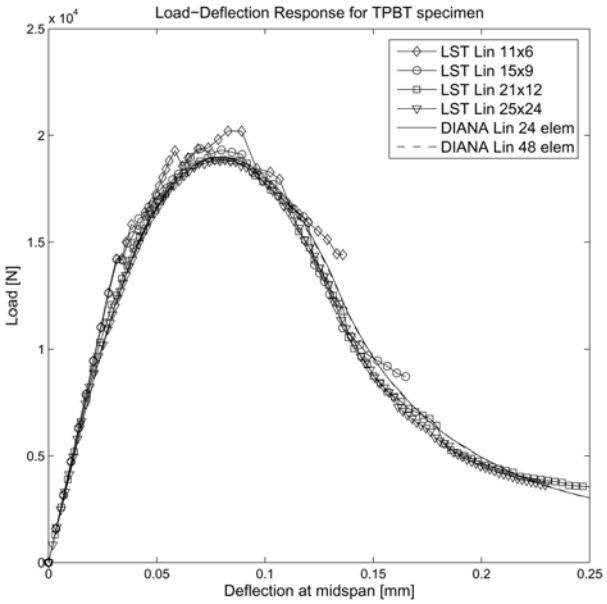

Fig. 12 Load-deformation-response for TPBT specimen modelled applying fully cracked LST elements

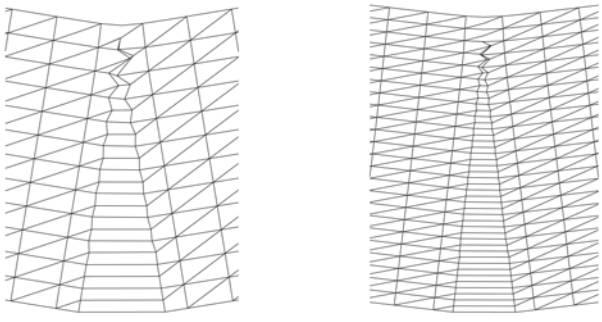

Fig. 13 Predicted crack path for LST computations of TPBT: (a) 21 by 12 Mesh. (b) 25 by 24 Mesh

elements remain uncracked the quality of the determined stress near the crack tip becomes low and hence influence the crack growth direction causing increasing tortuosity of the crack path. The conclusion is however that applying LST a sufficient accuracy concerning the crack growth direction is obtained by the local approach.

5.2. Four point shear beam

The four point shear beam serves to illustrate the capability of the suggested XFEM scheme to model curved cracks. The geometry of the four point shear beam (FPSB) - or the "double-edge notched specimen subjected to four point shear" is equivalent to the one investigated experimentally by Carpinteri, *et al*. (1992). In Carpinteri, *et al*. (1992) it is concluded that the FPSB may be modeled considering only mode I fracture, i.e. the shear stiffness in the crack may be ignored. The FPSB specimen was also analyzed by XFEM in Moës and Belytschko (2002). To maintain the basis for comparing the obtained results, fracture of the FPSB was also in the present case modeled considering only mode I fracture. The geometry of the test setup is shown in Fig. 14, while

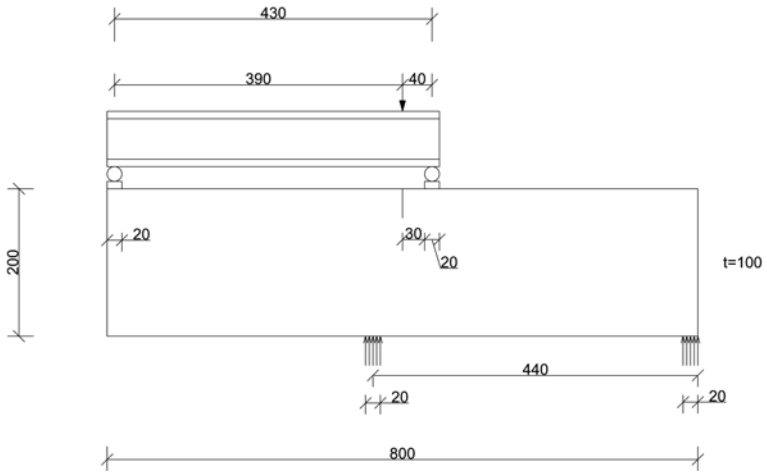

Fig. 14 Geometry of four point shear beam, all measures in mm

Table 3 Constitutive parameters FPSB

Parameter	Value
E_c	28000 MPa
o_c	0.1
f_t	2.4 MPa
G_f	145 N/m

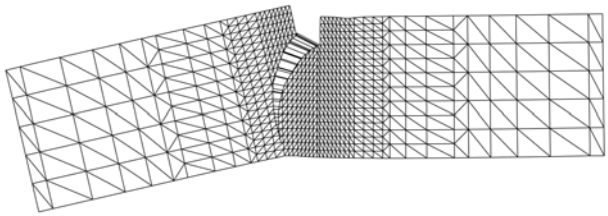

Fig. 15 Predicted crack path for FPSB specimen

constitutive parameters are given in Table 3. As for the TPBT specimen a linear softening curve (Fig. 8(b)) was applied.

A fairly coarse structured LST mesh, depicted in Fig. 15, consisting of 1222 elements and 2549 nodes was considered for the XFEM computation.

Fig. 15 depicts the computed crack path. The predicted crack path is in good agrement with the experimental findings in Carpinteri, *et al.* (1992). In Fig. 16 the computed load-deflection response is compared to the experimental load-deflection response obtained by Carpinteri, *et al.* (1992) and to the XFEM load-deflection response computed by Moës and Belytschko (2002). It is seen that the obtained results correlates well with the experimental results whereas some derivations are found when comparing to the results by Moës and Belytschko (2002).

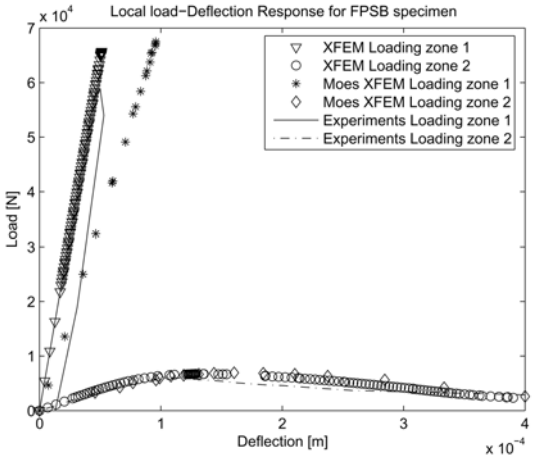

Fig. 16 Comparison of load-displacement response for FPSB obtained by present XFEM model, XFEM results by Moës and Belytschko (2002) and by experiments Carpinteri, *et al*. (1992). Loading zone 1 refers to the loading zone to the right in Fig. 14, while loading zone 2 refers to the left.

6. Conclusions

A direct enrichment of the displacement field has been implemented into an extended finite element scheme for modeling cohesive crack growth in concrete without remeshing. The XFEM scheme fits directly in the framework of standard finite element schemes. The XFEM scheme has been implemented for the three node constant strain triangle element (CST) and the linear strain six node triangle element (LST). Considering the CST element it was necessary to implement a nonlocal computation of crack growth direction to obtain good prediction of the crack path while for the LST element the crack path computation could be based on element local computations. Considering three point bending and four point shear, the efficiency of the suggested scheme was illustrated and it was found that even for relatively coarse meshes the scheme produces good results.

References

Asferg, J. L., Poulsen, P. N. and Nielsen, L. O. (2004), "Modeling of cohesive crack applying XFEM", *5th International PhD Symposium in Civil Engineering,* Walraven, J., Blaauwendraad, J., Scarpas, T. and Snijder, B. (Eds.), pages 1261-1269.

Barenblatt, G. I. (1962), "The mathematical theory of equilibrium of cracks in brittle fracture", *Advances in Applied Mech*., 7, 55-129.

Bažant, Z. P. and Oh, B. H. (1983), "Crack band theory for fracture of concrete", *Mater. Struct.*, *RILEM*, **16**(93), 155-177.

Belytschko, T. and Black, T. (1999), "Elastic crack growth in finite elements with minimal remeshing", *Int. J. Numer. Methods Eng.*, **45**(5), 601-620.

Belytschko, T., Krongauz, Y., Organ, D., Fleming, M. and Krysl, P. (1996), "Meshless methods: an overiew and recent developments", *Comput. Methods Appl. Mech. Eng.*, **139**, 3-47.

Bouchard, P. O., Bay, F. and Chastel, Y. (2002), "Numerical modelling of crack propagation: automatic remeshing and comparison of different criteria", *Comput. Methods Appl. Mech. Eng.*, **192**, 3887-3908.

Bouchard, P. O., Bay, F., Chastel, Y. and Tovena, I. (2000), "Crack propagation modelling using an advanced remeshing technique", *Comput. Methods Appl. Mech. Eng.*, **189**, 723- 742.

Carpinteri, A., Valente, S., Ferrara, G. and Melchiorri, G. (1992), "Is mode II fracture energy a real material property?", *Comput. Struct.*, **48**(3), 397-413.

Daux, C., Moës, N., Dolbow, J., Sukumar, N. and Belytschko, T. (2000), "Arbitrary branched and intersecting cracks with the extended finite element method", *Int. J. Numer. Methods Eng.*, **48**, 1741-1760.

Dugdale, D. S. (1960), "Yielding of steel sheets containing slits", *J. Mech. Phys. Solids,* **8**, 100-104.

Hillerborg, A., Modéer, M. and Peterson, P.-E (1976), "Analysis of crack formation and crack growth in concrete by means of fracture mechanics and finite elements", *Cement Concrete Res.*, **6**, 773-782.

Jirásek, M. (2000), "Comparative study on finite elements with embedded discontinuities", *Comput. Methods Appl. Mech. Eng.,* **188**, 307-330.

Jirásek, M. and Belytschko, T. (2002), "Computational resolution of strong discontinuities", in: H. Mang, F. Rammerstorfer, J. Eberhardsteiner (Eds.), *Proceedings of Fifth World Congress on Computational Mechanics*, WCCM V, Vienna University of Technology, Austria.

Karihaloo, B. L. (1995), *Fracture Mechanics and Structural Concrete.* Longman Scientific and Technial.

Karihaloo, B. L. and Xiao, Q. Z. (2002), "Modelling of stationary and growing cracks in FE framework without remeshing: a state-of-the-art review", *Comput. Struct.*, **81**, 119-129.

Krenk, S. (1995), "An orthogonal residual procedure for nonlinear finite element equations", *Int. J. Numer. Methods Eng.*, **38**, 823-839.

Melenk, J. M. and Babuŝka, I. (1996), "The partition of unity finite element method: basic theory and application", *Comput. Methods Appl. Mech. Eng.*, **139**, 289-314.

Mergheim, J., Kuhl, E. and Steinmann, P. (2005) "A finite element method for the computational modeling of cohesive cracks", *Int. J. Numer. Methods Eng.*, **63**, 276-289.

Moës, N. and Belytschko, T. (2002), "Extended finite element method for cohesive crack growth", *Eng. Fract. Mech.*, **69**, 813-833.

Moës, N., Dolbow, J. and Belytschko, T. (1999), "A finite element method for crack growth without remeshing", *Int. J. Numer. Methods Eng.*, **46**, 131-150.

Nielsen, M. P. (1999), *Limit Analysis and Concrete Plasticity.* CRC Press, second editon.

Patzák, B. and Jirásek, M. (2004), "Adaptive resolution of localized damage in quasi-brittle materials", *J. Eng. Mech.*, **130**, 720-732.

Stang, H., Olesen, J. F., Poulsen, P. N. and Dick-Nielsen, L. (2006), "Application of the cohesive crack in cementitious materials modelling", In Meschke, G. de Borst, R. Mang, H. and Bicanic, N., Editors, *Computational Modeling of Concrete Structures*, 443-449, Taylor & Francis.

Stolarska, M., Chopp, D. L, Moës, N. and Belytschko, T. (2001), "Modeling crack growth by level sets in the extended finite element method", *Int. J. Numer. Methods Eng.*, **51**, 943-960.

Sukumar, N., Moës, N., Moran, B. and Belytschko, T. (2000), "Extended finite element method for three dimensional crack modeling", *Int. J. Numer. Methods Eng.*, **48**, 1549-1570.

Vandewalle, L. (2000), "Test and design methods for steel fiber reinforced concret. Recommendations for bending test", *Mater. Struct.*, **33**, 3-5.

Wells, G. and Sluys, L. (2001), "A new method for modeling of cohesive cracks using finite elements", *Int. J. Numer. Methods Eng.*, **50**(12), 2667-2682.

Zi, G. and Belytschko, T. (2003), "New crack-tip elements for XFEM and applications to cohesive cracks", *Int. J. Numer. Methods Eng.,* **57**, 2221-2240.

NB

Paper II

A consistent partly cracked XFEM element for cohesive crack growth

International Journal for Numerical Methods in Engineering, 2007, vol 72, page 464-485.

INTERNATIONAL JOURNAL FOR NUMERICAL METHODS IN ENGINEERING
Int. J. Numer. Meth. Engng 2007; **72**:464–485
Published online 5 March 2007 in Wiley InterScience (www.interscience.wiley.com). DOI: 10.1002/nme.2023

A consistent partly cracked XFEM element for cohesive crack growth

J. L. Asferg, P. N. Poulsen*, † and L. O. Nielsen

Department of Civil Engineering, Technical University of Denmark, Brovej 1, DK-2800 Kgs. Lyngby, Denmark

SUMMARY

Present extended finite element method (XFEM) elements for cohesive crack growth may often not be able to model equal stresses on both sides of the discontinuity when acting as a crack-tip element. The authors have developed a new partly cracked XFEM element for cohesive crack growth with extra enrichments to the cracked elements. The extra enrichments are element side local and were developed by superposition of the standard nodal shape functions for the element and standard nodal shape functions for a sub-triangle of the cracked element. With the extra enrichments, the crack-tip element becomes capable of modelling variations in the discontinuous displacement field on both sides of the crack and hence also capable of modelling the case where equal stresses are present on each side of the crack. The enrichment was implemented for the 3-node constant strain triangle (CST) and a standard algorithm was used to solve the non-linear equations. The performance of the element is illustrated by modelling fracture mechanical benchmark tests. Investigations were carried out on the performance of the element for different crack lengths within one element. The results are compared with previously obtained XFEM results applying fully cracked XFEM elements, with computational results achieved using standard cohesive interface elements in a commercial code, and with experimental results. The suggested element performed well in the tests. Copyright © 2007 John Wiley & Sons, Ltd.

Received 11 September 2006; Revised 11 January 2007; Accepted 17 January 2007

KEY WORDS: XFEM; fracture mechanics; cohesive cracks; crack propagation; discontinuity; partition of unity

1. INTRODUCTION

The development of cracks is one of the governing factors for the structural behaviour of structures made of important materials such as concrete, fibre-reinforced composites, wood, etc. Common

*Correspondence to: P. N. Poulsen, Department of Civil Engineering, Technical University of Denmark, Brovej 1, DK-2800 Kgs. Lyngby, Denmark.
†E-mail: pnp@byg.dtu.dk

for these materials is that they belong to the group of quasibrittle materials for which the process of cracking may be described in terms of cohesive crack models [1–3].

In cohesive crack models, all non-linearities are assumed to be localized in the crack line, bridging stresses act near the crack tip, and it is assumed that no stress singularity is present at the crack tip.

Computational modelling of crack growth has been carried out applying various remeshing techniques, e.g. [4–8]. But remeshing is computationally costly and it involves the transferring of data between the different meshes and is therefore less attractive than approaches that allow the discontinuity to propagate independently of the mesh configuration by permitting the discontinuity to cross element boundaries.

The element-free Galerkin method [9] can model crack growth. However, due to major differences from standard finite element method (FEM), it cannot be directly implemented in existing FEM code.

The embedded crack models enable modelling of localized crack growth without remeshing. In models with a localization line [10–14], the displacement field may be discontinuous and hence the element may model the discontinuity within one element. However, even though an arbitrary displacement jump can be reproduced with this approach, the displacement fields on each side of the crack are not independent and this limits the modelling capabilities. For a more thorough discussion of elements with embedded discontinuities reference is made to [15, 16].

Among the latest developments in finite element modelling of crack propagation are the methods based on the partition of unity [17], of which the extended finite element method (XFEM) [18, 19] is probably the most widespread. In XFEM, the displacement field consists of two parts, one continuous and the other discontinuous. The continuous part is the standard displacement field corresponding to the situation without any cracks. The discontinuous displacement field is based on local partitions of unity and allows the element to include a discontinuity, in the present case a cohesive crack. XFEM uses a strong discontinuity approach for the modelling of the actual kinematics and at the same time generally allows the strains to be independent on the two sides of the discontinuity.

XFEM has been applied to various problems within the area of fracture mechanics. While it was first developed for linear elastic fracture mechanics [18–20], it has now been applied to problems like cohesive cracking [21–24], arbitrary branched and intersecting cracks [25], three-dimensional crack propagation [26, 27], and cracks in shells [28]. Apart from fracture mechanics, XFEM has also been applied to a number of other problems involving discontinuities, among which are the modelling of inclusions [29–31].

Wells and Sluys [21] applied the Heaviside step function as the only enrichment to a fully cracked element. Only nodes with a supporting side cut by the discontinuity were enriched. However, applying the Heaviside step function as in [21], the nodal enrichment influences not only the displacement field in the elements cut by the discontinuity, but also the displacement field in the elements sharing the enriched nodes—i.e. the enrichments typically have to be dealt with in a band of three elements along the line of discontinuity. Zi and Belytschko [23] formulated a partly cracked element in which the shifted sign function was used for the enrichment. In this set-up, the enrichment only involved the cracked elements. A formulation of a fully cracked element with the direct use of the Heaviside step function was presented in [24], also with the discontinuous displacement field limited to the cracked elements. In [32] a dual node strategy was applied and the displacement field was not decomposed into a continuous and discontinuous part in the same way as in the ‘standard’ XFEM approach. However, even though the basis for the shape functions

DOI: 10.1002/nme

is different, the scheme in [32] is capable of modelling the same variation in the displacement field as in the scheme in [23, 24].

Applying elements that may only be fully cracked does not allow for all possible load–displacement states to be computed, as, is normally required in a general solution of a non-linear problem. Therefore, the application of elements that are not allowed to be partly cracked may not only lead to an erroneous load–deformation response for a crack propagating through a given structure, but may also be the reason for numerical problems when solving the non-linear equations. An element that can be partly cracked is therefore preferable. Moës and Belytschko [22] proposed a partly cracked element in which the crack-tip element is enriched with a set of non-singular branch functions to model the displacement field around the tip of the discontinuity. But the application of branch functions is seen as less favourable in the case of cohesive cracks, where there is no need for asymptotic fields. Furthermore, the 'infinite' nature of branch functions is seen as contradictive, to the general finite element scheme, in which the displacement fields are element local. As previously mentioned, Zi and Belytschko proposed an element local enrichment of a partly cracked element in [23], applying the sign function for the enrichment.

With the enrichments as implemented in [21, 23, 33], the crack-tip element cannot model equal stresses on both sides of the crack as assumed in the cohesive model. With reference to [33] the problem is illustrated in Figure 1, which shows the displacement field that can be modelled in the element with the crack tip on its boundary. To ensure the continuity of the displacement field at the crack tip, the discontinuity degrees of freedom (DOFs) in nodes located at the crack-tip element boundary must be set to zero and this means that only one set of discontinuity DOFs is available in the tip element. Various non-local approaches have been applied to compensate for the inability of the tip element to model equal stresses on both sides of the discontinuity, especially when 3-node constant strain triangle (CST) elements are considered. In [21, 33] a non-local computation of the stresses in the near tip area was used to determine the principal stress direction at the tip, while the maximum hoop stress criterion utilizing stress intensity factors was applied in [23]. Recently Xiao and Karihaloo have extended their element local statically admissible stress recovery scheme [34] to cohesive cracks [35] and obtained good results for fairly dense meshes of higher-order elements.

A more direct way to obtain a better stress distribution on both sides of the crack in cohesive crack growth would be to formulate a tip element with the capability of modelling variations in the discontinuous displacement field on both sides of the discontinuity. This paper presents such a consistent approach to obtain a more correct stress distribution in a partly cracked tip element. The new enrichment scheme is based on additional enrichment of the cracked elements. The extra enrichment is constructed as a superposition of the standard nodal shape functions and standard nodal shape functions created for a sub-area of the cracked element. The suggested enrichment may

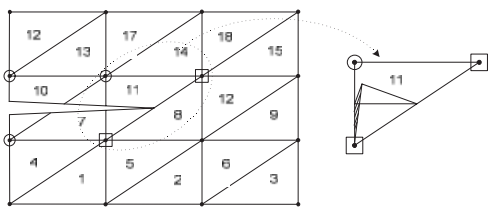

Figure 1. Discontinuous displacement field in CST 'tip' element [33].

DOI: 10.1002/nme

be seen as a natural extension of the enrichments applied in [21, 23, 24]. The extra enrichment allows the element to model equal stresses on both sides of the crack tip. Whereas only fully cracked elements are considered in [21, 33], the new enrichment scheme has been implemented so that the discontinuity in the crack-tip element may have any length. The concept behind the new enrichment was presented in [36].

The suggested XFEM scheme fits within the concept of standard finite element code and is applied to CST elements. The performance of the element is illustrated by modelling of fracture mechanical benchmark tests, such as the three-point beam bending test (TPBT) and the four-point shear beam (FPSB) test.

The paper is organized as follows: in Section 2, the enrichment of the displacement field will be introduced and the discontinuous displacement field developed and illustrated. Section 3 deals with the variational formulation, while matters of implementation are discussed in Section 4. Numerical examples are given in Section 5.

2. ENRICHMENT OF THE DISPLACEMENT FIELD

The displacement field for a cracked element is the sum of the continuous and the discontinuous displacement fields. The continuous displacement field is defined as equal to the displacement field for an uncracked element, i.e. the displacement field may be written

$$\mathbf{u}(x, y) = \mathbf{N}^{\mathrm{c}}(x, y)\mathbf{v}^{\mathrm{c}} + \mathbf{N}^{\mathrm{d}}(x, y)\mathbf{v}^{\mathrm{d}} \tag{1}$$

where $\mathbf{v}^{\mathrm{c}}$ and $\mathbf{v}^{\mathrm{d}}$ are the DOF vectors while $\mathbf{N}^{\mathrm{c}}$ and $\mathbf{N}^{\mathrm{d}}$ are the interpolation matrices. c refers to continuous and d to discontinuous. The element discontinuity interpolation matrix, $\mathbf{N}^{\mathrm{d}}$, is chosen as [24]

$$\mathbf{N}^{\mathrm{d}}(x, y) = \sum_{I} H_I(x, y)\mathbf{N}_I^*(x, y) \tag{2}$$

where $H_I(x, y)$ is the 2D Heaviside step function for node I and the set I is the number of enriched nodes. The step function $H_I(x, y)$ is 0 on the same side of the discontinuity as node I and 1 on the other side. $\mathbf{N}_I^*$ is the part of $\mathbf{N}^*$ from node I. In the standard case, $\mathbf{N}^*$ is chosen as $\mathbf{N}^{\mathrm{c}}$, but for the proposed element $\mathbf{N}^*$ is more general but able to describe the same variations as $\mathbf{N}^{\mathrm{c}}$. Figure 2 shows an example of the standard discontinuous displacement field for a CST element completely cut by a crack. The special enrichment applied in this work was developed from these standard enrichments.

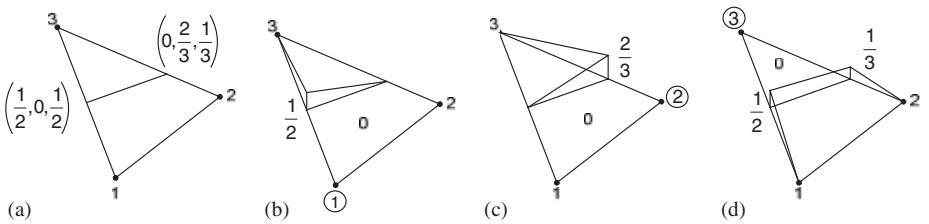

Figure 2. Example of the enrichment of the displacement field for cracked CST element. (a) Crack geometry, (b)–(d) discontinuous displacement field for discontinuity DOFs in nodes 1–3.

DOI: 10.1002/nme

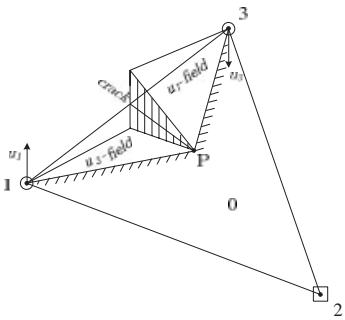

Figure 3. New XFEM crack-tip element.

The requirement for the new partly cracked tip element is that it must be able to model equal stresses on both sides of the discontinuity, i.e. the element must be able to perform as shown in Figure 3.

From Figure 3, it can be seen that an internal pseudo-node P, located at the crack tip, has been introduced. The pseudo-node does not hold any DOFs; it is just a point at which the discontinuous displacement field vanishes. Activating the enrichment of both nodes 1 and 3 allows for variations in the displacement fields on both sides of the crack as shown in the figure. This means that the element becomes capable of modelling the case where equal stresses are present on both sides of the crack. But the introduction of the pseudo-node defining the sub-displacement field 1-P-3 requires extra attention to the propagation of the crack from one element to another. Figure 4 illustrates the situation just before and just after the crack has crossed an element boundary. When the crack propagates within one element (upper part of Figure 4), the contribution to the displacement field from the discontinuity DOFs in node 3 can have a value. When the crack just has passed an element edge and starts to propagate into a new element (lower part of Figure 4), the contribution from the discontinuity DOFs in node 3 must increase from a value of 0. To deal with this discrepancy in the value of the DOFs, the nodes connected to the element edge cut just before the crack propagates into a new element are enriched with extra discontinuity DOFs—cf. Figure 5(c) and (d). As long as an element is acting as a crack-tip element, only the discontinuity DOFs corresponding to (a) and (b) will be active. When the crack propagates into the next element, the discontinuity DOFs corresponding to (c) and (d) becomes active in the element which is now the previous crack-tip element. The extra set of discontinuity DOFs can model a displacement field in the neighbour crack-tip element that is equal to the displacement field along the edge 2–3 in the lower figure in Figure 4, whereby the desired continuity across the element boundary is achieved.

The discontinuous displacement field in node 3 in relation to the tip edge (Figure 5(c)) is found by the superposition of the standard discontinuous displacement field in node 3 and a standard nodal displacement field for node 3 taking into account the sub-triangle 1-P-3 in Figure 3. The superposition is illustrated in Figure 6.

So far the two enrichments in node 3 have just been referred to as $u_{3,1}$ and $u_{3,2}$, however, it is evident from the figures, especially Figure 6 that the discontinuous DOFs in node 3 are element side local—$u_{3,1}$ refers to the 'entrance' side where the crack propagates into the element while $u_{3,2}$ refers to the 'exit' side where the crack leaves the element, and the element becomes fully cracked.

DOI: 10.1002/nme

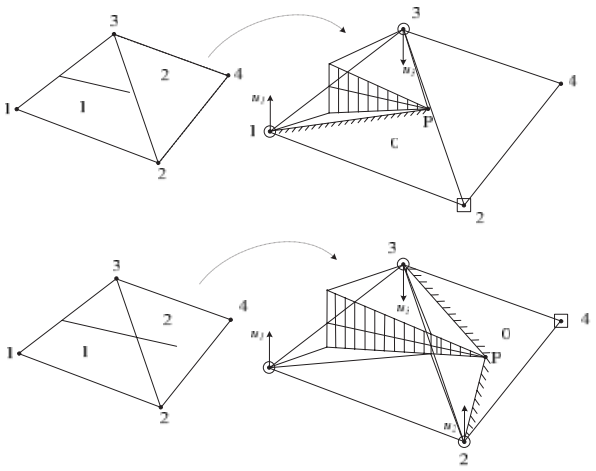

Figure 4. Propagation of a crack across an element boundary. The upper figures illustrate the situation just before the crack reaches the element boundary, while the lower figures illustrate the case where a crack continues into a new element.

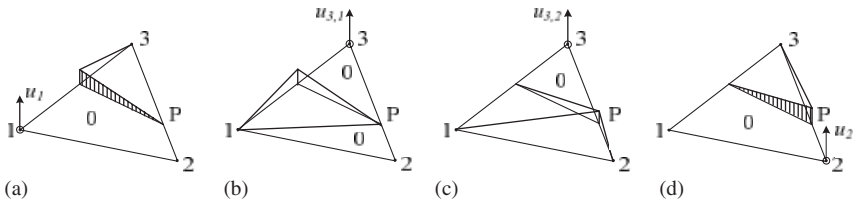

Figure 5. Nodal discontinuous displacement fields for the new crack-tip element: (a) field corresponding to node number 1; (b) field for node 3 referring to the 'entrance' side of the element; (c) field for node 3 referring to the 'exit' side of the element; and (d) field for node 2.

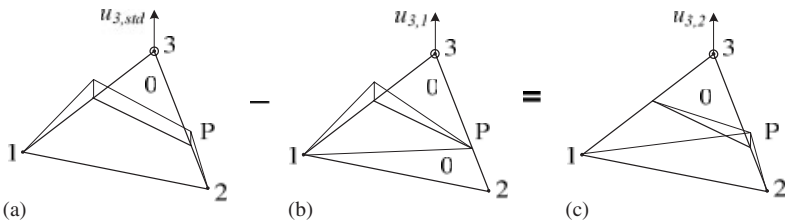

Figure 6. Construction of discontinuous displacement field $u_{3,2}$ by superposition.

The enrichment of a node in an element where two element sides are cut by the discontinuity may now be summarized by writing out the elements of the interpolation matrix N^* for the element. With reference to Figures 5 and 6, the local element co-ordinates in terms of area co-ordinates for the entire element (1–2–3) are termed $(\zeta_1, \zeta_2, \zeta_3)$, while the area co-ordinates for the sub-triangle (1-P-3) are termed $(\tilde{\zeta}_1, \tilde{\zeta}_2, \tilde{\zeta}_3)$. In line with the previously introduced notation, $N^*_{3,1}$ refers to the

DOI: 10.1002/nme

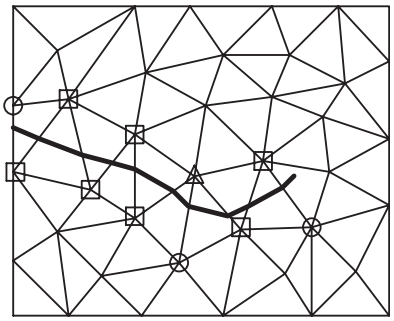

Figure 7. Enrichment at system level. Nodes marked with a circle have one set of discontinuity DOFs, nodes marked with a square have two sets, while the node marked with a triangle has three sets.

entrance side of the element and $N^*_{3,2}$ to the exit side of the element

$$\begin{aligned} N^*_1 &= \zeta_1 \\ N^*_2 &= \zeta_2 \\ N^*_{3,1} &= \tilde{\zeta}_3 \\ N^*_{3,2} &= \zeta_3 - \tilde{\zeta}_3 \end{aligned} \tag{3}$$

At the system level, the enrichment is limited to nodes whose support is cut by the discontinuity. In the above discussed case where focus was on the crack propagating from one element to another, one extra set of discontinuity DOFs was added to the node that is common for the element sides cut by the discontinuity. However, in the general case where several element sides cut by the discontinuity all share a given node, there will be as many active sets of discontinuity DOFs in that node as the number of element sides cut by the discontinuity sharing that node. The enrichment at system level is illustrated in Figure 7 where some nodes have one set of active discontinuity DOFs, some nodes have two active sets, and one node has three active sets.

However, the storage of a variable number of DOFs in the nodes is seen as less favourable due to the handling of the DOFs at system level. The enrichments are, therefore stored side-locally, depending on whether they belong to the 'entrance' or the 'exit' side of the element. This will be discussed in detail in Section 4, 'Aspects of implementation'.

3. VARIATIONAL FORMULATION

Given a cohesive crack in a structure in a state of plane stress or plane strain described in a Cartesian co-ordinate system x, y (cf. Figure 8), the arc length along the crack is termed s, and n, s is a curve linear co-ordinate system, n being normal to the crack face. The positive direction of s is seen in Figure 8. The orientation of n determines the positive side of the crack. The stress state in the crack may be defined by the normal stress σ_n and the shear stress τ_{ns} while work-conjugated generalized strains are the opening of the crack, $\Delta u_n = u_n^+ - u_n^-$ and the slip in the crack, $\Delta u_s = u_s^+ - u_s^-$. A small strain/small displacement static theory is used and the material outside the crack is assumed linear elastic.

DOI: 10.1002/nme

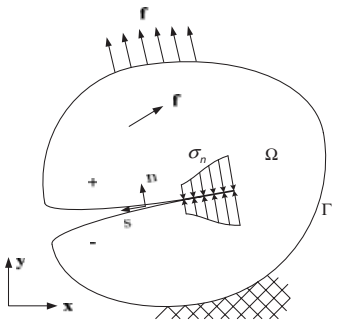

Figure 8. Cohesive crack in a two-dimensional domain with **f** representing both domain load and boundary load.

Let $[\![\ \ ]\!]$ denote a jump, then the stress increments $\mathrm{d}\boldsymbol{\sigma}^{\mathrm{cr}}$ across the crack surfaces are related to the increments in the displacement jump, $\mathrm{d}[\![\mathbf{u}]\!]$,—i.e. the separation of the crack surfaces—through the tangential material stiffness matrix $\mathbf{D}_{\mathrm{T}}^{\mathrm{cr}}$

$$\boldsymbol{\sigma}^{\mathrm{cr}}([\![\mathbf{u}]\!]) = \begin{bmatrix} \sigma_n([\![\mathbf{u}]\!]) \\ \tau_{ns}([\![\mathbf{u}]\!]) \end{bmatrix}, \quad [\![\mathbf{u}]\!] = \begin{bmatrix} \Delta u_n \\ \Delta u_s \end{bmatrix}, \quad \mathrm{d}\boldsymbol{\sigma}^{\mathrm{cr}}([\![\mathbf{u}]\!]) = \mathbf{D}_{\mathrm{T}}^{\mathrm{cr}}([\![\mathbf{u}]\!])\mathrm{d}[\![\mathbf{u}]\!] \tag{4}$$

For the uncracked part of the structure, the stress vector $\boldsymbol{\sigma}^{\mathrm{T}} = [\sigma_x \ \ \sigma_y \ \ \tau_{xy}]$ and the strain vector $\boldsymbol{\varepsilon}^{\mathrm{T}} = [\varepsilon_x \ \ \varepsilon_y \ \ \gamma_{xy}]$, $(\gamma_{xy} = 2\varepsilon_{xy})$ are defined as usual and related through the standard material stiffness matrix **D**, specified below for an isotropic material in plane stress

$$\mathrm{d}\boldsymbol{\sigma} = \mathbf{D}\mathrm{d}\boldsymbol{\varepsilon}, \quad \mathbf{D} = \frac{E}{1-\nu^2}\begin{bmatrix} 1 & \nu & 0 \\ \nu & 1 & 0 \\ 0 & 0 & \dfrac{1-\nu}{2} \end{bmatrix} \tag{5}$$

The virtual internal work-per-unit length of the crack δW_{cr}^i and the virtual internal work-per-unit area of the uncracked part of the structure δW_{c}^i may now be written, δ referring to a virtual quantity

$$\begin{aligned} \delta W_{\mathrm{cr}}^i &= \delta[\![\mathbf{u}]\!]^{\mathrm{T}}\boldsymbol{\sigma}^{\mathrm{cr}} = \sigma_n\delta\Delta u_n + \tau_{ns}\delta\Delta u_s \\ \delta W_{\mathrm{c}}^i &= \delta\boldsymbol{\varepsilon}^{\mathrm{T}}\boldsymbol{\sigma} = \sigma_x\delta\varepsilon_x + \sigma_y\delta\varepsilon_y + \tau_{xy}\delta\gamma_{xy} \end{aligned} \tag{6}$$

For the entire structure the virtual internal and external work becomes

$$\begin{aligned} \delta W^i &= \int_\Omega \delta\boldsymbol{\varepsilon}^{\mathrm{T}}\boldsymbol{\sigma}\,\mathrm{d}\Omega + \int_\Gamma \delta[\![\mathbf{u}]\!]^{\mathrm{T}}\boldsymbol{\sigma}^{\mathrm{cr}}\,\mathrm{d}\Gamma \\ \delta W^e &= \int_\Omega \delta\mathbf{u}^{\mathrm{T}}\mathbf{f}\,\mathrm{d}\Omega + \int_\Gamma \delta\mathbf{u}^{\mathrm{T}}\mathbf{f}\,\mathrm{d}\Gamma \end{aligned} \tag{7}$$

where **f** is the load on the structure.

DOI: 10.1002/nme

By applying incremental quantities, the incremental stiffness relation, can be obtained

$$\mathbf{K}_{\mathrm{T}}\Delta\mathbf{V} = \int_{\Omega} \mathbf{N}^{\mathrm{T}}\Delta\mathbf{f}\,\mathrm{d}\Omega + \int_{\Gamma} \mathbf{N}^{\mathrm{T}}\Delta\mathbf{f}\,\mathrm{d}\Gamma \tag{8}$$

where $\mathbf{V}$ is the system DOF vector and Δ refers to an incremental quantity.

Special attention must be paid to the internal work, because the contribution from each element to the tangential stiffness matrix $\mathbf{K}_{\mathrm{T}}$ depends on whether the element is cracked or not. The element tangential stiffness matrix, $\mathbf{k}_{\mathrm{T}}$, for a cracked element is found by the following procedure. From (1) and (2) the strain vector in a cracked element, except in the crack itself, is obtained

$$\boldsymbol{\varepsilon} = \mathbf{B}^{\mathrm{c}}\mathbf{v}^{\mathrm{c}} + \sum H_I \mathbf{B}_I^{\mathrm{c}}\mathbf{v}_I^{\mathrm{d}} = \mathbf{B}^{\mathrm{c}}\mathbf{v}^{\mathrm{c}} + \mathbf{B}^{\mathrm{d}}\mathbf{v}^{\mathrm{d}} \tag{9}$$

where $\mathbf{B}^{\mathrm{c}}$ and $\mathbf{B}^{\mathrm{d}}$ are the strain distribution matrixes corresponding to the interpolation matrix $\mathbf{N}^{\mathrm{c}}$, respectively, $\mathbf{N}^{\mathrm{d}}$.

Due to the displacement field from the first terms in (1) being continuous, the strains in the crack itself may be written as

$$[\![\mathbf{u}]\!](s) = \mathbf{T}(\mathbf{N}_{+}^{\mathrm{d}}(s) - \mathbf{N}_{-}^{\mathrm{d}}(s))\mathbf{v}^{\mathrm{d}} = \mathbf{B}^{\mathrm{cr}}\mathbf{v}^{\mathrm{d}} \tag{10}$$

Here, $\mathbf{B}^{\mathrm{cr}}$ is the strain distribution matrix in the crack, $\mathbf{T}$ is the transformation matrix between the (x, y) and (n, s) co-ordinate systems, while $\mathbf{N}_{+}^{\mathrm{d}}$ and $\mathbf{N}_{-}^{\mathrm{d}}$ are the discontinuous interpolation matrices on the positive and negative sides of the crack, respectively.

Applying the strain relations in (9) and (10), the virtual incremental internal work, $\mathbf{k}_{\mathrm{T}}$, defined by $\delta W^i = \delta\mathbf{v}^{\mathrm{T}}\mathbf{k}_{\mathrm{T}}\Delta\mathbf{v}$ where $\mathbf{v}^{\mathrm{T}} = [\mathbf{v}^{\mathrm{c}^{\mathrm{T}}}\ \ \mathbf{v}^{\mathrm{d}^{\mathrm{T}}}]$, is found to be

$$\mathbf{k}_{\mathrm{T}} = \begin{bmatrix} \int \mathbf{B}^{\mathrm{c}^{\mathrm{T}}}\mathbf{D}\mathbf{B}^{\mathrm{c}} & \int \mathbf{B}^{\mathrm{c}^{\mathrm{T}}}\mathbf{D}\mathbf{B}^{\mathrm{d}} \\ \int \mathbf{B}^{\mathrm{d}^{\mathrm{T}}}\mathbf{D}\mathbf{B}^{\mathrm{c}} & \int \mathbf{B}^{\mathrm{d}^{\mathrm{T}}}\mathbf{D}\mathbf{B}^{\mathrm{d}} + \int_{\mathrm{cr}} \mathbf{B}^{\mathrm{cr}^{\mathrm{T}}}\mathbf{D}^{\mathrm{cr}}\mathbf{B}^{\mathrm{cr}} \end{bmatrix} = \begin{bmatrix} \mathbf{k}^{\mathrm{cc}} & \mathbf{k}^{\mathrm{cd}} \\ \mathbf{k}^{\mathrm{dc}} & \mathbf{k}^{\mathrm{dd}} + \mathbf{k}_{\mathrm{T}}^{\mathrm{cr}} \end{bmatrix} \tag{11}$$

Due to a constant D-matrix outside the crack, the stiffness contribution from the areas outside the crack is constant and thus only the stiffness contribution from the crack itself is non-linear.

The element nodal forces, $\mathbf{q}$, depend like $\mathbf{k}_{\mathrm{T}}$ on the crack opening, and they are determined analogous to $\mathbf{k}_{\mathrm{T}}$. The contribution to $\mathbf{q}$ from the crack, $\mathbf{q}^{\mathrm{cr}}$, is found from the stresses in the crack. The stresses in the crack are related to the displacement jump across the crack according to (4). By adding this contribution to the contribution from the part of the element outside the crack, $\mathbf{q}$ is obtained as

$$\mathbf{q} = \begin{bmatrix} \mathbf{k}^{\mathrm{cc}} & \mathbf{k}^{\mathrm{cd}} \\ \mathbf{k}^{\mathrm{dc}} & \mathbf{k}^{\mathrm{dd}} \end{bmatrix} \begin{bmatrix} \mathbf{v}^{\mathrm{c}} \\ \mathbf{v}^{\mathrm{d}} \end{bmatrix} + \mathbf{q}^{\mathrm{cr}} \quad \text{where } \mathbf{q}^{\mathrm{cr}} = \int_{\mathrm{cr}} \mathbf{B}^{\mathrm{cr}^{\mathrm{T}}} \begin{Bmatrix} \sigma_n \\ \tau_{ns} \end{Bmatrix} \tag{12}$$

4. ASPECTS OF IMPLEMENTATION

This section concerns the implementation of the proposed element. The introduction of two sets of discontinuity DOFs in some of the nodes requires some extra bookkeeping and some comments will

DOI: 10.1002/nme

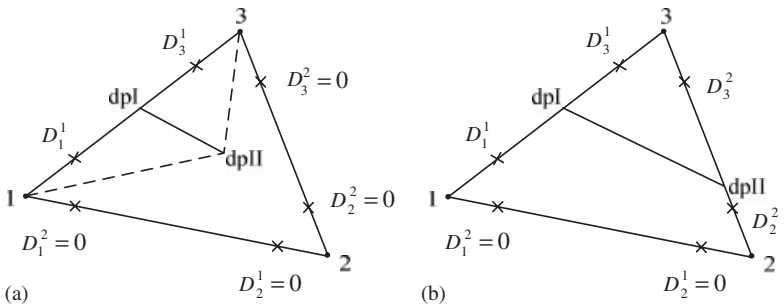

Figure 9. Element side local storage of discontinuous DOFs: (a) a partly cracked element and (b) a fully cracked non-tip element. D_{NO}^1 refers to discontinuity DOFs related to the 'entry' side of the element in node *NO* while D_{NO}^2 refers to discontinuity DOFs related to the 'exit' side of the element in node *NO*.

be given on the storage of these extra discontinuity DOFs. Hereafter the applied integration scheme will be presented. Then follows a discussion about the criterion for crack growth and smooth crack closure. The section concludes by illustrating the algorithm used to solve the non-linear equations in a schematic form.

4.1. Storage of discontinuity degrees of freedom

The additional discontinuous DOFs requires extra bookkeeping hence the affiliation of discontinuous DOFs to the element edges discussed in the previous section. Therefore, for storage purposes only, the discontinuous DOFs are related to the element edges, as illustrated in Figure 9. Figure 9(a) illustrates how the two active sets of discontinuous DOFs are stored when an element acts as a partly cracked tip element, while Figure 9(b) illustrates the storage of the four sets of discontinuous DOFs for a fully cracked non-tip element.

4.2. Integration scheme

Integration must be performed independently on each side of the discontinuity in elements cut by the discontinuity. For integration purposes, elements cut by the discontinuity are therefore divided into four sub-triangles in the case of partly cracked elements or into three sub-triangles in the case of fully cracked elements, as illustrated in Figure 10. One point Gauss quadrature is applied to each sub-triangle. Along the line of discontinuity, two point integration is applied. For elements not cut by the discontinuity standard, one point Gauss integration is performed.

4.3. Criteria for crack growth and smooth closure

A CST element is by default only able to model constant stresses in the element. Therefore, there is a need to construct a stress interpolation through the element when the element acts as a partly cracked tip element where stresses equal to the tensile strength are to be found at the tip. Furthermore, it is important to ensure a smooth transition when an element changes status from being uncracked to partly cracked and later changes status to being fully cracked. The smooth transition is of major importance for the capability of the element to model all possible crack lengths and for the stability of the iterative procedure.

DOI: 10.1002/nme

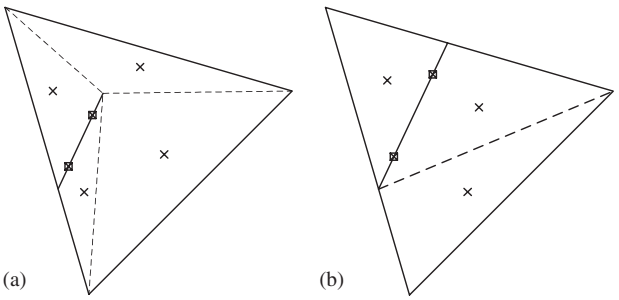

Figure 10. Integration scheme for: (a) a partly cracked element and (b) a fully cracked element. Crosses mark integration points in the continuum part of elements while boxes mark integration points on the line of discontinuity for integration of traction forces.

A stress interpolation is created from the average nodal stresses computed by weighting the contribution from each element to a given node with the area of that element—cf. (13)

$$\boldsymbol{\sigma}_{\mathrm{no}}^{\mathrm{ave}} = \left(\sum_{i=1}^{n_{\mathrm{el}}^{\mathrm{no}}} \boldsymbol{\sigma}_i A_i \right) \Bigg/ \sum_{i=1}^{n_{\mathrm{el}}^{\mathrm{no}}} A_i \tag{13}$$

where $\boldsymbol{\sigma}_{\mathrm{no}}^{\mathrm{ave}}$ is the average nodal stress, $n_{\mathrm{el}}^{\mathrm{no}}$ is the number of elements sharing a given node, $\boldsymbol{\sigma}_i$ is the stress in element i and A_i is the area of element i.

The contribution from fully cracked or partly cracked elements is weighted by using the relevant sub-areas when taking into account the contribution from the discontinuous displacement field. By weighting the stress contribution from the discontinuous field with the corresponding sub-areas in the partly cracked element, stress continuity across the element boundary is ensured when the discontinuity propagates from one element to another. From the nodal stresses, a linear interpolation is used for computation of the tip stresses.

Several strategies can be applied for the crack growth. In this work, the crack propagates when the tensile strength of the material is exceeded in the crack tip, and the crack is propagated in the normal direction for the principal stress direction in the crack tip. The crack may be incremented either in pre-specified increments or it may be propagated to the point where the continuous field yields tensile stresses equal to the tensile strength for a given load increment. The crack length is then kept constant in the load step for the following iterations. To keep the crack length constant in each load step, the iteration procedure has to ensure stresses equal to the tensile strength in the crack tip. This issue will be returned to below, when the algorithm used for solving the non-linear equations is discussed.

In a cohesive crack, tractions act at the crack surfaces near the tip, as illustrated in Figure 8, causing the crack to close smoothly. For an opening crack the tensile stresses at the crack tip will be equal to the tensile material strength, corresponding to vanishing stress intensity factors at the crack tip. Therefore, criteria for smooth closure can be imposed in terms of either a stress criterion or an equivalent stress intensity factor criterion. Investigations using interface cohesive crack elements [37] show that smooth crack closure is automatically achieved in a finite element formulation with a stress criterion when applying a sufficient number of elements for the cohesive zone, so no additional criterion for smooth closure is necessary.

DOI: 10.1002/nme

4.4. Algorithm

To remain within the framework of traditional FEM code, a general procedure, the orthogonal residual algorithm [38], was adopted for the XFEM scheme to solve the non-linear equations in [33]. The algorithm proved to be efficient for fully cracked elements and it was therefore also used here. In the present case, the algorithm is supplemented with a stress criterion for smooth crack closure—i.e. the iterative procedures ensures stresses equal to the tensile strength in the crack tip. The algorithm is summarized in Table I. The focus in this work was on the development and the performance of the new crack-tip element and the procedure for ensuring stresses equal to the material tensile strength at the crack tip was chosen as the simplest and most robust possible. In terms of speed, the algorithm could be improved by applying a more sophisticated strategy for the crack-tip stress iterations.

As a convergence criterion, an energy criterion was applied, and the elastic energy in the initial elastic load step was used as reference energy, E_{ref}. Furthermore, it will be noticed that it was decided to implement the orthogonal residual algorithm in a Newton–Raphson style, where the tangential stiffness matrix was updated in each iteration to take into account changes in crack opening and thus also changes in the contributions from the enriched nodes during the iterations.

5. NUMERICAL EXAMPLES

The performance of the new crack-tip element was tested by modelling of fracture in two fracture mechanical benchmark tests: the TPBT and the FPSB. The results will be compared to those obtained applying fully cracked elements in [33]. Furthermore, the XFEM results will be compared against results obtained by modelling fracture in the TPBT specimen applying standard cohesive interface elements in the commercial code DIANA. With regard to the FPSB, the XFEM results will be compared to experimental results obtained by Carpinteri and co-workers [39].

5.1. Three point beam bending test

The geometry of the TPBT specimen considered in this case is in accordance with RILEM recommendations [40]. The geometry is shown in Figure 11(a), the cross-section of the beam being a square. For the material parameters, standard values for a good-quality concrete were chosen, cf. Figure 12. A linear softening law, as illustrated in Figure 11(b), was applied for the normal stress in the crack. Only Mode I opening of the crack was considered and both the shear term and the coupling terms in the tangential material stiffness matrix for the crack were set to zero cf. (14).

$$\mathbf{D}_{\text{cr}}^{\text{T}} = \begin{bmatrix} \dfrac{-f_t}{\Delta u_{n,\text{ult}}^{\text{cr}}} & 0 \\ 0 & 0 \end{bmatrix} \tag{14}$$

Keeping in mind that the overall research perspective was to be able to model fracture in real size civil structures, investigations were carried out examining fairly coarse meshes compared to what may be found in the literature. For the TBTP specimen, a structured mesh of 25 by 24 elements (24 elements over the beam height—20 elements from the notch to the top of the beam) as well as an unstructured mesh of 709 elements holding 25 elements of varying size over the beam height

DOI: 10.1002/nme

Table I. Orthogonal residual algorithm for XFEM.

initial state: $\mathbf{u}_0, \mathbf{f}_0, \Delta\mathbf{u}_0 = 0, E_{\text{ref}}, \Delta\mathbf{f}_0$
load increments n=1,2...,$n_{\max}$
$\Delta\mathbf{u}_1 = \mathbf{K}_{\text{T},n-1}^{-1}\Delta\mathbf{f}_n$
$\Delta\mathbf{u} = \min(1, u_{\max}/\|\Delta\mathbf{u}\|)\Delta\mathbf{u}$
$\Delta\mathbf{u}_0^{\text{T}}\Delta\mathbf{u} < 0$ *then* $\Delta\mathbf{u} = -\Delta\mathbf{u}, \Delta\mathbf{f} = -\Delta\mathbf{f}$
$j = 1$
Iterations $i = 1, 2, \ldots i_{\max}$
$\Delta\mathbf{q} = \mathbf{q}(\mathbf{u} + \Delta\mathbf{u}) - \mathbf{f}_{n-1}$
$\zeta = \mathbf{q}^{\text{T}}\mathbf{u}/\mathbf{f}_n^{\text{T}}\Delta\mathbf{u}$ — ζ *is the optimal load scaling factor*
$\mathbf{r} = \zeta\Delta\mathbf{f}_n - \Delta\mathbf{q}$ — $\mathbf{r}$ *is the unbalanced force vector*
$\mathbf{K}_{\text{T},n} = \mathbf{K}_{\text{T}}(\mathbf{u} + \Delta\mathbf{u})$
$\delta\mathbf{u} = \mathbf{K}_{\text{T},n}^{-1}\mathbf{r}$ — $\delta\mathbf{u}$ *is the displacement correction*
$\delta\mathbf{u} = \min(1, u_{\max}/\|\delta\mathbf{u}\|)\delta\mathbf{u}$
$E_i = \mathbf{r}^{\text{T}}\delta\mathbf{u}$ — E_i *is the residual energy*
$\varepsilon_i = E_i/E_{\text{ref}}$
$\Delta\mathbf{u} = \Delta\mathbf{u} + \delta\mathbf{u}$
if $\varepsilon_i \leqslant$ *stop value*
$\Delta\sigma_{\text{tip}} = f_t - \sigma_{\text{tip}}$
if $\Delta\sigma_{\text{tip}} > \gamma f_t$ — γ *is the tolerance on* σ_{tip}
if $j = 1$
if $\Delta\sigma_{\text{tip}} > 0$
$\Delta\mathbf{f}_n = \Delta\mathbf{f} + \beta\Delta\mathbf{f}_0$ — β *is a load scaling factor*
if $\Delta\sigma_{\text{tip}} < 0$
$\Delta\mathbf{f}_n = \Delta\mathbf{f} - \beta\Delta\mathbf{f}_0$
end
else
$$\delta\mathbf{f}_n = (f_t - \sigma_{\text{tip}})\frac{\Delta\mathbf{f}(j) - \Delta\mathbf{f}(j-1)}{\sigma_{\text{tip}}(j) - \sigma_{\text{tip}}(j-1)}$$
$\Delta\mathbf{f}_n = \Delta\mathbf{f}_n - \phi\delta\mathbf{f}$ — ϕ *is a numerical damping factor*
end
$j = j+1, \quad \Delta\mathbf{u} = \mathbf{K}_{\text{T},n}^{-1}\Delta\mathbf{f}_n, \quad \varepsilon_i = 1$
end
end
stop iteration when $\varepsilon_i \leqslant$ *stop value*
$\mathbf{u}_n = \mathbf{u}_{n-1} + \Delta\mathbf{u}_n$
$\mathbf{f}_n = \mathbf{f}_{n-1} + \zeta\Delta\mathbf{f}_n$
$\Delta\mathbf{u}_0 = \Delta\mathbf{u}$
stop load increments when $\|\mathbf{u}_n\| > u_{\max}^{\text{check}}$

were considered. The structured mesh is depicted in Figure 13, which shows the fractured beam, while the unstructured mesh is depicted in Figure 14. In both cases, the crack path was achieved by propagating the crack half the way through one element in each step. For the structured mesh,

DOI: 10.1002/nme

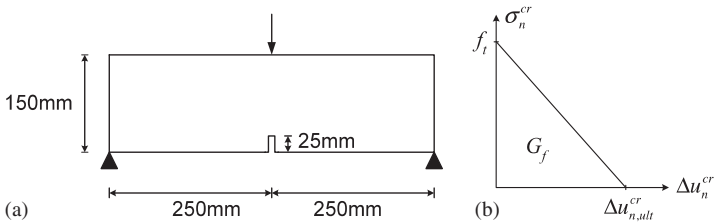

Figure 11. (a) Geometry of TPBT specimen and (b) applied linear softening curve.

Parameter	Value
E_c	37400MPa
ν_c	0.2
f_t	3.5MPa
G_f	160 N/m

Figure 12. Concrete parameters.

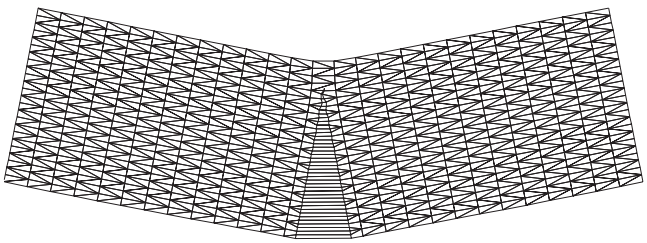

Figure 13. Crack path for a TPBT specimen, modelled applying partly cracked elements in a structured mesh of 25 by 24 elements. The crack was propagated half an element length in each step.

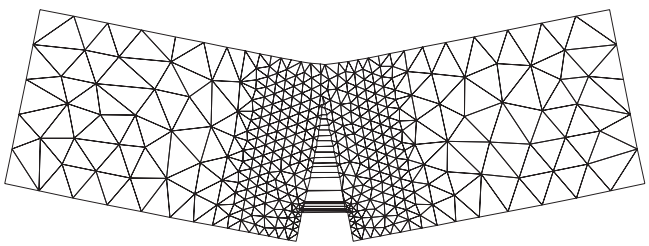

Figure 14. Crack path for a TPBT specimen, modelled applying partly cracked elements in an unstructured mesh of 709 elements. The crack was propagated half an element length in each step.

DOI: 10.1002/nme

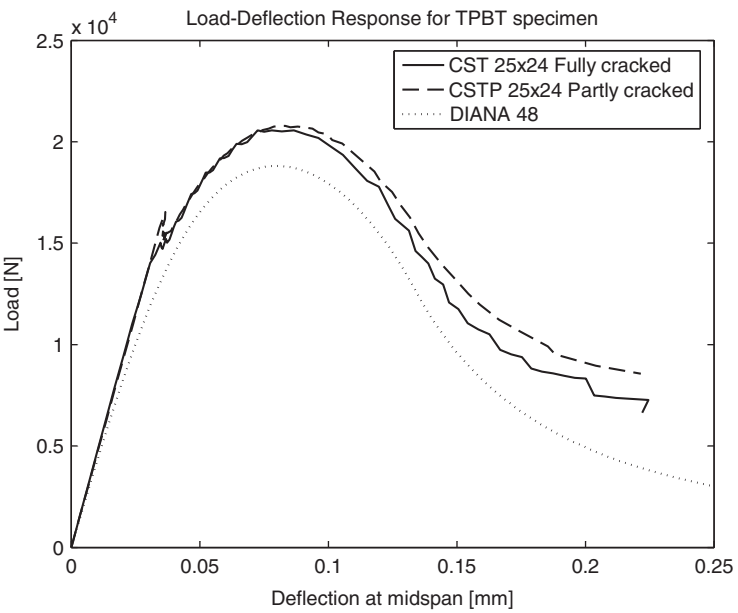

Figure 15. Crack path for TPBT specimen modelled applying partly cracked elements in a structured mesh of 25 by 24 elements. The crack was propagated half an element length in each step.

the notch was modelled as a pre-defined stress-free discontinuity. In the unstructured mesh, the notch was geometrically modelled, resulting in fairly small elements present just next to the tip of the notch. In both cases, the tolerance on crack-tip stress (γ in Table I) was set to 1% of the material tensile strength. In the last three steps for each mesh, slightly higher tolerance on the tip stress was allowed—for the structured mesh up to 2.6% error and for the unstructured mesh up to 4% error.

The load–displacement responses for the two models of fracture in the TPBT specimen are depicted in Figures 15 and 16. The deformation was computed as the difference between the vertical displacement of the centre point of the beam and the average vertical displacement of the mid-points of the beam ends. In both figures, the results obtained when using partly cracked CST elements are compared with results obtained using fully cracked CST elements, cf. [33], and with results obtained using 48 standard 3-node cohesive interface elements over the beam height in the commercial code DIANA.

In both cases, the application of the new partly cracked tip element produces a significantly smoother response than was obtained using fully cracked elements. The characteristics in terms of maximum load-carrying capacity and the overall shape of the response are, as expected, seen to be almost the same for fully cracked and partly cracked elements. With regard to the maximum load-carrying capacity, the structured mesh overestimates the load-carrying capacity by about 8%, while the unstructured mesh captures the maximum load-carrying capacity well. With regard to the post-peak response, the major part is captured well for both meshes. The difference in the determined load level for the last part of the post-peak response between the computations applying fully cracked and partly cracked elements is partly due to the fact that, when applying fully cracked elements,

DOI: 10.1002/nme

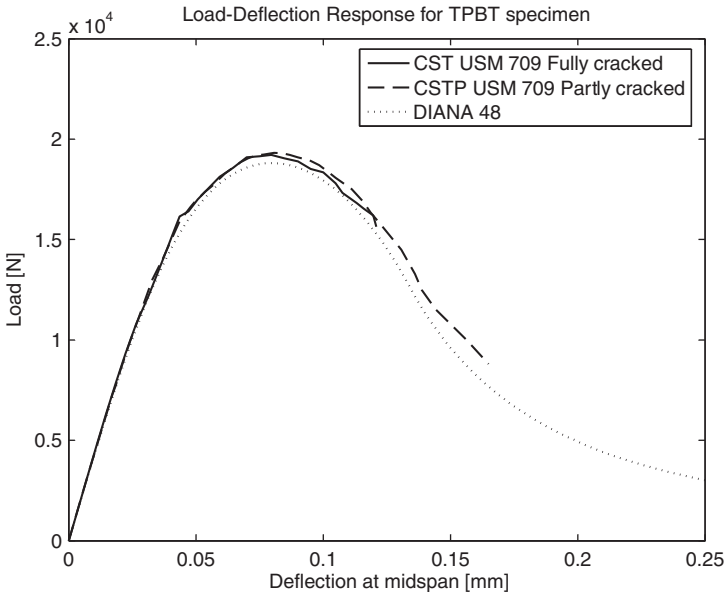

Figure 16. Crack path for TPBT specimen modelled applying partly cracked elements in a unstructured mesh of 709 elements. The crack was propagated half an element length in each step.

stresses equal to the material tensile strength are not assured in the crack tip. Another reason is that for fully cracked elements, the criterion for crack growth is based on element local stresses, while in the partly cracked case, crack growth is based on average nodal stresses. The difference compared with the DIANA computations is partly due to the difference in the applied number of elements, the different order of applied elements, and partly to the tortuosity of the last part of the XFEM crack path. When there are about four elements left between the crack tip and the top of the beam, the limited capability of CST elements does not allow for a reasonable stress variation across the remaining elements, and solutions where the tip stresses are equal to the material tensile stress may not be obtained.

From the load–deformation responses—in particular for the structured mesh—a sudden drop in the load-carrying capacity may be noted when the first element cracks. This non-smooth start of the non-linear response is due to the inability of one cracked CST element to produce a smooth closing crack and thus reproduce the required cohesive crack profile. About three elements are required to model the smooth closure and thus the nature of a cohesive crack. The smooth closure of the cohesive crack can also be seen in Figure 17 which shows different stages of the crack propagation in the structured mesh. From Figure 17 it may also be noticed that the tortuosity of the crack increases as the crack approaches the top of the beam. This is due to the difficulties of modelling the true stress distribution with only a few un-cracked elements available. With regard to the cohesive stresses across the crack, it should also be mentioned that the crack in the element next to the notch becomes stress free when the load has decreased to the level of the crack initiation ($\sim 15\,\mathrm{kN}$) on the post-peak response.

In the application of partly cracked elements, it is interesting to study the behaviour of the structural response when the crack propagates through a single element in more steps. In Figure 18,

DOI: 10.1002/nme

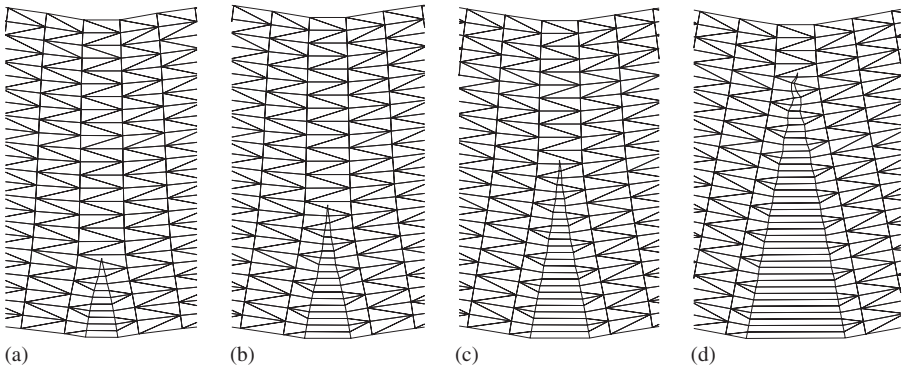

Figure 17. Propagation of crack in structured mesh: (a) $P = 15.3\,\text{kN}$, scaling factor 1140; (b) $P = 18.9\,\text{kN}$, scaling factor 762; (c) $P = 20.8\,\text{kN}$ (max load), scaling factor 526; and (d) $P = 8.6\,\text{kN}$, scaling factor 208.

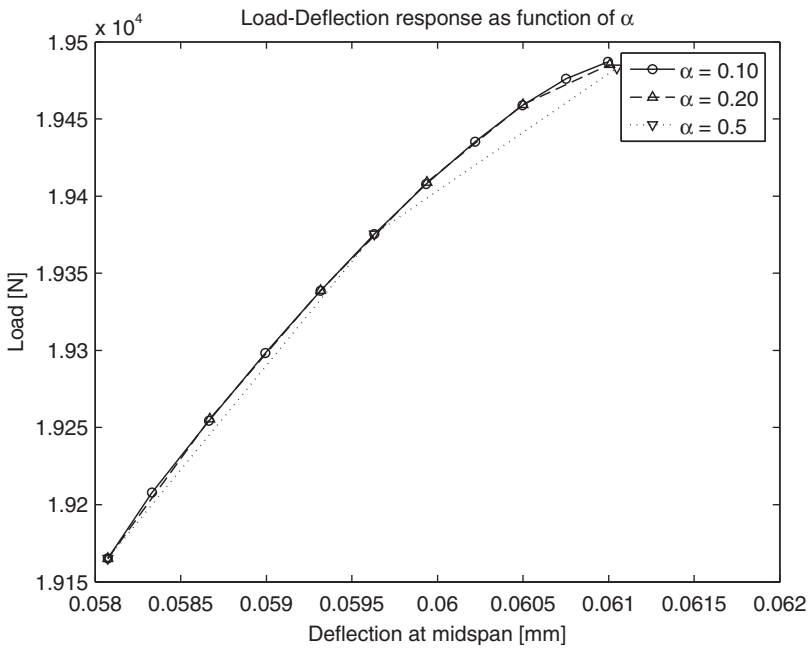

Figure 18. Load–deformation response as a function of crack-length increment when a crack propagates through one element (the element next to the tip element in 17(b)). α is the relative crack-length increment. $\alpha = 1$ corresponds to the element being fully cracked.

the load–deformation response is plotted for three different crack-length increments for a crack propagating through one element—in the present case when the crack is propagating through the element next to the tip element in Figure 17(b). The plots are obtained prescribing a tolerance on

DOI: 10.1002/nme

the tip stress of 0.01% of the tensile strength. From the figure, it can be seen that the deformation response depends only slightly on the size of the crack-length increment. If an even lower tolerance on the tip stresses is specified, even better results can be obtained. The figure also reveals that a very smooth response is obtained when the crack propagates through an element in several increments. The importance of a smooth response was discussed in the introduction and when discussing the criterion for crack growth. The ability of the proposed partly cracked element in principle to model all possible load–deformation states, and therefore to produce a smooth response for varying crack increments, represents a major improvement compared with elements only able to be fully cracked.

5.2. Four point shear beam

To test the ability of the suggested partly cracked tip element to model curved cracks, fracture of a FPSB was modelled. The geometry of the FPSB or the 'double-edge notched specimen subjected to four-point shear' is equivalent to that of the one investigated experimentally by Carpinteri and co-workers [39]. In [39], it is concluded that the FPSB may be modelled taking into account only mode I fracture. The FPSB specimen was also analysed by XFEM in [22, 33]. The geometry of the test set-up is shown in Figure 19, while constitutive parameters are given in Table II. As for the TPBT specimen, a linear softening curve (Figure 11(b)) was applied.

A fairly coarse structured mesh of 1222 elements and 2549 nodes was used for the XFEM computation. The mesh can be seen in Figure 20, which shows the crack path for the FPSB specimen. The results presented were obtained by propagating the crack in two increments across each element. This made it possible to test the modelling of a great variety of finite crack increments. In some cases, only a 'corner' of an element was cut, while in other cases the crack followed close to the longest possible path through the element.

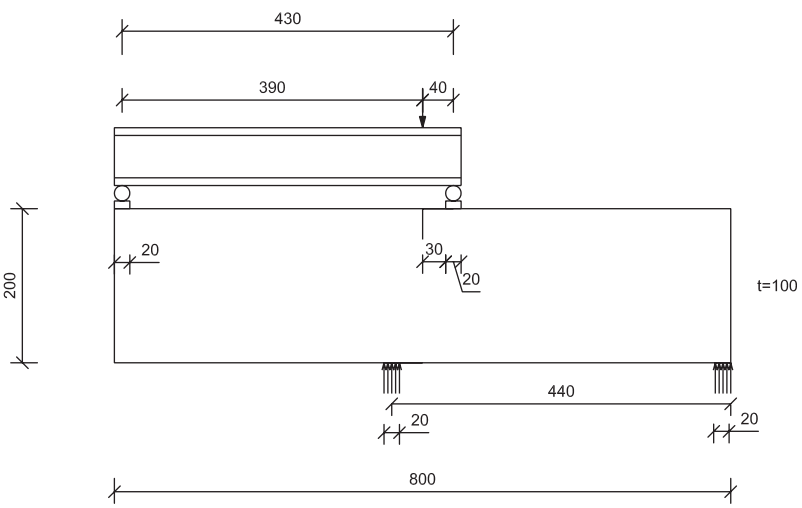

Figure 19. Geometry of four point shear beam, all measures in mm.

DOI: 10.1002/nme

Table II. Constitutive parameters FPSB.

Parameter	Value
E_c	28 000 MPa
ν_c	0.1
f_t	2.4 MPa
G_f	145 N/m

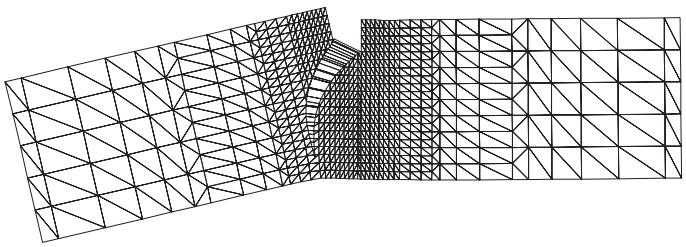

Figure 20. Crack path for fracture in the FPSB specimen.

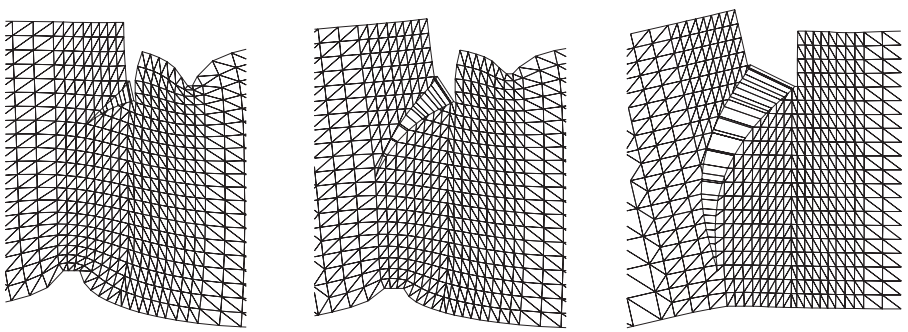

Figure 21. Propagation of crack in FPSB: (a) $P = 62.6$ kN, scaling factor 973; (b) $P = 73.8$ kN (Max load) scaling factor 581; and (c) $P = 21.2$ kN, scaling factor 154.

Figure 21 shows different stages of the developing crack. In Figure 22 the load–deformation response obtained when applying the new partly cracked XFEM element is compared with the experimental results of Carpinteri *et al*. [39] and with the results obtained when applying fully cracked XFEM LST elements [33].

From Figures 20 and 21, it can be seen that when applying the proposed partly cracked XFEM element, a nice smooth crack path is obtained that correlates well with what is observed in experiments. From the load–deformation response, it can also be seen that the results correlates

DOI: 10.1002/nme

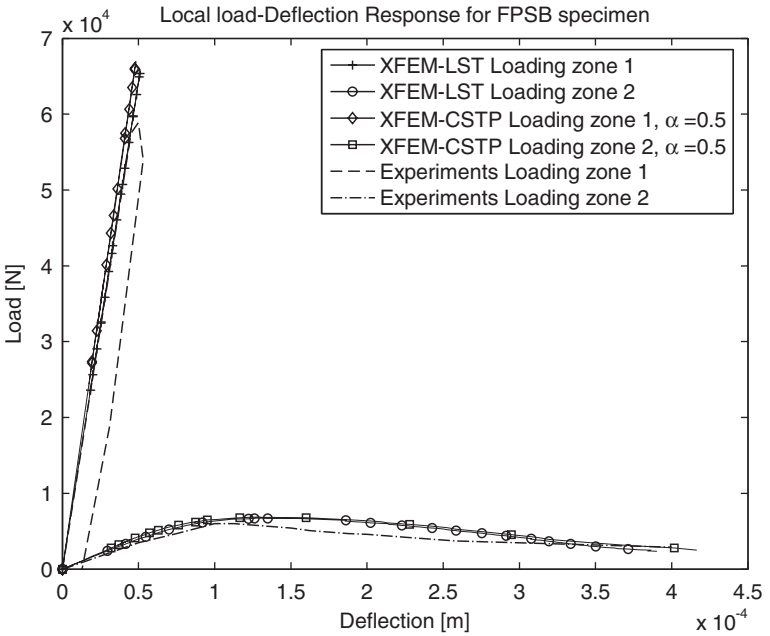

Figure 22. Comparison of load–displacement response for FPSB obtained by the new XFEM model, XFEM results obtained by applying fully cracked LST elements, and experimental results from [39]. Loading zone 2 refers to the loading zone to the left in Figure 19, while loading zone 1 refers to the loading zone to the right. Only every 5th data point in each XFEM LST series has been marked on the graphs.

well with the experimental results as well as with the previously obtained XFEM results for higher-order elements.

6. CONCLUSION

A new XFEM cohesive crack-tip element for cohesive cracking has been developed by the introduction of element side local enrichment of elements cut by the discontinuity. The new enrichment was developed by the superposition of the standard nodal shape functions and standard nodal shape functions for a sub-triangle of the cracked element. When the suggested enrichment is applied, the tip element becomes capable of modelling the situation where equal stresses are present on both sides of the crack. The enrichment was implemented for the three-node triangular constant-strain triangle (CST) element. Based on average nodal stresses for the crack-tip element, a stress interpolation was computed through the tip element and the ability of the tip element to hold the crack tip at different positions through the element was illustrated. The performance of the element in fracture mechanical benchmark tests was illustrated by modelling fracture in the notched TPBT and in the FPSB test. The numerical examples show the element performs well even for fairly coarse meshes.

DOI: 10.1002/nme

Further developments may include the extension of the scheme to higher-order elements and optimization of the algorithm, outlined in Table I, for solving the non-linear equations.

REFERENCES

1. Dugdale DS. Yielding of steel sheets containing slits. *Journal of the Mechanics and Physics of Solids* 1960; **8**:100–104.
2. Barenblatt GI. The mathematical theory of equilibrium of cracks in brittle fracture. *Advances in Applied Mechanics* 1962; **7**:55–129.
3. Hillerborg A, Moder M, Peterson P-E. Analysis of crack formation and crack growth in concrete by means of fracture mechanics and finite elements. *Cement and Concrete Research* 1976; **6**:773–782.
4. Martha L, Waarzynek PA, Ingraffea AR. Arbitrary crack propagation using solid modelling. *Engineering with Computers* 1993; **9**:63–82.
5. Carter BJ, Chen CS, Ingraffea AR, Wawrzynek PA. A topology-based system for modelling 3d crack growth in solid and shell structures. *Proceedings of the Ninth International Congress on Fracture ICF9*. Elsevier: Sydney, Australia, 1997; 1923–1934.
6. Bouchard PO, Bay F, Chastel Y, Tovena I. Crack propagation modelling using an advanced remeshing technique. *Computer Methods in Applied Mechanics and Engineering* 2000; **189**:723–742.
7. Bouchard PO, Bay F, Chastel Y. Numerical modelling of crack propagation: automatic remeshing and comparison of different criteria. *Computer Methods in Applied Mechanics and Engineering* 2002; **192**:3887–3908.
8. Patzák B, Jirásek M. Adaptive resolution of localized damage in quasi-brittle materials. *Journal of Engineering Mechanics* 2004; **130**:720–732.
9. Belytschko T, Krongauz Y, Organ D, Fleming M, Krysl P. Meshless methods: an overview and recent developments. *Computer Methods in Applied Mechanics and Engineering* 1996; **139**:3–47.
10. Dvorkin EN, Cuitiño AM, Gioia G. Finite elements with displacement interpolated embedded localization lines insensitive to mesh size and distortions. *Computer Methods in Applied Mechanics and Engineering* 1990; **90**:829–844.
11. Klisinski M, Runesson K, Sture S. Finite element with inner softening band. *Journal of Engineering Mechanics* (ASCE) 1991; **117**:575–587.
12. Simo JC, Oliver J. A new approach to the analysis and simulation of strain softening in solids. In *Fracture and Damage in Quasibrittle Structures*, Bažant ZP, Bittnar Z, Jirasek M, Mazars J (eds). E & FN Spon: London, 1994; 25–39.
13. Olofsson T, Klisinski M, Nedar P. Inner softening bands: a new approach to localization in finite elements. In *Computational Modeling of Concrete Structures*, Mang H, Bićanić N, de Borst R (eds). Pineridge: Swansea, 1998; 373–382.
14. Oliver J. Modelling strong discontinuities in solid mechanics via strain softening constitutive equations. Part 1: Fundamentals. Part 2: Numerical simulation. *International Journal for Numerical Methods in Engineering* 1996; **39**:3575–3623.
15. Jirásek M. Comparative study on finite elements with embedded discontinuities. *Computer Methods in Applied Mechanics and Engineering* 2000; **188**:307–330.
16. Jirásek M, Belytschko T. Computational resolution of strong discontinuities. In *Proceedings of Fifth World Congress on Computational Mechanics*, Mang HA, Rammerstorfer FG, Eberhardsyeiner J (eds), Vienna, Austria, 2002.
17. Mellenk JM, Babuška I. The partition of unity finite element method: basic theory and application. *Computer Methods in Applied Mechanics and Engineering* 1996; **139**:289–314.
18. Belytschko T, Black T. Elastic crack growth in finite elements with minimal remeshing. *International Journal for Numerical Methods in Engineering* 1999; **45**(5):601–620.
19. Moës N, Dolbow J, Belytschko T. A finite element method for crack growth without remeshing. *International Journal for Numerical Methods in Engineering* 1999; **46**:131–150.
20. Stolarska M, Chopp DL, Moës N, Belytschko T. Modeling crack growth by level sets in the extended finite element method. *International Journal for Numerical Methods in Engineering* 2001; **51**:943–960.
21. Wells GN, Sluys LJ. A new method for modelling of cohesive cracks using finite elements. *International Journal for Numerical Methods in Engineering* 2001; **50**(12):2667–2682.
22. Moës N, Belytschko T. Extended finite element method for cohesive crack growth. *Engineering Fracture Mechanics* 2002; **69**:813–833.

DOI: 10.1002/nme

23. Zi G, Belytschko T. New crack-tip elements for XFEM and applications to cohesive cracks. *International Journal for Numerical Methods in Engineering* 2003; **57**:2221–2240.
24. Asferg JL, Poulsen PN, Nielsen LO. Modeling of cohesive crack applying XFEM. In *Fifth International PhD Symposium in Civil Engineering*, Walraven J, Blauwendraad J, Scarpas T, Snijder B (eds), 2004; 1261–1269.
25. Daux C, Moës N, Dolbow J, Sukumar N, Belytschko T. Arbitrary branched and intersecting cracks with the extended finite element method. *International Journal for Numerical Methods in Engineering* 2000; **48**:1741–1760.
26. Sukumar N, Moës N, Moran B, Belytschko T. Extended finite element method for three-dimensional crack modelling. *International Journal for Numerical Methods in Engineering* 2000; **48**:1549–1570.
27. Areias PMA, Belytschko T. Analysis of three-dimensional crack initiation and propagation using the extended finite element method. *International Journal for Numerical Methods in Engineering* 2005; **63**:760–788.
28. Areias PMA, Belytschko T. Non-linear analysis of shells with arbitrary evolving cracks using XFEM. *International Journal for Numerical Methods in Engineering* 2005; **62**:384–415.
29. Belytschko T, Moës N, Usui S, Parimi C. Arbitrary discontinuities in finite elements. *International Journal for Numerical Methods in Engineering* 2001; **50**:993–1013.
30. Sukumar N, Chopp DL, Moës N, Belytschko T. Modeling holes and inclusions by level sets in the extended finite-element method. *Computer Methods in Applied Mechanics and Engineering* 2001; **190**:6183–6200.
31. Chessa J, Wang H, Belytschko T. On the construction of blending elements for local partition of unity enriched finite elements. *International Journal for Numerical Methods in Engineering* 2003; **57**:1015–1038.
32. Mergheim J, Kuhl E, Steinmann P. A finite element method for the computational modelling of cohesive cracks. *International Journal for Numerical Methods in Engineering* 2005; **63**:276–289.
33. Asferg JL, Poulsen PN, Nielsen LO. A direct XFEM formulation for modeling of cohesive crack growth in concrete. *Computers and Concrete* 2007, in press.
34. Xiao QZ, Karihaloo BL. Improving the accuracy of XFEM crack tip fields using higher order quadrature and statically admissible stress recovery. *International Journal for Numerical Methods in Engineering* 2005; **66**:1378–1410.
35. Xiao QZ, Karihaloo BL. Asymptotic fields at frictionless and frictional cohesive crack tips in quasi-brittle materials. *Journal of Mechanics of Materials and Structures* 2006; **1**:881–910.
36. Asferg JL, Poulsen PN, Nielsen LO. Cohesive crack-tip element for XFEM. In *Proceedings of 11th International Conference on Fracture*, Carpinteri A (ed.), Turin, Italy, 2005.
37. Stang H, Olesen JF, Poulsen PN, Nielsen LD. Application of the cohesive crack in cementitious material modelling. In *Computational Modelling of Concrete Structures*, Meschke G, de Borst R, Mang H, Bićanić N (eds). Taylor & Francis: London, 2006; 443–449.
38. Krenk S. An orthogonal residual procedure for nonlinear finite element equations. *International Journal for Numerical Methods in Engineering* 1995; **38**:823–839.
39. Carpinteri A, Valente S, Ferrara G, Melchiorri G. Is mode II fracture energy a real material property? *Computers and Structures* 1992; **48**(3):397–413.
40. Vandervalle L. Test and design methods for steel fiber reinforced concrete. Recommendations for bending test. *Materials and Structures* 2000; **33**:3–5.

DOI: 10.1002/nme

Paper III

Partly Cracked XFEM Interface

Paper in: *Fracture of Nano and Engineering Materials and Structures, Proceedings of the 16 European Conference of Fracture, Alexndroupolis, Greece, July 3-7, 2006. E.E. Gdoutos (eds), page 397-398, (Full paper on CD).*

PARTLY CRACKED XFEM INTERFACE

J.L. Asferg[†], T. Belytschko,[‡] P.N. Poulsen,[†] L.O. Nielsen[†]

[†] *Department of Civil Engineering, Technical University of Denmark*
DK-2800 Kgs. Lyngby, Denmark.
[‡] *Department of Mechanical Engineering, Northwestern University*
Evanston, IL, USA

E-mail:
jla@byg.dtu.dk, tedbelytschko@northwestern.edu, pnp@byg.dtu.dk, lon@byg.dtu.dk

Summary

Modeling of crack propagation in reinforced concrete structures may be carried out applying the XFEM concept. Several authors have proposed methods for cohesive crack modeling within the framework of XFEM Wells and Sluys (2001), Moës and Belytschko (2002), Zi and Belytschko (2003), Asferg et al. (2006), that are applicable for modeling of crack propagation in the bulk concrete of reinforced concrete structures. Cracking in the bond zone between concrete and reinforcement, however, plays an important role in the load carrying behavior of reinforced concrete structures and requires special attention. As a step towards a more consistent method for modeling of reinforced concrete structures, a new 6 node XFEM interface element for cohesive cracking is developed. The interface element is able to hold the crack tip within the interior of the element and it is based on a partition of unity. The performance of the element is illustrated by modeling of crack growth in a notched three point bending beam.

Keywords *Extended finite elements - XFEM, Fracture mechanics, cohesive crack growth.*

1 Introduction

Throughout the last century intense research has been carried out regarding methods to determine the ultimate strength of reinforced concrete structures. Today well documented methods are available for estimating the ultimate strength of most reinforced concrete structures. However, most of these methods require the use of empirical factors and do not consider phenomena such as size effects and reinforcement arrangement in detail.

Regarding reinforced concrete structures in the serviceability limit state the predictive capability of existing methods of analysis is limited. Complex models dealing with the serviceability limit state requires prediction of the complex cracking which takes places in the concrete during loading. Modeling of cracks in plain concrete has been a focus area in the research community since the mid seventies where Hillerborg et al. (1976) presented their fictitious crack model and Bažant and Oh (1983) proposed the concept of a crack band. Today several FEM codes have interface elements suitable for discrete cracking and elements for smeared cracking. The use of

interface elements however requires the crack path to be known beforehand, while crack modeling applying the smeared approach is not well-suited for modeling of localized crack growth.

Among the methods that allow modeling of discrete crack growth without knowing the crack path beforehand is the extended finite element method - XFEM, Belytschko and Black (1999), Moës et al. (1999). XFEM has been applied to a number of different problems within the area of fracture mechanics among which are cohesive cracking, Wells and Sluys (2001),Moës and Belytschko (2002) and Zi and Belytschko (2003). XFEM modeling of crack growth in plain concrete for benchmark tests such as three point bending and four point shear bending was also considered in Asferg et al. (2006) applying a simplified concept for the enrichment of the displacement field.

Modeling of reinforced concrete beams applying the FEM was first carried out by Ngo and Scordelis (1967). Since then several approaches for modeling of the interaction between reinforcement and concrete have emerged. Today the most widely used concept for modeling the interaction between steel and concrete is the application of interface elements for the bond zone e.g. Lundgren (1999).

The use of standard interface elements, however, poses some difficulties. Generation of more complex models with multidirectional reinforcement is cumbersome and special attention is required whenever two reinforcement bars cross each other. When the aim is to model crack growth without knowing the crack path beforehand applying, e.g. the XFEM concept for the bulk concrete, traditional interface elements are not applicable for the bond zone between reinforcement and concrete.

The goal of the present research project is to develop a more consistent method for modeling of reinforced concrete structures and a superelement may be the final goal of the project. However before such an element can be formulated, an XFEM interface element for the bond zone has to be formulated. One of the requirements to the XFEM interface element is that it should be able to handle intersecting cracks - longitudinal cracking along the reinforcement initiated by cracks crossing the reinforcement. Furthermore the interface element should be formulated as an element that is able to partly crack. Bond between concrete and reinforcement is a 3D problem and the confining pressure is one of the key effects for the stress transfer between concrete and reinforcement. However, initially the XFEM interface is considered in a plane version. c.f. Figure 1

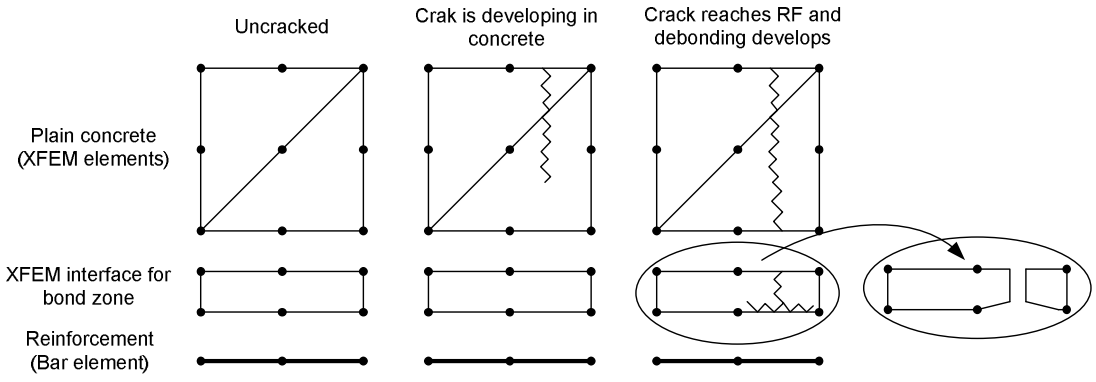

Figure 1: Development of crack in interface between concrete and reinforcement

This papers presents the interface formulation that allows the longitudinal crack to develop in the interface, the tip of the crack being within the interior of the element. At present the element is not able to model intersecting cracks. The paper is organized as follows. First the enrichment concept is presented, then the variational formulation is developed and then the implementation aspects as integration scheme and crack growth are discussed. The last part of the paper concerns the numerical example.

2 Enrichment of Displacement field

In the extended finite element method the displacement field is decomposed into two parts, a continuous and a discontinuous part. The continuous part is the standard displacement field corresponding to the situation without any crack while the enrichment with the discontinuous displacement field enables the element to include a cohesive crack. The displacement field is enriched only in elements cut by the discontinuity. The enriched field may be written as

$$\mathbf{u}\left(x,y\right)=\mathbf{N}^{c}(x,y)\mathbf{v}^{c}+\mathbf{N}^{d}(x,y)\mathbf{v}^{d} \tag{1}$$

where $\mathbf{v}^c$ and $\mathbf{v}^d$ are the dof vectors while $\mathbf{N}^c$ and $\mathbf{N}^d$ are the interpolation matrices. c refers to continuous and d to discontinuous.

In Moës and Belytschko (2002) an XFEM scheme was proposed for cohesive cracking considering elements capable of treating the crack tip within the interior of the element. In this scheme fully cracked elements are enriched with the signed distance function by applying the jump function while the crack tip element is enriched with a set of branch functions to model the near tip field. Cohesive cracking was also considered in Zi and Belytschko (2003). Here a XFEM scheme based on a true partition of unity enrichment for all elements cut by the discontinuity was proposed. In Zi and Belytschko (2003) all elements, including the tip element are enriched by the sign function as the only enrichment.

The enrichment of the displacement field for the new interface element is also based on true local partition of unity and follows the enrichment scheme suggested in Asferg et al. (2006). In Asferg et al. (2006) the discontinuous interpolation matrix, $\mathbf{N}^d$, is chosen as

$$\mathbf{N}^{d}\left(x,y\right)=\sum_{I}H_{I}(x,y)\mathbf{N}_{I}^{c}(x,y) \tag{2}$$

where $H_I(x,y)$ is the Heaviside step function for node I. The step function $H_I(x,y)$ is 0 on the same side of the discontinuity as node I and 1 on the other side.

For the element to be able to hold the crack tip within the interior of the element a more general formulation is however required: in (2) $\mathbf{N}^c$ is replaced by $\mathbf{N}^*$ that is more general but able to describe the same variations as $\mathbf{N}^c$. Referring to Figure 2, $\mathbf{N}^*$ is formulated in terms of the standard shape functions by introducing the relative crack length $\alpha \in [0,1]$ as additional variable. The element consists of two superimposed elements, the first with a continuous field as shown in Figure 2(B), the second with a discontinuous field defined on $-1<\zeta<-1+2\alpha$, $-1\leq\eta\leq 1$, c.f. Figure 2(C) The element is not isoparametric, so ζ and η are scaled coordinates of a rectangle. The enrichment of the displacement field refers only to the cracked part of the element. It has to be emphasized that figure 2(C) only serves to illustrate the interpretation of

the enrichment; no extra nodes are added to the element, the discontinuous degrees of freedom are stored in the standard nodes c.f. Figure 2(A). For completeness the shape functions $\mathbf{N}^*$ are written out in (3).

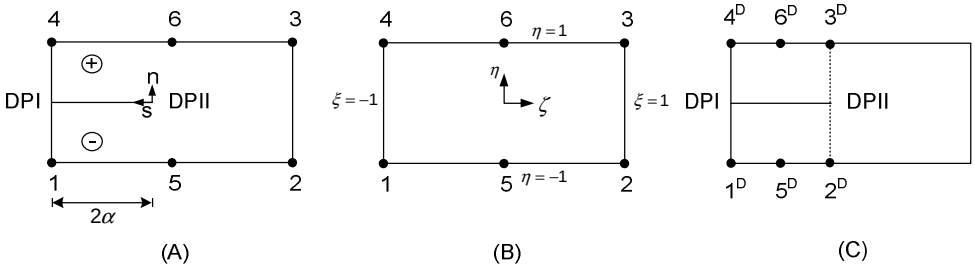

Figure 2: Topology of interface element. (A) Topology of partly cracked interface element . (B) Standard element coordinates. (C) "Discontinuity" nodes in partly cracked interface element.

$$
\begin{aligned}
N_1^* &= \tfrac{-1}{4\alpha^2}\,(\zeta+1-\alpha)\,(\zeta+1-2\alpha)\,(\eta-1)\\
N_2^* &= \tfrac{-1}{4\alpha^2}\,(\zeta+1)\,(\zeta+1-\alpha)\,(\eta-1)\\
N_3^* &= \tfrac{1}{4\alpha^2}\,(\zeta+1)\,(\zeta+1-\alpha)\,(\eta+1)\\
N_4^* &= \tfrac{1}{4\alpha^2}\,(\zeta+1-\alpha)\,(\zeta+1-2\alpha)\,(\eta+1)\\
N_5^* &= \tfrac{1}{2\alpha^2}\,(\zeta+1)\,(\zeta+1-2\alpha)\,(\eta-1)\\
N_6^* &= \tfrac{-1}{2\alpha^2}\,(\zeta+1)\,(\zeta+1-2\alpha)\,(\eta+1)
\end{aligned}
\tag{3}
$$

where α is shown in Figure 2(A)

We apply the enrichment above only to elements cut by the discontinuity; the enrichment is purely local hence the discontinuous displacement field will always be zero on edges where elements not cut by the discontinuity joins the enriched element. To ensure that the crack closes at the tip the discontinuity dofs corresponding to the tip are set to zero. Figure 3 illustrates a possible discontinuous displacement field modeled by applying the discontinuous shape functions in (3). Notice the capability to model smooth closure of the crack.

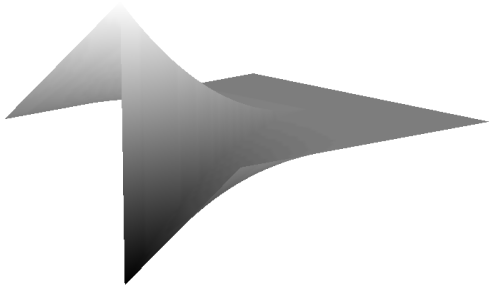

Figure 3: Discontinuous displacement field for partly cracked interface element

3 Variational formulation

Considering a cohesive crack in a plane stress or strain structure described in a Cartesian coordinate system x,y (cf. Figure 4), the arc length along the crack is termed s, and n,s is a Cartesian coordinate system, n being normal to the crack face. The orientation of n determines the positive side of the crack. The stress state in the crack may be defined by the normal stress σ_n and the shear stress τ_{ns} while work conjugated strains are the opening of the crack, $\Delta u_n = u_n^+ - u_n^-$ and the slip in the crack, $\Delta u_s = u_s^+ - u_s^-$. A small strain / small displacement static theory is used and the bulk material is assumed linear elastic.

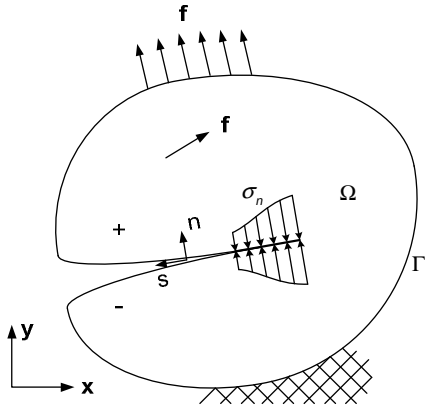

Figure 4: Cohesive crack in two dimensional domain with f representing both domain load and boundary load

The stress increments $d\boldsymbol{\sigma}^{cr}$ across the crack surfaces are related to the increments in the displacement jump - i.e. the separation of the crack surfaces - $d[\![\boldsymbol{u}]\!]$ of the crack through the tangential material stiffness matrix $\mathbf{D}_T^{cr}$

$$\boldsymbol{\sigma}^{cr}(\boldsymbol{u}) = \begin{bmatrix} \sigma_n(u_n) \\ \tau_{ns}(u_s) \end{bmatrix} \qquad d[\![\boldsymbol{u}]\!] = \begin{bmatrix} \Delta u_n \\ \Delta u_s \end{bmatrix} \qquad d\boldsymbol{\sigma}^{cr}(\boldsymbol{u}) = \mathbf{D}_T^{cr}(\boldsymbol{u})\, d[\![\boldsymbol{u}]\!] \tag{4}$$

For the bulk material the stress vector $\boldsymbol{\sigma}^T = [\sigma_x \quad \sigma_y \quad \tau_{xy}]$ and strain vector $\boldsymbol{\epsilon}^T = [\epsilon_x \quad \epsilon_y \quad \gamma_{xy}]$, $(\gamma_{xy} = 2\epsilon_{xy})$ are related through the standard material stiffness matrix $\mathbf{D}$, specified below for an isotropic material.

$$d\boldsymbol{\sigma} = \mathbf{D} d\boldsymbol{\epsilon} \qquad , \qquad \boldsymbol{D} = \frac{E}{1-\nu^2} \begin{bmatrix} 1 & \nu & 0 \\ \nu & 1 & 0 \\ 0 & 0 & \frac{1-\nu}{2} \end{bmatrix} \tag{5}$$

The virtual internal work per unit length of the crack δW_{cr}^i and the internal work per unit area of the uncracked part of the structure δW_c^i may now be written, δ referring to a virtual quantity

$$\begin{aligned} \delta W^i_{cr} &= \delta\boldsymbol{\epsilon}^{crT}\boldsymbol{\sigma}^{cr} = \sigma_n\delta\Delta u_n + \tau_{ns}\delta\Delta u_s \\ \delta W^i_c &= \delta\boldsymbol{\epsilon}^T\boldsymbol{\sigma} = \sigma_x\delta\epsilon_x + \sigma_y\delta\epsilon_y + \tau_{xy}\delta\gamma_{xy} \end{aligned} \tag{6}$$

For the entire structure the internal and external work becomes

$$\begin{aligned} \delta W^i &= \textstyle\int_\Omega \delta\boldsymbol{\epsilon}^T\boldsymbol{\sigma}d\Omega + \int_\Gamma \delta[\![\boldsymbol{u}]\!]^T\boldsymbol{\sigma}^{cr}d\Gamma \\ \delta W^e &= \textstyle\int_\Omega \delta\mathbf{u}^T\mathbf{f}d\Omega + \int_\Gamma \delta\mathbf{u}^T\mathbf{f}d\Gamma \end{aligned} \tag{7}$$

Leading to the usual discrete equilibrium equation in its ordinary form

$$\mathbf{K}_T\Delta\mathbf{V} = \int_\Omega \mathbf{N}^T\Delta\mathbf{f}d\Omega + \int_\Gamma \mathbf{N}^T\Delta\mathbf{f}d\Gamma \tag{8}$$

where $\boldsymbol{V}$ is the system dof vector and Δ refers to incremental.

Special attention must be paid to the internal work, hence the contribution from each element to the tangential stiffness $\mathbf{K}_T$ depends on whether the element is cracked or not. The element tangential stiffness matrix, $\mathbf{k}_T$, for a cracked element is developed by the following procedure. From (1, 2) the strain vector in a cracked element, except in the crack, is obtained

$$\boldsymbol{\epsilon}(x,y) = \mathbf{B}^c(x,y)\,\mathbf{v}^c + \sum H_I(x,y)\,\mathbf{B}^c_I(x,y)\mathbf{v}^d_I = \mathbf{B}^c\mathbf{v}^c + \mathbf{B}^d\mathbf{v}^d \tag{9}$$

Where $\mathbf{B}^c$ is the strain distribution matrix corresponding to the interpolation matrix N^c.

Since the displacement field from the first terms in (1) is continuous, the displacement jump in the crack may be written as

$$[\![\boldsymbol{u}]\!](s) = \mathbf{T}\left(\mathbf{N}^d_+(s) - \mathbf{N}^d_-(s)\right)\mathbf{v}^d = \mathbf{B}^{cr}\mathbf{v}^d \tag{10}$$

Here $\mathbf{B}^{cr}$ is the strain distribution matrix in the crack, $\mathbf{T}$ is the transformation matrix between the (x,y)- and (n,s)-coordinate systems while $\mathbf{N}^d_+$ and $\mathbf{N}^d_-$ are the discontinuous interpolation matrices at the positive, respectively, negative side of the crack.

Applying the strain relations in (9) and (10) when formulating the virtual internal work, $\mathbf{k}_T$ defined by $\delta W^i = \delta\mathbf{v}^T\mathbf{k}_T d\mathbf{v}$, where $\mathbf{v^T} = [\mathbf{v}^{cT} \quad \mathbf{v}^{dT}]$, is found to be

$$\mathbf{k}_T = \begin{bmatrix} \int \mathbf{B}^{cT}\mathbf{D}\mathbf{B}^c & \int \mathbf{B}^{cT}\mathbf{D}\mathbf{B}^d \\ \int \mathbf{B}^{dT}\mathbf{D}\mathbf{B}^c & \int \mathbf{B}^{dT}\mathbf{D}\mathbf{B}^d + \int_{cr}\mathbf{B}^{crT}\mathbf{D}^{cr}\mathbf{B}^{cr} \end{bmatrix} = \begin{bmatrix} \mathbf{k}^{cc}_T & \mathbf{k}^{cd}_T \\ \mathbf{k}^{dc}_T & \mathbf{k}^{dd}_T + \mathbf{k}^{cr}_T \end{bmatrix} \tag{11}$$

Performing the equilibrium iteration solving the non-linear finite element equations the element nodal forces, $\mathbf{q}$, are required. $\mathbf{q}$ depends like $\mathbf{k}_T$ on the crack opening and is determined analogous to $\mathbf{k}_T$. The contribution to $\mathbf{q}$ from the crack, $\mathbf{q}^{cr}$, is found from the stresses in the crack. The stresses in the crack are related to the displacement jump according to (4). Adding this contribution to the contribution from the part of the element outside the crack, $\mathbf{q}$ is obtained as

$$\mathbf{q} = \begin{bmatrix} \mathbf{k}^{cc}_T & \mathbf{k}^{cd}_T \\ \mathbf{k}^{dc}_T & \mathbf{k}^{dd}_T \end{bmatrix}\begin{bmatrix} \mathbf{v}^c \\ \mathbf{v}^d \end{bmatrix} + \mathbf{q}^{cr} \qquad where \qquad \mathbf{q}^{cr} = \int_{cr}\mathbf{B}^{crT}\begin{Bmatrix} \sigma_n \\ \tau_{ns} \end{Bmatrix} \tag{12}$$

4 Implementation

In this section some of the key aspects of the implementation of the interface element will be discussed. First the applied integration scheme will be outline, then crack growth and criterions for smooth crack closure will be discussed briefly.

4.1 Integration of enriched elements

To ensure sufficient accuracy of the strain field at both side of the discontinuity in elements cut by the discontinuity, integration must be performed independently on both sides of the discontinuity. For fully cracked elements, (Wells and Sluys (2001) and Asferg et al. (2006)) the integration has been carried out considering the same subdomain for the continuous field and the discontinuous field. In this case, where partly cracked elements are considered, the integration of the continuous field is carried out by considering the entire area of the element. For the discontinuous field the area cut by the discontinuity is divided into two parts and individual integration performed on those subdomains. For the three subdomains a standard seven point Gauss integration scheme is applied. Concerning the line of discontinuity three integration points are applied for the integration of traction forces across the discontinuity. Figure 5 illustrates the integration scheme.

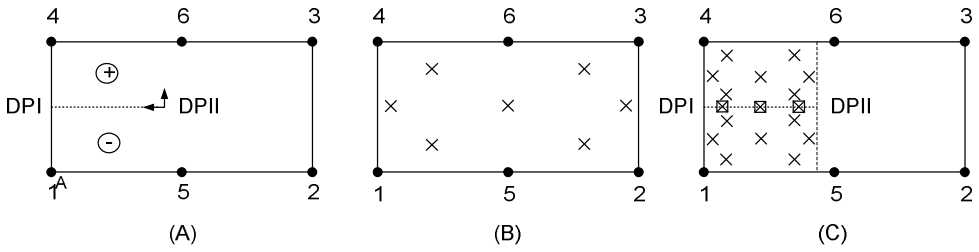

Figure 5: Applied integration scheme. (A) Element partly cut by discontinuity. (B) Integration point for continuous field. (C) Integration point for discontinuous field, crosses mark integration points i continuum, crossed square marks integration point in discontinuity.

4.2 Crack Growth and Condition for smooth crack closure

For an interface element, one of the often discussed issues, determination of the crack growth direction, is not an issue. The interface element limits the crack growth to the longitudinal direction of the interface element; the crack propagates along the centerline of the element. When the element is applied to practical modeling problems, the thickness of the element is small compared to the element length.

In the case of cohesive cracking, cohesive tractions act at the crack surface near the tip and no singularity is present at the crack tip. The criterion for a stable crack is that the tensile stresses at the crack tip are equal to the tensile strength of the material, f_t. When the tensile stresses at the crack tip are equal to f_t smooth closure of the crack is achieved. When a crack is propagated element by element as in Wells and Sluys (2001), Asferg et al. (2006) often no criterion is applied for smooth crack closure. In Zi and Belytschko (2003) a smooth crack closure criterion is imposed at the system level by requiring the stress projection in the normal direction

to the crack to be equal to f_t at the crack tip. For the interface element we are investigating possibilities for imposing a smooth closure criterion on element level. However for the results given in this paper no criterion has been applied to ensure smooth crack closure. As a first test the crack was propagated element by element and an element became cracked when the tensile stresses in the element exceeded f_t. Allowing the elements to be partly cracked the crack length in a given load step was determined from the stress field in the uncracked part of the element and the crack then propagated to the point where the tensile stresses were equal to f_t.

4.3 Algorithm

To remain within the framework of traditional FEM codes a general procedure, the orthogonal residual algorithm Krenk (1995), was adopted for the XFEM scheme to solve the non-linear equations. As a convergence criterion a energy criterion was applied and the elastic energy in the initial elastic load step was used as reference energy.

5 Numerical example

As initial test case three point bending of a notched beam is considered. The geometry of the test specimen is chosen in accordance with the RILEM specifications for the notched three point bending test (TPBT) of concrete beams Vandervalle (2000). The geometry and applied constitutive parameters are seen in Figure 6. Only mode I cracking is considered, though the scheme allows for mixed mode coupling. A simple linear softening law is applied as the constitutive relation for the crack.

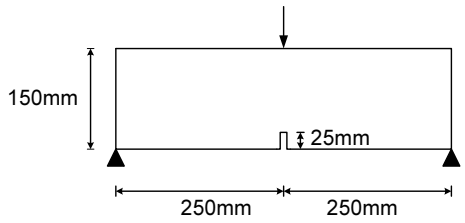

Parameter	Value
E_c	37400MPa
ν_c	0.2
f_t	3.5MPa
G_f	160 N/m

Figure 6: Geometry and constitutive parameters for TPBT specimen

A narrow band of interface elements has been used at the center section of the beam, and results will be given for two fairly coarse meshes. One mesh is with 12 elements, the other with 24 through the beam height. The mesh with 24 elements over the beam height is depicted in Figure 7. The notch is modeled by an initial stress free crack through the number of elements that corresponds to 25mm - i.e. in the case of 12 elements through the beam height the 2 lower elements are cut by an initial stress free crack while the number is 4 in the case of 24 elements through the beam hight.

Results in terms of load displacement curves for the two considered meshes are given in Figure 8. The XFEM results are compared to results obtained by modeling the TPBT specimen applying standard interface element in the commercial code DIANA from TNO. Figure 8(a)

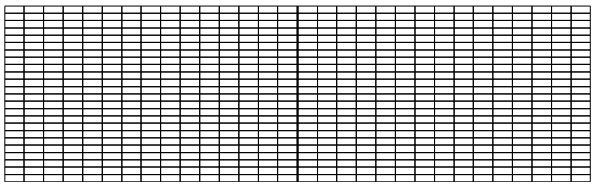

Figure 7: Mesh of TPBT specimen, 24 elements through the beam hight.

compares the load deflection response obtained using fully cracked elements to partly cracked elements for the 21 by 12 mesh while Figure 8(b) illustrates the results for the 31 by 24 mesh. Figure 9 shows the propagation of the crack through the beam at different load levels.

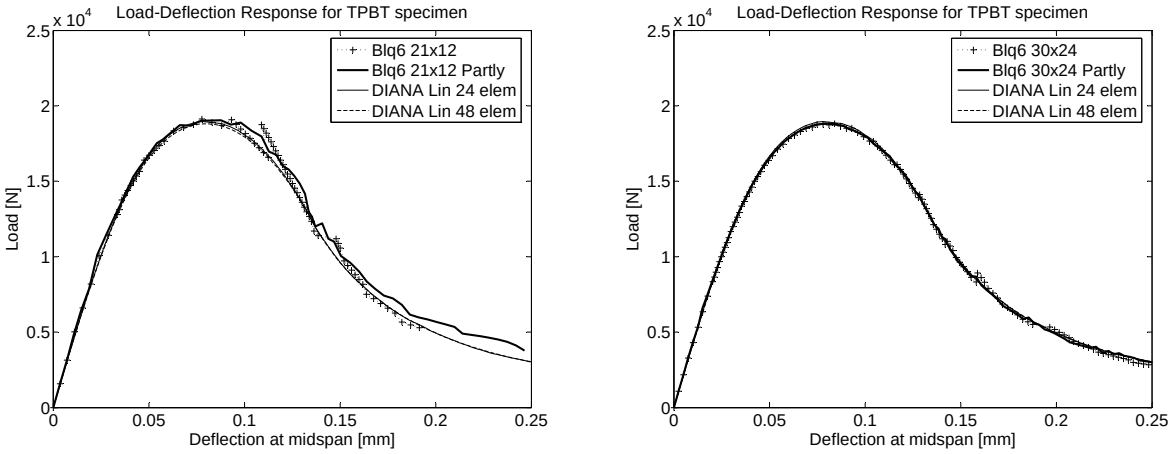

(a) (b)

Figure 8: Load deflection response for TPBT specimen. (a) Mesh of 21x12 elements (b) Mesh of 31x24 elements.

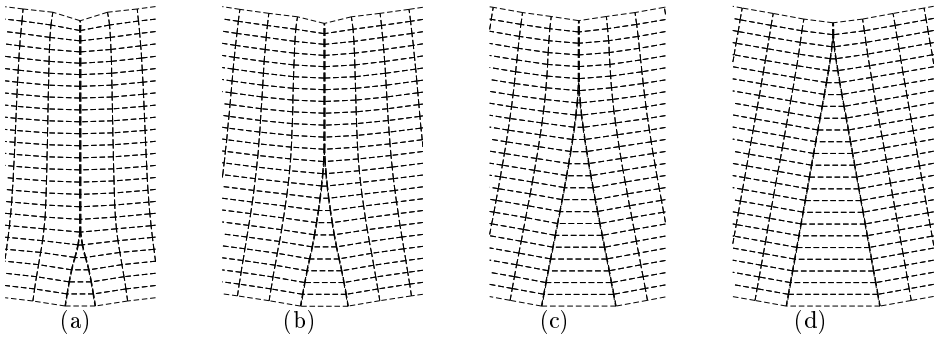

(a) (b) (c) (d)

Figure 9: Propagation of crack through TPBT specimen. (a) Crack has propagated through 3 elements, P=11.2kN. (b) Crack has reached midpoint of beam, P=18.4kN. (c) Crack has propagated 3/4 of the way through the beam, P=14.6kN. (d) Crack has reached top of beam., P=2.5kN

From Figure 8 it is seen that even with as few as 12 elements through the beam height,

the overall load deformation response is captured pretty well. However increasing the number of elements through the beam height smoothes out the response significantly. As expected the use of partly cracked interface elements results in a more smooth response than the use of elements that are allowed only to be fully cracked. By implementing a iteration control procedure that ensures that the stresses at the crack tip equals f_t it may be expected that an even smoother response is obtained.

6 Conclusion

As a step towards a more consistent method for modeling of reinforced concrete, a new six node interface element has been proposed. In this paper a first version of the proposed interface element being able to hold the crack tip within the interior of the element has been presented. By modeling of fracture in a three point bending beam, the performance of the element has been illustrated. Is is seen that for even fairly coarse meshes the XFEM scheme produces good results, as expected the use of partly cracked element results in a more smooth response than when fully cracked elements are applied.

Further work on the interface elements involves first and foremost an control method for the iteration procedure that ensures that the tensile stress at the crack tip in all steps are equal to the tensile strength of the material. Then the capability to handel intersecting cracks as sketched on Figure 1 shall be considered and finally an appropriate bond model for the interaction between concrete and reinforcement shall be applied.

7 Acknowledgment

The second author acknowledges the support of the Army Research Office.

References

Asferg, J. L., Poulsen, P. N., and Nielsen, L. O. (2006). A direct XFEM formulation for modelling of cohesive crack growth in concrete. *Submitted to Computers and Concrete*.

Bažant, Z. P. and Oh, B. H. (1983). Crack band theory for fracture of concrete. *Materials and structures, RILEM*, 16 (93):155–177.

Belytschko, T. and Black, T. (1999). Elastic crack growth in finite elements with minimal remeshing. *International Journal for Numerical Methods in Engineering*, 45 (5):601–620.

Hillerborg, A., Modéer, M., and Peterson, P.-E. (1976). Analysis of crack formation and crack growth in concrete by means of fracture mechanics and finite elements. *Cement and Concrete Research*, 6:773–782.

Krenk, S. (1995). An orthogonal residual procedure for nonlinear finite element equations. *International Journal for Numerical Methods in Engineering*, 38:823–839.

Lundgren, K. (1999). *Three-Dimensional Modeling of Bond in Reinforced Concrete*. PhD thesis, Division of Concrete Structures, Department of Structural Engineering, Chalmers University of Technology.

Moës, N. and Belytschko, T. (2002). Extended finite element method for cohesive crack growth. *Engineering Fracture Mechanics*, 69:813–833.

Moës, N., Dolbow, J., and Belytschko, T. (1999). A finite element methode for crack growth without remeshing. *International Journal for Numerical Methods in Engineering*, 46:131–150.

Ngo, D. and Scordelis, C. (1967). Finite element analysis of reinforced concrete beams. *ACI Journal*, 64:152–163.

Vandervalle, L. (2000). Test and design methods for steel fiber reinforced concrete. Recommendations for bending test. *Materials and Structures*, 33:3–5.

Wells, G. N. and Sluys, L. (2001). A new method for modeling of cohesive cracks using finite elements. *International Journal for Numerical Methods in Engineering*, 50 (12):2667–2682.

Zi, G. and Belytschko, T. (2003). New crack-tip elements for XFEM and applications to cohesive cracks. *International Journal for Numerical Methods in Engineering*, 57:2221–2240.

Report no R-171
ISSN 1601-2917
ISBN 978-87-7877-214-1